

Neural Prosthetics and Parietal Cortex

Thesis by  
Boris Revechkis

In Partial Fulfillment of the Requirements for the Degree of  
Doctor of Philosophy



California Institute of Technology  
Pasadena, California

2015  
(Defended May 29, 2015)

© 2015

Boris Revechki

All Rights Reserved

**Acknowledgements**

I'd like to thank my advisor, Richard Andersen, for giving me the rare privilege of listening to neurons both primate and human, Tyson Aflalo for persistent advice and guidance, Bijan Pesaran for giving me my first glimpse of real neuroscience when I was just a curious undergraduate, and our clinical study subject for having the courage and fortitude to turn her profound hardships into learning opportunities for all of us.

I'd also like to thank Dr. Nader Pouratian for his critical surgical expertise and enthusiasm, Ueli Rutishauser, Chess Stetson, Eunjung Hwang, Markus Hauschild, helpful for scientific discussion, Tessa Yao for administrative omnipresence, Kelsie Pejsa for animal care, and Viktor Shcherbatyuk and Spencer Kellis for technical assistance. I thank the National Institutes of Health for providing the funding that allowed this thesis to be undertaken.

**Dedication**

I dedicate this thesis to my family:

To my parents and grandparents for abandoning their former lives, friends, and homes, and traveling halfway across the planet so that their children could live better.

To my brother, for asking my parents for a little brother.

And, again, to my parents, for agreeing.

**Abstract**

In the last decade, research efforts into directly interfacing with the neurons of individuals with motor deficits have increased. The goal of such research is clear: Enable individuals affected by paralysis or amputation to regain control of their environments by manipulating external devices with thought alone. Though the motor cortices are the usual brain areas upon which neural prosthetics depend, research into the parietal lobe and its subregions, primarily in non-human primates, has uncovered alternative areas that could also benefit neural interfaces. Similar to the motor cortical areas, parietal regions can supply information about the trajectories of movements. In addition, the parietal lobe also contains cognitive signals like movement goals and intentions. But, these areas are also known to be tuned to saccadic eye movements, which could interfere with the function of a prosthetic designed to capture motor intentions only. In this thesis, we develop and examine the functionality of a neural prosthetic with a non-human primate model using the superior parietal lobe to examine the effectiveness of such an interface and the effects of unconstrained eye movements in a task that more closely simulates clinical applications. Additionally, we examine methods for improving usability of such interfaces.

The parietal cortex is also believed to contain neural signals relating to monitoring of the state of the limbs through visual and somatosensory feedback. In one of the world's first clinical neural prosthetics based on the human parietal lobe, we examine the extent to which feedback regarding the state of a movement effector alters parietal neural signals

and what the implications are for motor neural prosthetics and how this informs our understanding of this area of the human brain.

**Table of Contents**

Acknowledgements.....	ii
Abstract.....	iv
List of Abbreviations .....	ix
List of Illustrations and Tables .....	x
1. Introduction .....	1
2. Background.....	3
2.1 Brain Machine Interfaces .....	5
2.2 Parietal Cortex.....	7
2.3 References .....	10
3. Non-Human Primate Parietal Cortex and Neural Prosthetics .....	13
3.1 Parietal Neural Prosthetic Control of a Computer Cursor in a Graphical-User-Interface Task.....	13
3.1.1 Introduction.....	13
3.1.2 Methods.....	15
3.1.2.1 Behavioral Setup .....	16
3.1.2.2 Neural Recordings.....	16
3.1.2.3 Behavioral Task.....	18
3.1.2.4 Performance Measures .....	20
3.1.2.5 Decoder Training.....	22
3.1.2.6 Decoder Calculation .....	24
3.1.2.7 Saccade Task .....	25
3.1.3 Results.....	26
3.1.3.1 Saccade Task .....	26
3.1.3.2 Behavioral Task – Manual Control .....	27
3.1.3.3 Behavioral Task – Brain Control.....	30
3.1.4 Discussion.....	36
3.1.5 References.....	39
3.2 State Decoding Improves Use of a Computer Cursor for Neuroprosthetic Applications .....	41
3.2.1 Introduction.....	41
3.2.2 Methods.....	42
3.2.2.1 Behavioral Setup .....	42
3.2.2.2 Neural Recordings.....	43
3.2.2.3 Behavioral Task.....	44

3.2.2.4	Performance Measures .....	46
3.2.2.5	Statistical Tests.....	47
3.2.2.6	Decoder Training Procedure .....	47
3.2.2.7	Velocity Decoder Computation.....	48
3.2.2.8	State Decoder Computation.....	50
3.2.3	Results.....	51
3.2.4	Discussion.....	55
3.2.5	References.....	57
4.	Human Parietal Cortex .....	58
4.1	Selectivity for Hand Movement Execution and Feedback in Human Parietal Neurons and Local Fields .....	58
4.1.1	Introduction.....	58
4.1.2	Methods.....	60
4.1.2.1	Human Subject Recruitment .....	60
4.1.2.2	Experimental Setup .....	61
4.1.2.3	Behavioral Tasks .....	62
4.1.2.3.1	Effector Specificity in Decoding Delayed Reaches .....	62
4.1.2.3.2	Limb Tuning Task .....	66
4.1.2.3.3	Effector Specificity in Hand Gestures.....	69
4.1.2.3.4	Online Gesture Control .....	72
4.1.3	Results.....	76
4.1.3.1	Delayed Reach Task .....	76
4.1.3.2	Limb Tuning Task.....	81
4.1.3.3	Gesture Task .....	83
4.1.3.3.1	LFP Response .....	83
4.1.3.3.2	Single/Multi-unit Response .....	86
4.1.3.4	Online Gesture Control Task .....	89
4.1.4	Discussion.....	93
4.1.5	References.....	98
	Appendices.....	100
A.	Tuning and Decoding Properties of Neural Populations .....	100
1.	Human Neural Population.....	100
2.	NHP Neural Population.....	102

B. Clinical Implant Targeting Methodology .....	103
C. Supplementary Data .....	108
D. Descriptions of Video Files .....	110

**List of Abbreviations**

AIP	Anterior Intraparietal Area
BA	Brodmann Area
BOLD	Blood-oxygen-level Dependent
BMI	Brain Machine Interface
FDR	False Discovery Rate
FMRI	Functional Magnetic Resonance Imaging
FOV	Field of View
HMD	Head-Mounted Display
IQR	Inter-Quartile Range
ITI	Inter-Trial Interval
LFP	Local Field Potential
LIP	Lateral Intraparietal Area
LOOCV	Leave-One-Out Cross Validation
NHP	Non-Human Primate
PCA	Principal Component Analysis
PPC	Posterior Parietal Cortex
PRR	Parietal Reach Region
PSTH	Peristimulus Time Histogram
TTA	Time To Acquire
TTH	Time To Hold
TTR	Time To Reward
VR	Virtual Reality

**List of Illustrations and Tables**

Figure 3.1.2.3-1 Face in the Crowd Task Trial Structure. .... 18

Figure 3.1.3.1-1 Manual Control Performance. .... 27

Figure 3.1.3.2-1 Effect of the Crowd on Gaze During Manual Control. .... 28

Figure 3.1.3.2-2 Gaze with Crowd on during Manual vs Brain Control. .... 29

Figure 3.1.3.3-1 Performance Measures Across Training and Assessment Conditions (Brain Control). .... 31

Table 1 Statistics for All Combinations of Conditions and Measures. .... 32

Figure 3.1.3.3-2 Hand and Cursor Position During Decoding ..... 35

Figure 3.2.2.3-1 Face in a Crowd Task Structure. .... 44

Figure 3.2.2.3-1 Encoding of Movement versus Non-movement By the Neural Data .... 46

Figure 3.2.3-1 Summary State Decoder Performance. .... 52

Figure 3.2.3-2 Effect of State Decoding on TTH Per Decoder ..... 54

Figure 4.1.2.3.1-1 Example Frame from Stereoscopic Display. .... 62

Figure 4.1.2.3.1-2 Reaching Task Progression. .... 65

Figure 4.1.2.3.2-1 Limb Tuning Task Diagram. .... 67

Figure 4.1.2.3.2-1 Gesture Task Progression. .... 69

Figure 4.1.2.3.4-1 Online Gesture Control Task And Training Task. .... 73

Figure 4.1.3.1-1 Delayed Reaching Task Offline Decoding Performance. .... 77

Figure 4.1.3.1-2 Time Course of Decoding Performance Throughout the Trial. .... 79

Figure 4.1.3.1-3 Limb Tuning Task Results. .... 81

Figure 4.1.3.3.1-1 Responses in the Local Field Potentials of Array 1 to Task Variables. .... 84

Figure 4.1.3.3.2-1 Example Neural Responses during the Gesture Task. .... 88

Figure 4.1.3.4-1 Online Gesture Control Performance Summary. .... 90

Figure 4.1.3.4-2 Change in Activity of Units Used For Decoding. .... 93

Figure A-1 PSTHs of Tuned Units Used for Offline Decoding of Delayed Reach Task. .... 100

Figure A-1 Neuron Dropping Curves for Delayed Reach Task By Effector. .... 101

Figure A-2 PSTHs of Tuned Neurons Recorded during a Delayed Reach Center-out Task. .... 102

Figure B-1 Targeting Task 3 Schematic. .... 105

Figure B-2 fMRI Results and Array Implant Locations. .... 106

Figure C-1 Local Field Potential Power for Array 1 During the Gesture Task, Collapsed in Time. .... 108

Figure C-2 Local Field Potentials of Array 2 During the Gesture Task. .... 109

Figure C-3 Local Field Potential Power for Array 2 During the Gesture Task, Collapsed in Time. 2. .... 109

## **1. Introduction**

Ever since it was discovered that the activity of individual neurons in the mammalian brain correlate with specific sensory stimuli, decisions, and, movements, a tantalizing and profound question has loomed large. Is it possible to predict thoughts and intentions from neural activity? Can those predictions be used to connect brains and their owners directly with the world through artificial devices, bypassing the body? Though many envisioned incarnations of such technology remain outside the scope of modern neuroscience, one subset has proven an active and fruitful area of research over the last 20 years. A small number of paralysis patients have successfully been able to manipulate computer cursors and robotic limbs based on the activity of tens to a few hundreds of neurons in their primary motor cortices. However, many technical and scientific challenges remain to be conquered before these technologies can be applied beyond the proof of concept.

The vast majority of Brain Machine Interface (BMI) or neural prosthetic research has depended on recording of primary motor cortical neurons. Another brain area, the parietal lobe, and more specifically, the superior parietal lobule, has also been an active venue of basic research over the last half-century. Studied for its role in sensory-motor transformations, movement and motor planning, and decision making, it has been suggested as a viable and rich alternative for neuroprosthetic applications. Preliminary work in non-human primates has shown that this area can indeed be used for this purpose. In this thesis, we examine further the applications of this brain area for use in neural

prosthetics in both non-human primates and humans. In applying the neural signals located in the parietal lobe, we improve upon the technology as a whole while also learning more about how this part of the primate brain contributes to motor behavior.

In Chapter 2, we give an overview of the history of recording of neural activity at the single-unit level, the properties of parietal cortex, as well as an overview of neural prosthetics research to date. In Chapter 3, we present two studies of neural prosthetics carried out with a non-human primate subject. In the first, we examine the effect of eye movements on the ability of a prosthetic user to perform neural control of a cursor. Because some areas in parietal cortex are sensitive to gaze direction and movements of the eye, it is important to determine whether or not record from hand-related areas can be done without interference of eye-related signals. In the second study, we describe a paired decoder system, one state-based and one continuous, that reduces unwanted noise in a neurally controlled cursor and improves upon the state of the art.

In Chapter 4, we assess the sensitivity of neurons and local field potentials recorded from the superior parietal lobule of a tetraplegic human to different forms of visual feedback during observed and attempted motion of various types of movement effectors. We also examine if the degree of anthropomorphism of a movement effector affects decoding performance in one offline reaching task and one online gesture control task.

## 2. Background

Ever since the link between the brain and mind has been considered, generations of natural philosophers, scientists, and even pseudoscientists have been examining and investigating the workings of this organ. But, it was not until Luigi Galvani's experiments at end of the 18<sup>th</sup> century that the association between the nervous system and electricity was observed. Galvani determined that injecting current into the severed frog leg caused its muscles to contract (Piccolino 1997). With this, modern electrophysiology was born.

However, its infancy was long. Little was known about the brain during Galvani's time. Over the next century, biologists and anatomists steadily investigated the brain and its various structures at progressively smaller scales. In the late 1880s, Santiago Ramón y Cajal transformed neuroscience as a whole through detailed drawings and descriptions of what he deemed the functional units of the brain: the neuron. But scientists still lacked the technology to investigate such tiny structures and what their function might be.

The next leap in that direction was made by Edgar Adrian, a British electrophysiologist. On a lark, Adrian combined the valve amplifier and capillary electrometer to see how they might improve his recordings of the electrical activity of muscle fibers of the frog leg. While testing the newly assembled apparatus, Adrian initially mistook mysterious oscillations he observed in the electrical potential for noise corrupting his signal. He quickly realized that the noise he was recording was actually trains of action potentials traveling along the muscle fibers. We now know that action potentials are the basic unit of

communication between neurons in the periphery as well as in the brain. Adrian was the first to record them directly, albeit from muscle fibers.

Not long after, Adrian was able to make similar recordings from the optic nerve of the toad. During those experiments, Adrian played the electrical recordings of the nerve over a loudspeaker so that he could listen to the impulses while working with the preparation in a nearly dark room. Eventually, he noticed that the intensity of impulses played over the loudspeaker varied with his own movements around the room. He realized that he was in the field of view of the toad's eye, and that the rate of activity along the optic nerve was responding to his movement. This and related work garnered Adrian and his colleague Sir Charles Scott Sherrington the Nobel prize in Physiology or Medicine in 1932 (Hodgkin 1979).

Over the next half-century, engineering and medical techniques for recording electrophysiological signals gradually improved. Beginning in the late 1950s, Nobel laureates David H. Hubel and Torsten Wiesel described neurons in visual cortex of anaesthetized cats that responded sensitively to the presence of bright edges in the animal's field of view (Hubel and Wiesel 1959, 1962). This marked the cornerstone of research into the neural basis for vision that has continued since. But, these preparations required that the animals be partially sedated and stationary.

By the late 1960s, it was well established through lesion and stimulation of the precentral gyrus that this area was critically important for generating movements, garnering it the title “motor cortex” (Kandel 2013). However, it was not until that time that techniques were developed to record individual neurons in the cortices of awake, behaving animals such as the macaque monkey (Evarts 1968, 1966). Studies in this era observed the close relationship between direction of motion of an animal’s arm and the discharge rates of the neurons of its motor cortex.

## **2.1 Brain Machine Interfaces**

Nearly as soon as it was possible to record cortical neurons of awake, behaving primates, scientists began training these animals to volitionally control the output of their own cortical neurons (Fetz 1969). In a seminal work, Georgopoulos and colleagues (Georgopoulos et al. 1982) observed that motor cortical neurons fired preferentially for certain directions of motion of the arm and less so in the opposite direction with a gradual decline in discharge rate for directions in between the two extremes. They postulated that a so-called “population code” distributed across many of these types of neurons would allow downstream brain areas to “read out” or decode the intended motion of the animal by summing across many neurons with such tuning properties in a population. In theory, if enough electrodes could be inserted simultaneously, the intended motion could be accurately read out by a machine and used to manipulate an external device. This could allow individuals missing limbs or with paralysis to control prosthetic devices just by thinking. Around the same time, Schmidt and colleagues were testing the possibility of

implanting electrodes for long periods of time in order to record from such neurons and allow primates and eventually humans to manipulate external devices (Schmidt 1980).

By the late 1990s, the improvements in neural recording technology and computer hardware made this possible. Arrays of 16 or more electrodes could now be implanted chronically in the mammalian brain. Computers were fast and cheap enough to allow detection, analysis, decoding, and transmission of neural control signals in real-time. Though it was not known for certain how many individual neurons would need to be recorded simultaneously to allow useful decoding, Nicolelis and colleagues demonstrated this capability in several landmark studies using only a few dozen: first in the rat (Chapin et al. 1999) and shortly thereafter in non-human primates (Wessberg et al. 2000). These studies involved so-called “open-loop” control, wherein the animal generating the neural signals did not get direct feedback about the prosthetic device being manipulated. Shortly thereafter, 3D “closed-loop” control was achieved in primates where in the animals received real-time visual feedback regarding the effector being controlled via neural signals (Taylor, Tillery, and Schwartz 2002).

Not long after, clinical trials were carried out to attempt these same experiments with paralyzed human subjects. In 2006, the first successful pilot study demonstrated useful neural control of a computer cursor and a simple robot limb by a tetraplegic human subject (Hochberg et al. 2006). The subject was implanted with a 96 channel electrode array in the arm area of the primary motor cortex. He was able to successfully manipulate the cursor

even when recording or distracted by other stimuli. Rapid improvements followed. By 2013, another human subject was able to manipulate a sophisticated robot arm with 17 degrees of freedom to feed herself and even shake hands with others (Collinger et al. 2013).

However, many challenges remain. The recording technology used in the human clinical trials and in this thesis only maintains the ability to record action potentials for 6 months to a few years. It requires connecting hardware that must permanently break the skin, providing a potential root for infection. Furthermore, the number of neurons recorded on a single array is still low enough that the loss of only a few can lead to significant degradation of decoding capabilities. And, slight disruptions can significantly impact recording quality on the arrays as a whole. Though these challenges are significant, further improvements in recording and implantation technologies could eventually lead to practical and transformative prosthetic technologies.

## **2.2 Parietal Cortex**

In the 1970s, just as studies in motor cortex and other areas of awake, behaving primates were becoming more and more numerous, another lobe of the primate brain was investigated intently by Vernon Mountcastle and colleagues. Building on single-unit and lesion studies in the primate (Desiraju 1972, Hartje and Ettlinger 1973, Hyvarinen and Poranen 1974, Sakata et al. 1973) and lesion studies in humans (Hecaen et al. 1956), they hypothesized that the parietal cortex subserves coordination of movements of the body in space, specifically of the limbs, hands, and eyes. They also noted that this function centers

on behavioral goals and not “the details of muscular contraction during execution”, which could be processed by downstream motor areas. Parietal regions receive “signals that describe the position and movement of the body in space”, making it ideally situated between sensory and motor areas to carry out the hypothesized function (Mountcastle et al. 1975).

In the years that followed, numerous other groups investigated the parietal lobe. Kalaska and colleagues echoed many of these observations of primate PPC and Brodmann’s area 5 in particular (Kalaska, Caminiti, and Georgopoulos 1983, Scott, Sergio, and Kalaska 1997), noting that area 5 neurons had similar properties to motor cortical neurons. But, area 5 neurons were less sensitive to movement properties like dynamics but retained tuning to kinematics (Cohen et al. 1990).

Further studies by Richard Andersen and colleagues suggested that the PPC represents movement plans and intentions (Andersen and Cui 2009, Cui and Andersen 2007, 2011, Snyder, Batista, and Andersen 1997, Quiñero et al. 2006). They hypothesized that PPC’s unique properties would also make it an effective substrate for closed-loop, real-time neural prosthetic devices (Musallam et al. 2004, Pesaran, Musallam, and Andersen 2006), and demonstrated this in primate studies (Hauschild et al. 2012, Mulliken, Musallam, and Andersen 2008a) as well as the first clinical trial with human subjects based on parietal cortex (Aflalo et al. in press).

Additionally, the parietal cortex was found to contain behavior and decision-related information encoded in the local field potential. This signal is the “background” electrical oscillations recorded by an extracellular electrode, filtering out the action potentials caused by neurons close to the electrode tip. This signal is thought to reflect the averaged extracellular currents of entire populations of neurons surrounding the electrode tip (Mitzdorf 1985). In 2002, Pesaran and colleagues (Pesaran et al. 2002) found that the gamma band (60-100Hz) of the local field potential of the Lateral Intraparietal Area encoded spatial information about upcoming saccades, at times exceeding the information content of even the simultaneously recorded action potentials. Additionally, the beta band (typically around 15-30Hz) of the local field potential (LFP) has been actively studied for its role in motor behavior and movement planning (Engel and Fries 2010). The LFP, being easier to record and more stable, has offered a potential alternative to action potentials for applications in neural prosthetics.

## 2.3 References

- Aflalo, T. N. S., R. A. Andersen, S. Kellis, and C. Klaes. in press. "Decoding Motor Imagery from the Posterior Parietal Cortex of a Tetraplegic Human." *Science*.
- Andersen, Richard A., and He Cui. 2009. "Intention, Action Planning, and Decision Making in Parietal-Frontal Circuits." *Neuron* 63 (5):568--583.
- Chapin, J. K., K. A. Moxon, R. S. Markowitz, and M. A. Nicolelis. 1999. "Real-time control of a robot arm using simultaneously recorded neurons in the motor cortex." *Nat Neurosci* 2 (7):664-70. doi: 10.1038/10223.
- Cohen, M., Kalaska Jf, Prud'homme M, and Hyde Ml. 1990. "Parietal area 5 neuronal activity encodes movement kinematics, not movement dynamics." *Experimental Brain*.
- Collinger, J. L., B. Wodlinger, J. E. Downey, W. Wang, E. C. Tyler-Kabara, D. J. Weber, A. J. McMorland, M. Velliste, M. L. Boninger, and A. B. Schwartz. 2013. "High-performance neuroprosthetic control by an individual with tetraplegia." *Lancet* 381 (9866):557-64. doi: 10.1016/S0140-6736(12)61816-9.
- Cui, H., and R. A. Andersen. 2007. "Posterior parietal cortex encodes autonomously selected motor plans." *Neuron* 56 (3):552-9. doi: 10.1016/j.neuron.2007.09.031.
- Cui, H., and R. A. Andersen. 2011. "Different representations of potential and selected motor plans by distinct parietal areas." *J Neurosci* 31 (49):18130-6. doi: 10.1523/JNEUROSCI.6247-10.2011.
- Desiraju, T. 1972. "Discharge properties of neurons of the parietal association cortex during states of sleep and wakefulness in the monkey." *Brain Res* 47 (1):69-75.
- Engel, A. K., and P. Fries. 2010. "Beta-band oscillations -- signalling the status quo?" *Current opinion in neurobiology*.
- Evarts, E. V. 1966. "Pyramidal tract activity associated with a conditioned hand movement in the monkey." *J Neurophysiol* 29 (6):1011-27.
- Evarts, E. V. 1968. "A technique for recording activity of subcortical neurons in moving animals." *Electroencephalogr Clin Neurophysiol* 24 (1):83-6.
- Fetz, E. E. 1969. "Operant conditioning of cortical unit activity." *Science* 163 (3870):955-8.
- Georgopoulos, A. P., J. F. Kalaska, R. Caminiti, and J. T. Massey. 1982. "On the relations between the direction of two-dimensional arm movements and cell discharge in primate motor cortex." *J Neurosci* 2 (11):1527-37.
- Hartje, W., and G. Ettlinger. 1973. "Reaching in light and dark after unilateral posterior parietal ablations in the monkey." *Cortex* 9 (4):346-54.
- Hauschild, M., G. H. Mulliken, I. Fineman, G. E. Loeb, and R. A. Andersen. 2012. "Cognitive signals for brain-machine interfaces in posterior parietal cortex include continuous 3D trajectory commands." *Proc Natl Acad Sci U S A* 109 (42):17075-80. doi: 10.1073/pnas.1215092109.

- Hecaen, H., W. Penfield, C. Bertrand, and R. Malmö. 1956. "The syndrome of apractognosia due to lesions of the minor cerebral hemisphere." *AMA Arch Neurol Psychiatry* 75 (4):400-34.
- Hochberg, Leigh R., Mijail D. Serruya, Gerhard M. Friehs, Jon A. Mukand, Maryam Saleh, Abraham H. Caplan, Almut Branner, David Chen, Richard D. Penn, and John P. Donoghue. 2006. "Neuronal ensemble control of prosthetic devices by a human with tetraplegia." *Nature* 442 (7099):164--171.
- Hodgkin, A. 1979. "Edgar Douglas Adrian, Baron Adrian of Cambridge, 30 November 1889 - 4 August 1977." *Biogr Mem Fellows R Soc* 25:1-73.
- Hubel, D. H., and T. N. Wiesel. 1959. "Receptive fields of single neurones in the cat's striate cortex." *J Physiol* 148:574-91.
- Hubel, D. H., and T. N. Wiesel. 1962. "Receptive fields, binocular interaction and functional architecture in the cat's visual cortex." *J Physiol* 160:106-54.
- Hyvarinen, J., and A. Poranen. 1974. "Function of the parietal associative area 7 as revealed from cellular discharges in alert monkeys." *Brain* 97 (4):673-92.
- Kalaska, J. F., R. Caminiti, and A. P. Georgopoulos. 1983. "Cortical mechanisms related to the direction of two-dimensional arm movements: relations in parietal area 5 and comparison with motor cortex." *Exp Brain Res* 51 (2):247-60.
- Kandel, Eric R. 2013. *Principles of neural science*. 5th ed. New York: McGraw-Hill.
- Mitzdorf, U. 1985. "Current source-density method and application in cat cerebral cortex: investigation of evoked potentials and EEG phenomena." *Physiol Rev* 65 (1):37-100.
- Mountcastle, V.B., J. C. Lynch, A. Georgopoulos, H. Sakata, and C. Acuna. 1975. "Posterior parietal association cortex of the monkey: command functions for operations within extrapersonal space." *Journal of Neurophysiology* 38 (4):871-908.
- Mulliken, G. H., S. Musallam, and R. A. Andersen. 2008a. "Decoding Trajectories from Posterior Parietal Cortex Ensembles." *Journal of Neuroscience* 28 (48):12913--12926.
- Musallam, S., B. D. Corneil, B. Greger, H. Scherberger, and R. A. Andersen. 2004. "Cognitive control signals for neural prosthetics." *Science* 305 (5681):258-62. doi: 10.1126/science.1097938.
- Pesaran, B., S. Musallam, and R. A. Andersen. 2006. "Cognitive neural prosthetics." *Curr Biol* 16 (3):R77-80. doi: 10.1016/j.cub.2006.01.043.
- Pesaran, B., J. S. Pezaris, M. Sahani, and P. P. Mitra. 2002. "Temporal structure in neuronal activity during working memory in macaque parietal cortex." *Nature* \dots
- Piccolino, M. 1997. "Luigi Galvani and animal electricity: two centuries after the foundation of electrophysiology." *Trends Neurosci* 20 (10):443-8.
- Quiñ Quiroga, R., L. H. Snyder, A. P. Batista, H. Cui, and R. A. Andersen. 2006. "Movement intention is better predicted than attention in the posterior parietal cortex." *J Neurosci* 26 (13):3615-20. doi: 10.1523/JNEUROSCI.3468-05.2006.
- Sakata, H., Y. Takaoka, A. Kawarasaki, and H. Shibutani. 1973. "Somatosensory properties of neurons in the superior parietal cortex (area 5) of the rhesus monkey." *Brain Research*.

- Schmidt, E. M. 1980. "Single neuron recording from motor cortex as a possible source of signals for control of external devices." *Ann Biomed Eng* 8 (4-6):339-49.
- Scott, S. H., Sergio, and J. F. Kalaska. 1997. "Reaching movements with similar hand paths but different arm orientations. II. Activity of individual cells in dorsal premotor cortex and parietal area 5." *Journal of Neurophysiology*.
- Snyder, L. H., A. P. Batista, and R. A. Andersen. 1997. "Coding of intention in the posterior parietal cortex." *Nature* 386 (6621):167-70. doi: 10.1038/386167a0.
- Taylor, D. M., S. I. Tillery, and A. B. Schwartz. 2002. "Direct cortical control of 3D neuroprosthetic devices." *Science* 296 (5574):1829-32. doi: 10.1126/science.1070291.
- Wessberg, J., C. R. Stambaugh, J. D. Kralik, P. D. Beck, M. Laubach, J. K. Chapin, J. Kim, S. J. Biggs, M. A. Srinivasan, and M. A. Nicolelis. 2000. "Real-time prediction of hand trajectory by ensembles of cortical neurons in primates." *Nature* 408 (6810):361-5. doi: 10.1038/35042582.

### **3. Non-Human Primate Parietal Cortex and Neural Prosthetics**

#### **3.1 Parietal Neural Prosthetic Control of a Computer Cursor in a Graphical-User-Interface Task**

Note: Section 3.1 is adapted from Revechkis et al., 2014, under the Creative Commons License (CC BY 3.0). Minor modifications have been to the text to correct typographical errors in the published text. Figure locations, formatting, references, and captions have been modified to accommodate this thesis.

##### **3.1.1 Introduction**

Neural prosthetics hold great promise for allowing disabled individuals to regain agency over their environment by directly manipulating robotic limbs or computer interfaces. When tested in the laboratory, computer or motor-based interfaces tend to only involve series of individual targets (Collinger et al., 2013, Velliste et al., 2008, Gilja et al., 2012, Hauschild et al., 2012). When multiple targets have been used, the effects of the greater task complexity themselves were not evaluated (Ifft et al., 2013, O’Doherty et al., 2011) or the cognitive component of the tasks have been minor (Hochberg et al., 2006, Shanechi et al., 2012), limiting clinical usefulness. These studies do not replicate the function of a modern graphical user interface (GUI), i.e., selecting a remembered or desired target from a group of alternatives. Such function would be clinically relevant and useful to patients with motor deficits.

To this end, we designed a task for non-human primates (NHPs) that incorporated these behavioral elements and assessed its effect on an interface driven by neural activity in the PPC. The “Face in a Crowd” task required selecting a single, icon-like stimulus, the “face”, from a group, the “crowd”. The correct target was indicated by an initial sample face stimulus. The targets were refined so as to naturally require a visual search of several saccades to locate the matching stimulus without imposing any artificial constraints on eye movements, i.e., during free gaze. After visually locating the matching target, it was selected by manipulating a manually or neurally controlled computer cursor. This task created a NHP analog to human use of a GUI. In the “Crowd Off” task condition, no Crowd appeared, reducing behavior to a traditional center-out task.

Increasing task complexity from one to many possible targets may seem like a simple change, but the associated cognitive and behavioral requirements are not: more eye movements to and between visual stimuli, more complex decision making, and greater demands on working memory and attention. Prosthetics driven by neural activity in motor cortex may be influenced by these variables, as motor (Rao and Donoghue, 2014) and premotor areas (Pesaran et al., 2008) exhibit strong transients to the onset of visual stimuli. Posterior parietal cortex (PPC), which has also been used to drive cortical prosthetics (Musallam et al., 2004, Mulliken et al. 2008, Hauschild et al., 2012, Ifft et al., 2013) in NHPs, is well known to be sensitive to many of these behavioral variables (Buneo & Andersen, 2006, Colby and Goldberg, 1999, Louie et al., 2011, Pesaran et al., 2010). It is

therefore relevant to determine if these added task demands and their neural correlates interfere with the signals upon which a useful neural prosthetic would depend.

Area 5d, a subregion of PPC, was chosen as the substrate for Brain Control due to its selectivity for arm kinematics (Bremner and Andersen, 2012, Crammond and Kalaska, 1989, Cui and Andersen, 2011, Graziano et al., 2000). Neural decoders were repeatedly trained to transform neural activity from this region into cursor commands during both the Crowd On and Crowd Off task conditions to determine whether the Crowd's presence during training or thereafter adversely affected decoding performance.

Some of the behavioral variables mentioned above, e.g., attention and working memory, are difficult to measure directly. Eye movements are closely related to them (Soto et al., 2005) and much more readily recorded. Therefore, we examined eye movements during the various phases of the Face in a Crowd task as well as during a saccade-only task to a) assess the degree of eye tuning in the recorded population of neurons, b) ensure the Face in a Crowd task required a visual search, and c) examine whether task performance under Brain Control was impaired as a result. Furthermore, we sought to determine if cursor movement under Brain Control could be dissociated from eye movements as during natural hand eye coordination.

### **3.1.2 Methods**

A male rhesus monkey participated in this study. All procedures were approved by the California Institute of Technology Institutional Animal Care and Use Committee and were performed in accordance with NIH guidelines.

### **3.1.2.1 Behavioral Setup**

The monkey was seated in a chair and viewed all visual stimuli on a vertical LCD monitor placed about 40 cm from the eyes. The NHP's head was held in place by a surgically implanted headpost. When Brain Control was performed, both arms were gently restrained to prevent large arm movements. Eye position was recorded using the ISCAN system (ISCAN Inc., Woburn, MA). Hand position was tracked at 120 Hz with a magnetic 6 degree of freedom trakStar sensor (Ascension Technology Corporation, Milton, VT) affixed to the hand. View of the hand was blocked by an opaque plate placed at neck height. Stimulus presentation was performed with the PsychoPy psychophysics library for Python (Peirce, 2007). Task control and recordings were performed with the Simulink real-time system (The MathWorks Inc., Boston, MA).

### **3.1.2.2 Neural Recordings**

The monkey was implanted with two 96-channel electrode Cereport arrays (Blackrock Microsystems, Salt Lake City, UT) on the convexity of the superior parietal lobule near the posterior half of the IPS, i.e., the approximate location of neurons functionally ascribed to Area 5d in previous studies (Bremner and Andersen, 2012, Cui and Andersen, 2011). The Cereport (formerly known as the "Utah" array) has been commonly used in human

neuroprosthetic studies and was thus used in the present study to more closely mimic clinical techniques for recording extracellular potentials (Rothschild 2010). Neural activity was amplified, digitized, and recorded with the Cerebus neural signal processor. In the Central software suite (Blackrock Microsystems), thresholds for action potential detection for each channel were set at -4.5 times the root-mean-square of the raw signal sampled over a 1 second window on a daily basis. In real-time, the time of threshold crossings were transmitted to MATLAB software (The MathWorks Inc., Boston, MA) and counted in non-overlapping, 50ms time bins. No spike sorting was used, as spike sorting itself presents a significant difficulty to maintain from day to day in human trials (Franke et al., 2012), and has been reported to confer little benefit upon BMI performance (Fraser et al., 2009). From the two arrays combined, approximately 105 active channels were reliably recorded with spiking activity of some kind as judged by the experimenter. Active channels that met the simple criterion of firing at an average rate of 1 crossing per second during the Training block were used in online decoding. This resulted in  $85 \pm 2$  channels being used for decoding each day.

### 3.1.2.3 Behavioral Task

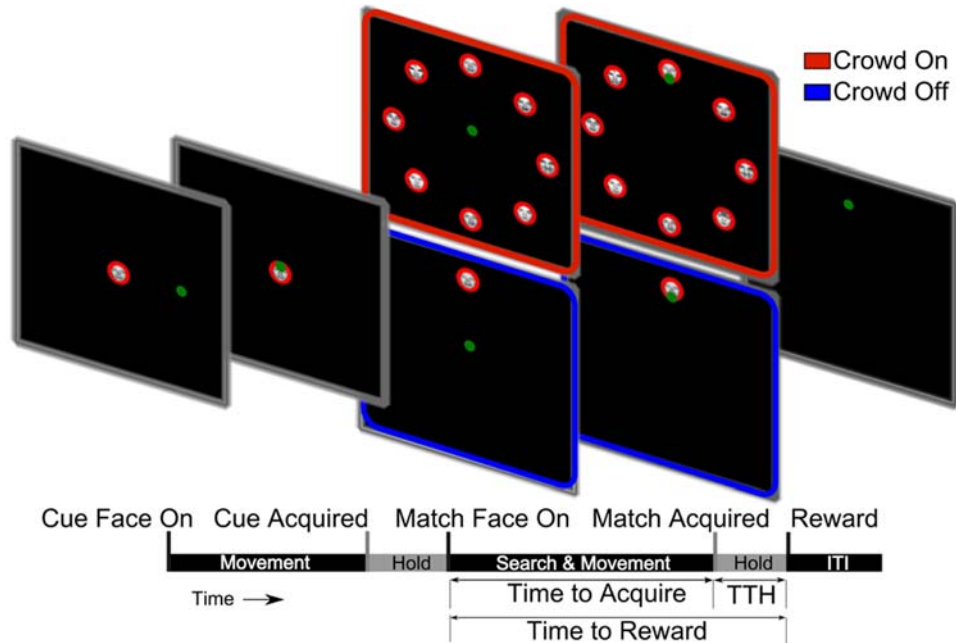


**Figure 3.1.2.3-1 Face in the Crowd Task Trial Structure** The timeline pictured schematizes the phases of the task and associated events. The start of each phase of the task is marked with a tick, labeled, and pictured above with a screenshot of the task display. The behavioral measures used and their corresponding temporal extents are also indicated below the timeline. Target 1 is the Cue Face, and Target 2 is the Match Face. In the Crowd On Condition, Target 2 is accompanied by 7 other faces of different individuals. In Crowd Off, it appears alone. The green dot represents the cursor.

A green cursor of radius 0.7cm was continuously presented on the screen. The cursor was controlled either by the monkey's hand moving in the horizontal plane above a flat, table-top surface immediately in front of his body (Manual Control mode), or by the output of a neural decoder (Brain Control mode) with hands gently restrained on the table surface in a relaxed position with elbows bent at approximately 90 degrees.

The purpose of the task was to create an animal paradigm that mimics human use of a GUI. The Crowd task naturally required a period of visual search for a cued stimulus via repeated saccades followed by a cursor movement to, and selection of, the chosen target. We chose

visual stimuli/targets consisting of images of various human faces taken from the Psychological Image Collection at Stirling (PICS) database (<http://pics.stir.ac.uk>). Face targets consisted of a photographic head-on image of one of 3 facial expressions of 12 individuals. One individual was chosen for use as the “goal” face or individual for the current study. All faces were normalized for size with a red surrounding mask that obscured the overall shape of the head and hair. The faces were also normalized for total brightness. These manipulations made the stimuli subtle enough in their differences that they required fixation for correct identification of the goal individual. The goal individual’s expression varied from trial to trial but not within a trial. The outer diameter of all the face stimuli, red mask included, was 3 cm. Acceptance windows for all targets and the cursor were identical in size to their respective visual representations.

A trial began when a sample face cue (Target 1) of the goal individual appeared at the center of the screen (**Figure 3.1.2.3-1**). The subject moved the cursor to overlap the cue for a contiguous Hold Period of 400ms. If overlap was broken during the Hold Period before 400ms elapsed, an entire new 400ms Hold Period would need to be performed. This rule was applied for all Hold Periods in the task. For the Crowd On condition, after the Hold Period, Target 1 disappeared, and a “crowd” of face stimuli of 8 individuals appeared. One of the 8 faces in the crowd (Target 2) was an identical match to the initial cue face, Target 1. Each face in the crowd was situated on a circle of radius 9cm centered on the middle of the screen and separated by 45 degrees on the circle (**Figure 3.1.2.3-1**). The monkey then had 20 seconds to locate the matching face and move the cursor to overlap it

for another Hold Period of 400ms. After this second Hold Period, a juice reward was delivered via a tube placed in front of the monkey's mouth. Simultaneously, all targets disappeared and a reward beep was sounded. A new trial began after an inter-trial interval (ITI) of 0.5s. Failure to locate, select, and Hold Target 2 within the 20s period resulted in termination of the trial: the disappearance of all targets, an auditory cue signifying trial failure, and a penalty ITI of 5-10s. Overlap with an incorrect target for 400ms or more also resulted in termination of the trial. An overlap of less than 400ms with an incorrect Target in the Crowd was permitted. The cursor was continuously controlled during the trials and ITI. In the "No Crowd" task condition, Target 2 appeared somewhere on the same circle described above, but with no other face stimuli present (**Figure 3.1.2.3-1**).

#### **3.1.2.4 Performance Measures**

Task performance was assessed by the fraction of trials successfully completed and by measuring the time required to perform the various stages of the task (**Figure 3.1.2.3-1**). Time to Acquire, or TTA, spanned the time between Target 2 Onset (with or without the Crowd) and initial contact with Target 2. This period included the time required to visually locate the matching face whether the Crowd was present or not. The time from initial Acquisition of Target 2 to Reward, or Time to Hold (TTH), measured how long the subject took to "settle" the cursor down on the Target. Time to Hold could be no shorter than 400ms, but could be longer if overlap of the cursor and Target 2 was broken and reestablished before completing the trial. Time to Reward, or TTR, captured the time from Target 2 Onset to Reward and so would be the sum of TTA and TTH for a given trial.

In order to assess the effect of Brain Control on cursor control without the influence of task difficulty, we calculated the change in Time to Acquire, or  $\Delta TTA$ , by subtracting average daily TTA in Manual Control from each subsequent Brain Control trial TTA, i.e.,

$$\Delta TTA_k^{BC} = TTA_k^{BC} - \overline{TTA^{MC}} \quad (1)$$

where superscripts *MC* or *BC* indicate Manual Control or Brain Control and *k* indicates Brain Control trial *k*. The average TTA in Manual Control,  $\overline{TTA^{MC}}$ , was computed per day and per task condition (Crowd On or Off) and was only subtracted from Brain Control trials with the corresponding task condition on the same day. This calculation isolated the difference in TTA that was attributable solely to the use of Brain Control rather than Manual Control by eliminating time consumed by other aspects of the task, e.g., searching for and reacting to the presence of the correct target. This calculation thereby gave a direct indication of the effectiveness of Brain Control of the cursor independent of the influence of other, task-related factors. This measure was then examined as a function of Assessment condition and Training condition (described below) in subsequent analyses.

*P* values reported are the result of a non-parametric, two-sample Kolmogorov-Smirnov test for differences in distributions. Where reported, inter-quartile range (IQR) was computed by taking the difference between the third quartile (Q3) and the first quartile (Q1) of the data. Reported R-squared values were computed by taking the square of the Pearson's correlation coefficient (R) between the variables specified.

### **3.1.2.5 Decoder Training**

Each day began with the monkey performing 160 trials of both the Crowd and No Crowd task conditions alternating every 20 trials under Manual Control. This allowed assessment of daily variation in basic task performance without the influence of Brain Control quality. Next, the monkey's hands were gently restrained.

A previously computed neural decoder, a Training Decoder, was used by the NHP to manipulate the cursor during an initial 250s Training Block in either the Crowd On or Crowd Off condition. The Training Decoder and computer assistance functioned like a set of training wheels on a bicycle, allowing the NHP to use neural activity to drive the cursor, though not fully independently.

The Training Decoder was computed in a previous behavioral session using the same methods described here. The task used during training of the Training Decoder was the Crowd Off task condition of the Face in a Crowd task. We attempted to use the same Training Decoder for every Training Block in the current study in order to keep initial conditions for each Training Block as similar as possible; however, after one to four days, Training Decoders stopped generating useful output even with substantial assistance during the Training. When that occurred, the most recently computed decoder (trained with the Crowd Off) was substituted in as a Training Decoder. The dataset for the current study spanned 7 days and 23 decoders. The decoders trained in the first 4 days all used the same

Training Decoder during training. The next Training Decoder was used for 2 days, and the third for one day. All analyses described below were repeated on a restricted data set using only decoders trained with the first Training Decoder (days 1-4). The results of those analyses did not differ substantially from the results described below.

Furthermore, using a Training Decoder (itself trained on the Crowd Off task condition) to compute a new decoder with the Crowd On task condition could be considered a sort of worst-case scenario in which the task type changes from one training block to the next. We reasoned that if we find no impairment of decoding function caused by the “switch” to the Crowd On condition, there is no reason to expect an impairment would arise if the two tasks were fully segregated with respect to training and assessment. It would be feasible that it might provide an advantage, but our main goal in the study was to examine whether or not these task contexts reduced decode performance.

During the Training Block, output of the Training Decoder was assisted by removing some fraction of the error in cursor movement in each time bin. Error was defined as the component of the instantaneous movement vector that did not point directly at the Target. When no target was present on the screen, any movement of the cursor was considered error. Typically, the assistance level was adjusted such that 30% of the error was removed in each time bin. During Training, the ITI was set to 0s. The neural activity and cursor kinematics during the Training Block were subsequently used as input to compute a new decoder.

When computing the new decoder after performing the Training Block, the noisy velocities of the cursor during the Training Block were reoriented to point towards the instantaneous goal to more accurately capture the assumed intentions of the subject (Gilja et al., 2012). For each time bin, the intention of the NHP was assumed to be either move the cursor towards the current correct face target or hold the cursor steady if the cursor already overlapped the correct target. Reaction times were accounted for by assuming an intention to hold the cursor steady until 200ms after Target 2 onset in the No Crowd condition and after initial cue onset and 400ms after onset of Target 2 and the other targets in the Crowd condition. These values were chosen based on average reaction times during Manual Control.

Once the new decoder was computed, it was then used for Brain Control by the NHP without assistance to perform the task in both Crowd On and Off conditions in 10 alternating blocks of 20 trials, yielding a total of 200 Assessment trials per decoder. This process of Training and Assessment of performance was repeated so that the effect on performance of the Crowd (during Training and/or Decoding) could be measured. Twenty-three decoders were trained and assessed across seven days. The task condition of the first Training Block on a given day was alternated to remove any order effects.

### **3.1.2.6 Decoder Calculation**

For transforming neural activity into cursor position and velocity, we used a linear decoding model coupled with a linear state space model of the cursor dynamics. (For further detail, see Section [3.2.2.7](#)). The final decoder form closely resembled that described by Gilja and colleagues (Gilja et al., 2012).

### **3.1.2.7 Saccade Task**

To assess the correlation between eye kinematics and neural activity, the monkey was trained to perform a task in which a trial consisted of repeated fixation on a series of 4 yellow circular targets placed on a 2 by 2 equally spaced grid measuring 14cm square. After fixating a target for the required period of 500ms, the target would turn from yellow to grey. After successfully fixating on all 4 targets in any sequence, the targets would all disappear and juice reward would be delivered. An ITI of 0.5s followed. The position of the hand (which was not required to perform the task) was recorded along with neural signals during this task, though the hand rarely moved.

Two days, each consisting of approximately 1500 trials, were recorded. R-squared values between a) linear predictions of eye kinematics based on neuronal firing with b) actual eye kinematics were computed and validated using Leave One Out Cross-Validation (LOOCV) on 20 equally sized segments of the data.

Additionally, segments of neural data were used to decode the spatial locations of the endpoints of saccades during this task. Saccades that began on one of the four targets and

ended on any of the other 3 targets were preselected from the data. Each saccade was labeled by the target at which the saccade ended. Observations were comprised of total number of spikes summed for each neural channel across a window beginning 0.150s before a saccade onset and 0.300s after. Linear discriminant analysis was used to classify the neural data into one of four possible targets/categories. LOOCV was used to obtain a measure of the performance of neural classification of saccade targets, whereby all observations save one were used as training data. The class of the “left out” trial was then predicted using the classifier. This was repeated using each available trial as the excluded trial. Performance was computed as the percentage of “left out” trials that were correctly classified. A permutation test, whereby target labels were randomly shuffled and LOOCV repeated, was used to generate a null distribution of performance in order to assess whether classification of the actual data exceeded chance levels ( $n = 10^3$  permutations).

### **3.1.3 Results**

#### **3.1.3.1 Saccade Task**

Ideally, the neurons recorded would not at all be sensitive to eye movements. However, Area 5d neurons show some eye position tuning (Bremner and Andersen, 2012). To quantify the degree of eye position tuning in the population recorded for the current study, we recorded neural activity while the NHP performed a task involving saccades only. Cross-validated R-squared values between neural activity and eye movements were computed. Though highly significant for x and y position, ( $p_x = 1.5e^{-4}$  and  $p_y = 6.4e^{-3}$ )

R-squared values of 0.05 and 0.02, respectively, were obtained, indicating a measurable but small relationship with eye position. P values were not significant ( $\gg 0.05$ ) for eye velocity.

When trying to decode the goal of individual saccades from amongst the 4 possible targets in the saccade task based only on neural data, 41.54% correctness was achieved for  $n = 674$  saccades. Though modest, this performance significantly exceeded chance level of 25% ( $p < 10^{-5}$ , permutation test.) Thus, the neural activity correlated with saccades could not account for the 98% success rate achieved with the neural cursor during the Face in the Crowd task.

### 3.1.3.2 Behavioral Task – Manual Control

During the Manual Control block of each day, the monkey was able to successfully complete  $> 99\%$  of the trials correctly, i.e.,

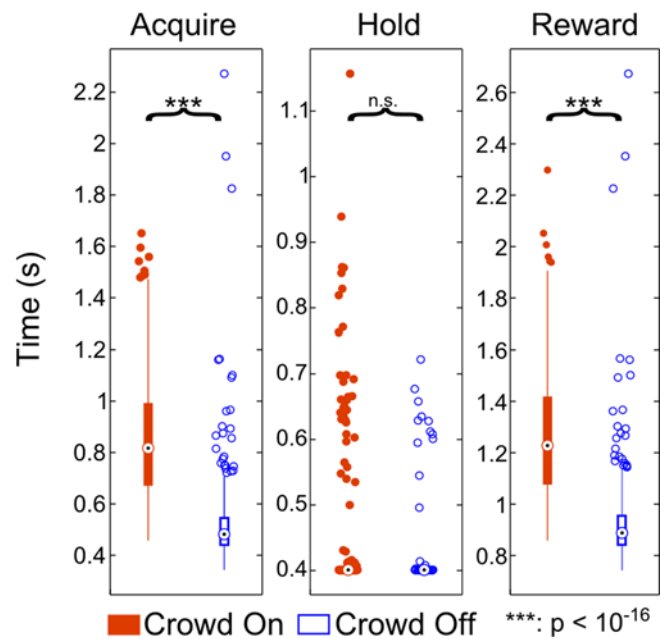


**Figure 3.1.3.1-1 Manual Control Performance** Boxplots of performance measures during Manual Control in Crowd On ( $n = 567$  trials) and Crowd Off ( $n = 560$  trials) task conditions. Wide, middle band represents the middle two quartiles. Thinner bands on top and bottom represent the top and bottom quartiles, respectively. Circles with dots indicate medians. Outliers are small circles jittered in the horizontal axis for visibility. Filled (Crowd On) or empty (Crowd Off) bands and circles indicate the Crowd On or Crowd Off task condition. Values exceeding  $(Q3 + 1.5 \times (Q3 - Q1))$  are considered outliers, where  $Q1$  and  $Q3$  are the 25th and 75th percentiles, respectively. The Crowd On condition resulted in an increase in Acquisition and Reward time relative to the Crowd Off condition. Time to Hold was not significantly affected, as the vast majority of the Hold Times in both conditions were the minimum possible value of 400ms.

selecting the correct face before time ran out. This performance indicated that the animal had no difficulty in reliably finding the matching Face in the Crowd. Basic task performance statistics under Manual Control for all days (Crowd On n= 567 trials, Crowd Off n = 560 trials) revealed the desired effect (**Figure 3.1.3.2-1**). As expected, the presence of the Crowd significantly increased TTA (Crowd On Median = 0.82, IQR = 0.32, Crowd Off Median = 0.48, IQR = 0.11,  $p < 10e^{-16}$ ) and TTR (Crowd On Median = 1.23, IQR = 0.34, Crowd Off Median = 0.89, IQR = 0.12,  $p < 10e^{-16}$ ), but not TTH (Crowd On Median = 0.40, IQR =  $1.4e^{-14}$ , Crowd Off Median = 0.40, IQR =  $2.8e^{-14}$ ,  $p = 0.08$ ). This is because the Crowd causes a visual search which delays Acquisition time, but not the time required to Hold the target once it has been initially contacted. The delay in Acquisition time of course results in slower overall task performance as measured by TTR.

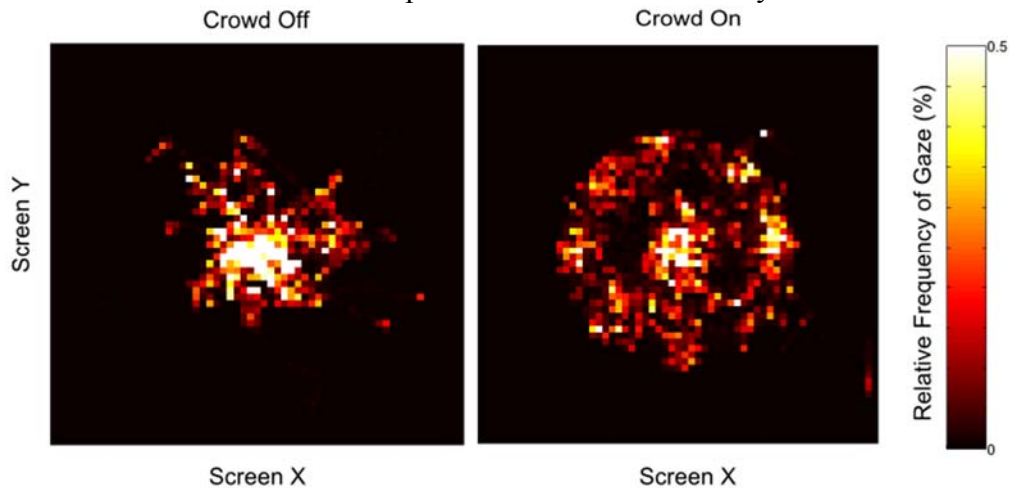


**Figure 3.1.3.2-1 Effect of the Crowd on Gaze During Manual Control** Heat maps of eye position during Manual Control averaged across n = 80 trials in each panel. Data was taken between onset of Target 2 and movement onset of the Hand. Data for each trial was rotated such that the location of Target 2 falls on the 3 o'clock position. (During task performance, Target 2 appeared in any one of the 8 possible positions.) The data demonstrated the NHP's tendency to gaze around the screen before moving the cursor when the Crowd was On. When the Crowd Was off, the NHP was able to initiate his hand movement to the target even before making a saccade to it. This explains why the left panel does not capture the position of the target at the 3 o'clock position.

To verify that TTA was increased because the Crowd required the animal to search and identify the target face, we examined eye behavior prior to movement onset and between movement onset and target acquisition for each day. Eye positions for each trial were rotated to place Target 2 at the 3 o'clock position. Two-dimensional histograms of eye position for each task condition clearly reveal the monkey's tendency to visually search through the faces in the Crowd On task condition before initiating his hand movement (**Figure 3.1.3.2-1**). Histograms for the period between Movement Onset and Target 2 acquisition looked similar, indicating that the monkey continued scanning the faces even during and after movement to select the correct target (**Figure 3.1.3.2-2**, left panel).

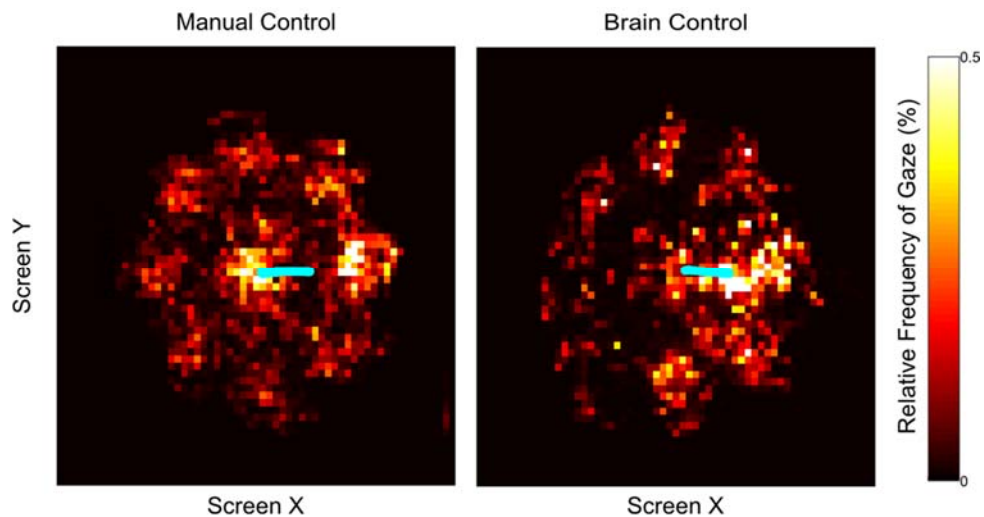


**Figure 3.1.3.2-2 Gaze with Crowd on during Manual vs Brain Control.** Heat maps of eye position as in **Figure 3.1.3.2-1** averaged across  $n = 160$  trials and  $n = 100$  in left and right panels, respectively. Data was again rotated for each trial to place the correct target at the 3 o'clock position. Here, data was taken during a 1 second window ending on Target Acquisition, guaranteeing that the cursor was in motion. We compared this epoch between Manual and Brain Control to confirm that the NHP was able to freely gaze at the targets even while maintaining straight cursor motion. For Brain Control, the trials with the straightest cursor trajectories were preselected by only analyzing the fastest 15% of trials. Average cursor trajectory during the same period for each control type is superimposed on the images in cyan. Video 2 also demonstrates dissociation of neural cursor movement from eye movements.

### 3.1.3.3 Behavioral Task – Brain Control

During the Brain Control sessions, the monkey was able to successfully complete > 98% of the trials correctly, i.e., selecting the correct face before time ran out (Video 3.1-1). The fraction of trials that were completed successfully did not significantly differ between Manual and Brain Control blocks ( $p = 0.75$ ).

Each decoder was trained during a Training Block either with the Crowd On or Crowd Off and then assessed for performance with the Crowd On or Off. This comprised a 2 x 2 factorial design with the “main effects” being Training Condition and Assessment Condition.

The task condition in which the decoders were trained, the Training Condition, did not significantly influence the TTA achieved (Crowd On Median = 1.65, IQR = 1.00,  $n = 1508$  trials, Crowd Off Median = 1.69, IQR = 1.05,  $p = 0.22$ ,  $n = 1871$  trials, **Figure 3.1.3.3-1**, left panel). We also examined whether or not the task condition used during Training of a decoder had any systematic effect on the  $\beta$  weights for any channel or dimension ( $x$  or  $y$  velocity). After using the Bonferroni method to correct for multiple comparisons, there were no significant differences in the decoder weights among all channel/dimension combinations as a function of task condition. Thus, the task condition used during Training did not seem to affect subsequent performance or the decoders themselves.

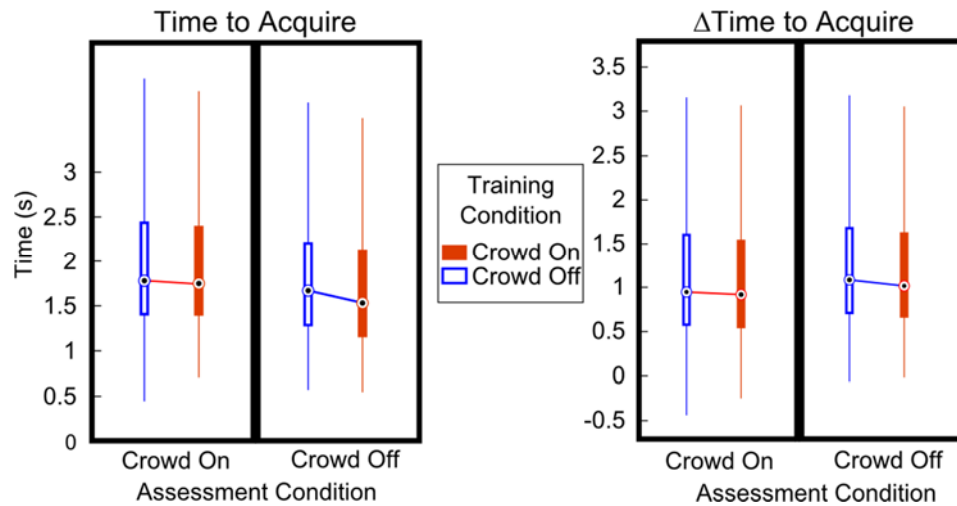


**Figure 3.1.3.3-1 Performance Measures Across Training and Assessment Conditions (Brain Control)** Boxplots as in **Figure 3.1.3.1-1** of performance measures. Outliers have been excluded for clarity. Assessment Condition, indicated by the label on the abscissa, denotes the task used during full Brain Control with no assistance. Training Condition, indicated by filled (Crowd On) or empty (Crowd Off) bands, denotes task used during Training of decoders. For Time to Acquire (left panel), only Assessment Condition reached significance ( $p < 10^{-16}$ ). For  $\Delta$ Time to Acquire, both the Training Condition ( $p = 0.03$ ) and Assessment Condition ( $p = 1.3e^{-6}$ ) were significantly better in the Crowd On conditions, though only by small margins. No pairwise comparisons, indicated by lines joining adjacent medians, reached statistical significance. All group statistics are listed in Table 1.

But, as in Manual Control and as expected, the presence of the Crowd during Assessment blocks slowed task performance (Crowd On Median = 1.75, IQR = 1.05,  $n = 1656$  trials; Crowd Off Median = 1.55, IQR = 1.00,  $n = 1723$  trials;  $p < 10e^{-16}$ , **Figure 3.1.3.3-1**, left panel). While this effect on performance was almost certainly due in part to the visual search required when the Crowd was present, it was also possible that the presence of the Crowd impaired Brain Control of the cursor by interfering with the neural signals used to determine cursor position. To test this possibility, we devised a second measure,  $\Delta$ TTA, to directly assess the quality of Brain Control under the various Training and Assessment conditions.

Assess Condn	Time to Acquire				$\Delta$ Time to Acquire			
	Crowd On		Crowd Off		Crowd On		Crowd Off	
Train Condition	Crowd Off	Crowd On	Crowd Off	Crowd On	Crowd Off	Crowd On	Crowd Off	Crowd On
Median	1.779	1.748	1.597	1.531	0.969	0.940	1.106	1.038
IQR	1.062	1.01	1.000	0.984	1.055	1.012	0.999	0.978
n (Trials)	893	763	978	745	893	763	978	745

**Table 1 Statistics for All Combinations of Conditions and Measures** Table of data for all combinations of Training and Assessment conditions for both main measures. Layout of each group from left to right corresponds to layout in **Figure 3.1.3.3-1**. Note that both measures (Time to Acquire and  $\Delta$ Time to Acquire) were computed using the same trials, thus the correspondence in number of trials between the left and right halves of the table.

The  $\Delta$ TTA was computed for all trials to quantify how Brain Control affected the Acquisition of Target 2 relative to Manual Control in isolation from other factors. We then used the same statistical comparisons that were computed for the unadjusted TTA values to determine whether or not the Crowd's presence during Training or Assessment influenced the  $\Delta$ TTA. While the comparison revealed a significant effect of Training condition (Crowd On Median = 0.99, IQR = 1.00, n = 1508 trials; Crowd Off Median = 1.04, IQR = 1.03, n = 1871 trials; p = 0.03, **Figure 3.1.3.3-1**, right panel), and the trend favored the Crowd On condition, the small difference in the medians suggested only a negligible advantage. We found a significant influence of Assessment Condition on  $\Delta$ TTA (Crowd On Median = 0.95, IQR = 1.04, n = 1656 trials; Crowd Off Median = 1.08, IQR = 0.97, n = 1723 trials; p =  $1.3e^{-6}$ , **Figure 3.1.3.3-1**, right panel), indicating that decoding with the Crowd On yielded slightly better brain control quality. Again, however, the magnitude of this difference was only 45ms, so we considered this difference small enough to be negligible.

Taken together, these results indicated that the additional eye movements and various behavioral demands of the Crowd On task condition did not interfere directly with decoding of a neurally controlled cursor. The more complex task condition might have conferred a small albeit negligible advantage to performance of neural decoding.

These results suggest the NHP was able to simultaneously gaze freely around the screen while independently controlling cursor position. However, an alternative hypothesis that saccades did negatively impact cursor control would also account for this result if the NHP simply learned to minimize extraneous saccades when the Crowd was present. To rule out this possibility, we once again examined 2D histograms of eye position during a phase in the trials when the cursor was actively being transported to the target (**Figure**, right panel). These histograms include eye positions across a one second window ending on Acquisition of Target 2. This window was chosen to capture the time when the cursor is still in motion in both Manual (left panel) as well as Brain Control (right panel). For Brain Control, the trials with straightest cursor trajectories were preselected for this analysis by choosing the fastest 15% of trials. For this representative set, it is clear that, on average, even during active cursor movement in both Manual and Brain Control, the animal made many saccades to the faces around the screen. Additionally, ample saccades during cursor movement are evident in videos of task performance under Brain Control wherein playback speed was slowed and the animal's gaze position was added post hoc (Video 3.1-2).

Though the NHP was able to gaze around the screen with the Crowd On during Brain Control as well as in Manual Control, it should be noted that the overall number of saccades was reduced in Brain Control. We compared the number of saccades landing on a peripheral target (and not the correct target or the cursor) in a one second window ending on initial acquisition of Target 2 for each trial. We then compared the occurrence of these saccades in Manual (mean = 2.04 saccades, s.d. = 1.54) vs. Brain Control (mean = 0.82 saccades, std = 1.18) trials, revealing that there were significantly more in Manual Control ( $p < 10^{-16}$ ). One possible explanation for this outcome is the increased difficulty and imperfect accuracy of Brain Control, i.e., on trials where cursor control is worse, the subject would need to gaze at the cursor longer to maintain closed-loop control. An alternative explanation is extraneous saccades reduced decode accuracy, and the subject learned to make fewer saccades to maintain cursor control. To distinguish these possibilities, we computed the correlation between number of saccades to peripheral targets (as above) in each trial to the TTA across all  $n = 1718$  trials. A correlation of  $r = -0.12$  ( $p < 10e-7$ , T test) supports the former account and rules out the latter. Trials with many saccades to locations not occupied by the cursor were amongst the shortest, while the longest trials involved prolonged periods of gazing at the cursor, presumably to accommodate feedback control.

In a separate session, the brain control task was run with long (1s) ITIs to determine if the animal was able to move the cursor back to the middle of the screen, the location where Target 1 appears at the start of each trial, before there is any overt visual cue to do so. The

animal's performance clearly demonstrated his ability to move the cursor back to the middle of the screen before Target 1 appeared in anticipation of the upcoming trial (Video 3.1-3). Additionally, in separate sessions, we confirmed that the decoders trained in this center-out style task could generalize to a 3x3 grid of the same face targets spaced evenly on an 18cm x 18cm square. While performance in terms of trial length was inherently slower than the circular, center-out task ( $p < 10^{-16}$ ) due to the longer cursor movements required (Time To Acquire: Median = 2.405s, IQR = 1.433, Time to Reward: Median = 3.226s IQR = 1.540), control of the cursor itself was qualitatively no different (Video 3.1-4).

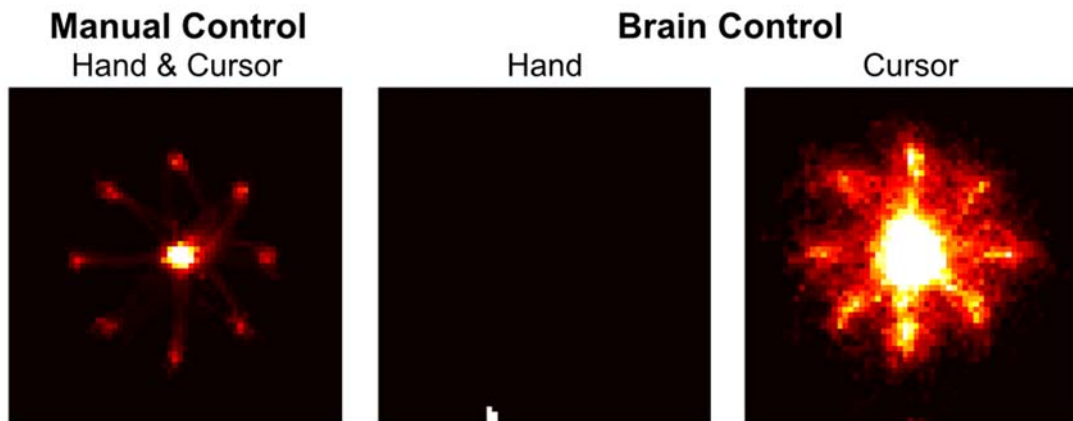


**Figure 3.1.3.3-2 Hand and Cursor Position During Decoding** Heat maps of Hand and Cursor positions during Manual & Brain Control. Hotter colors indicate greater fraction of time spent in that location. Left panel: Hand and Cursor (which are causally linked and thus represented with one image) during Manual Control averaged across  $n = 161$  trials. Hand position (middle panel) and Cursor position (right panel) averaged across the same set of  $n = 465$  Brain Control trials. For the brain control session shown, the signal measured by the hand sensor was very close to its static measurement noise.

While the subject's arms were prevented from making large movements during Brain Control, he was still able to make small wrist and finger movements, though these

movements as measured by the tracking sensor did not directly influence cursor position. On most days both hands were observably and measurably still (**Figure 3.1.3.3-2**), however on other days small, residual movements were made during performance of the task under Brain Control. We used the measured hand kinematics (in the horizontal plane that would typically be used to control the cursor in Manual Control) to predict the kinematics of the neural cursor. Cross-validated R-squared values never exceeded 0.03 for either dimension for any day, indicating little influence of residual hand movements on the decoded cursor.

#### **3.1.4 Discussion**

Despite the known sensitivity of motor control areas to numerous cognitive and motor variables (Rao and Donoghue, 2014, Buneo & Andersen, 2006, Colby and Goldberg, 1999, Louie et al., 2011, Pesaran et al., 2010), we showed robust use of a neurally controlled cursor driven by signals from the parietal cortex in a context cognitively and visually richer than those created to date for use by primates. The task created a primate model of human use of GUI interfaces, e.g., tablet computers or smartphones. The performance measures indicated that training and decoding with the Crowd On did not impair neural cursor control, but may have actually conferred a small (albeit negligible) advantage. These small differences may simply have arisen as a result of motivational factors, i.e., more “interesting” stimuli being present on the screen with the Crowd On.

By targeting Area 5d for implant, we were able to obtain neural signals that reflected intended movements of the limb. Though residual eye-related signals were measurable in a control task, it was clear that they did not interfere with the functioning of the interface, whether during use of an existing decoder or during training. To our knowledge, this study is the first confirmation that unconstrained gaze does not interfere with prosthetic control, even in a visually complex task environment. Furthermore, we demonstrated the ability of the subject to decouple gaze position, i.e., sensing, from control of the cursor, i.e., the motor intention. This is a crucial capability for providing natural, intuitive control.

This capability was further emphasized given the ability of the subject to manipulate the cursor even in the absence of overt visual targets during the trials with extended ITIs. This result suggests that neural activity in parietal cortex can capture motor intentions without the need for overt visual representations of movement goals.

We hope in upcoming clinical work that human subjects will be able to control parietal neuroprosthetics by naturally manipulating their internal representation of the limb. Or with training, perhaps patients will mentally manipulate the cursor or end effector directly without remapping imagined actions or using other indirect strategies. This capability could reasonably be expected to occur given the observed mechanisms of tool use and/or extension of the body schema in parietal neurons by Iriki and colleagues (Iriki et al., 2001).

These findings as a whole strengthen the case for the use of the parietal cortex in human clinical neuroprosthetic applications. They suggest that a human subject controlling a neural cursor driven by spiking activity in the parietal cortex could elicit similar results: robust 2D control that is insensitive to the visual and behavioral nuances of a modern computing interface.

### 3.1.5 References

- Bremner, L.R. and Andersen, R.A. (2012). Coding of the Reach Vector in Parietal Area 5d. *Neuron*. 75, 342-351.
- Buneo, C., & Andersen, R (2006). The posterior parietal cortex: sensorimotor interface for the planning and online control of visually guided movements. *Neuropsychologia*. 44, 2594-2606.
- Colby, C., & Goldberg, M (1999). Space and attention in parietal cortex. *Annual Review of Neuroscience*. 22, 319-349.
- Collinger JL, Wodlinger B, Downey JE, Wang W, Tyler-Kabara EC, Weber DJ, McMorland AJC, Velliste M, Boninger ML, Schwartz AB (2013). High-performance neuroprosthetic control by an individual with tetraplegia. *Lancet* 6736:61816-61819.
- Crammond, D., & Kalaska, J (1989). Neuronal activity in primate parietal cortex area 5 varies with intended movement direction during an instructed-delay period. *Experimental Brain Research*. (1989) 76, 458-462.
- Cui, H., & Andersen, R. A (2011). Different Representations of Potential and Selected Motor Plans by Distinct Parietal Areas. *Journal of Neuroscience*, 31(49), 18130-18136.
- Franke F, Jackel D, Dragas J, Muller J, Radivojevic M, Bakkum D, Hierlemann A. (2012) High-density microelectrode array recordings and real-time spike sorting for closed-loop experiments: an emerging technology to study neural plasticity. *Front Neural Circuits*., 20;6:105.
- Fraser G W, Chase S M, Whitford A and Schwartz A B (2009) Control of a brain–computer interface without spike sorting *Journal of Neural Engineering*, 6 1–8.
- Gilja V, Nuyujukian P, Chestek CA, Cunningham JP, Yu BM, Fan JM, Churchland MM, Kaufman MT, Kao JC, Ryu SI, Shenoy KV., (2012). A high-performance neural prosthesis enabled by control algorithm design. *Nature Neuroscience*, 15(12), 1752-1757.
- Graziano M S A, Cooke D F, Taylor C S R 2000 Coding the Location of the Arm by Sight *Science* 290 1782–6.
- Hauschild, M., Mulliken, G., & Fineman, I (2012). Cognitive signals for brain–machine interfaces in posterior parietal cortex include continuous 3D trajectory commands. *Proceedings of the National Academies of Science*. 109(42), 17075–17080.
- Hochberg, L. R., Serruya, M. D., Friehs, G. M., Mukand, J. A., Saleh, M., Caplan, A. H., et al (2006). Neuronal ensemble control of prosthetic devices by a human with tetraplegia. *Nature*, 442(7099), 164-171.
- Ifft, P., Shokur, S., Li, Z., Lebedev, M., & Nicolelis, M (2013). A Brain-Machine Interface Enables Bimanual Arm Movements in Monkeys. *Science Translational Medicine*, 5(210), 210ra154-210ra154.
- Iriki, A., Tanaka, M., Obayashi, S., & Iwamura, Y (2001). Self-images in the video monitor coded by monkey intraparietal neurons. *Neuroscience Research*, 40, 163-173.

- Louie, K., Grattan, L. E., & Glimcher, P. W (2011). Reward Value-Based Gain Control: Divisive Normalization in Parietal Cortex. *Journal of Neuroscience*, 31(29), 10627-10639.
- Mulliken, G. H., Musallam, S., & Andersen, R. A (2008). Decoding Trajectories from Posterior Parietal Cortex Ensembles. *Journal of Neuroscience*, 28(48), 12913-12926.
- Musallam, S., Corneil, B., Greger, B., & Scherberger, H (2004). Cognitive control signals for neural prosthetics. *Science*, 305, 258-262.
- O'Doherty JE, Lebedev MA, Ifft PJ, Zhuang KZ, Shokur S, Bleuler H, Nicolelis MA. Active tactile exploration using a brain-machine-brain interface. *Nature*. 2011 Oct 5; 479(7372):228-31.
- Peirce, JW (2007) PsychoPy - Psychophysics software in Python. *Journal of Neuroscience Methods*, 162(1-2), 8-13.
- Pesaran, B., Nelson, M. J., & Andersen, R. A (2010). A Relative Position Code for Saccades in Dorsal Premotor Cortex. *Journal of Neuroscience*, 30(19), 6527-6537.
- Pesaran, B., Nelson, M. J., & Andersen, R. A (2008). Free choice activates a decision circuit between frontal and parietal cortex. *Nature*, 453(7193), 406-409.
- Rao, N., & Donoghue, J (2014). Cue to action processing in motor cortex populations. *Journal of Neurophysiology*, 111, 441-453.
- Revechkis, B., Aflalo, T.N.S., Andersen, R., Use of a posterior parietal cortex brain-machine interface in a cognitive face-in-a-crowd task. Poster presented at: Society for Neuroscience 2013; November 13 2013; San Diego, CA.
- Revechkis, B., T. N. Aflalo, S. Kellis, N. Pouratian, and R. A. Andersen. 2014. "Parietal neural prosthetic control of a computer cursor in a graphical-user-interface task." *J Neural Eng* 11 (6):066014. doi: 10.1088/1741-2560/11/6/066014.
- Rothschild RM. Neuroengineering tools/applications for bidirectional interfaces, brain-computer interfaces, and neuroprosthetic implants - a review of recent progress. *Front Neuroeng*. 2010 ;15;3:112.
- Shanechi, M. M., Hu, R. C., Powers, M., Wornell, G. W., Brown, E. N., & Williams, Z. M (2012). Neural population partitioning and a concurrent brain-machine interface for sequential motor function. *Nat Neurosci*, 15(12), 1715-1722.
- Soto, D., Heinke, D., Humphreys, G. W., & Blanco, M. J. (2005). Early, Involuntary Top-Down Guidance of Attention From Working Memory. *Journal of Experimental Psychology: Human Perception and Performance*, 31(2), 248-261.
- Velliste, M., Perel, S., Spalding, M. C., Whitford, A. S., & Schwartz, A. B (2008). Cortical control of a prosthetic arm for self-feeding. *Nature*, 453(7198), 1098-1101.

## **3.2 State Decoding Improves Use of a Computer Cursor for Neuroprosthetic Applications**

### **3.2.1 Introduction**

A common problem with computer-based neural prosthetics lies in the generally noisy output of the decoders (Wang et al., 2013, Ifft et al., 2013, Vargas-Irwin et al., 2010). This noise is present and particularly noticeable when the cursor or other effector is intended to be kept stationary, e.g., when attempting to select a target. Even if “clicking” is decoded separately for target selection (Kim et al., 2011), noisy positioning of the cursor would result in many wasted and potentially frustrating clicks if the cursor is not held in place at the correct time. Easily selecting targets is crucial for a neural prosthetic that utilizes a graphical user interface (GUI). Additionally, noisy cursor movement during other periods in which a stationary cursor is desired, e.g., during visual search of the screen or attentional disengagement from the interface altogether, would also make the interface more difficult to use. Additionally, it has not been demonstrated whether the intention to move at all can be decoded in the absence of limb movement, as would be relevant in a clinical setting.

We developed a neural prosthetic tested with a non-human primate (NHP) using neural activity from Brodmann’s Area 5 in posterior parietal cortex. The interface, driven by a linear velocity decoder, was used to perform a GUI-like task using a “point and hold” strategy to select targets. We observed that jittery movement of the cursor often made holding the targets for the required time very difficult (Video 3.2-1).

Rather than simply relaxing the behavioral requirements of the task, we coupled the existing linear velocity decoder with a categorical state decoder. Such decoders have been used in studies involving parietal and motor cortex for offline reconstructions of behavior (Shenoy et al., 2003, Kemere et al., 2008, Aggarwal et al., 2013, Darmanjian et al., 2003), and for decoding “clicks” or selection in tetraplegic human subjects with motor cortical prosthetics (Kim et al., 2011). Additionally, previous work (Hwang and Andersen, 2009) has shown that local field potentials (LFPs) in the PPC can be used to detect the onset of an intended cursor movement even without production of limb movement. Thus, in the current study, we coupled state decoding with continuous control of a computer cursor in a GUI-like NHP task. We found that decoding of movement state conferred significantly better performance.

### **3.2.2 Methods**

One male rhesus monkey participated in this study. All animal and surgical procedures were approved by the California Institute of Technology Institutional Animal Care and Use Committee and followed guidelines set forth by the National Institutes of Health.

#### **3.2.2.1 Behavioral Setup**

The primate was seated in a chair and viewed an LCD monitor that presented task stimuli. The arms were gently restrained in a relaxed position when performing Brain Control. Eye position was tracked with an infrared camera (ISCAN Inc., Woburn, MA). Hand position was tracked with a 6DOF magnetic sensor (Ascension Technology Corporation, Milton,

VT). The PsychoPy psychophysics library was used for stimulus presentation (Peirce, 2007) and Simulink software (The MathWorks Inc., Boston, MA) for task control.

### **3.2.2.2 Neural Recordings**

Two 96-channel Cereport arrays (Blackrock Microsystems, Salt Lake City, UT), implanted on the superior parietal lobule, were used to record neural activity. Electrical potentials were amplified, digitized, and recorded with the Cerebus hardware and Central software suite (Blackrock Microsystems). Thresholds for action potential detection were set -4.5 times the RMS of the raw signal. Threshold crossing rates were calculated in non-overlapping 50ms bins by custom MATLAB software (The MathWorks Inc, Boston, MA). About 85 channels of discernible spike activity were used each day.

Power in the local field potentials (LFPs) was calculated using fast Fourier transforms of the raw neural signal for each available channel over a 100ms sliding window at 50ms intervals. By using a step size identical to the spike bin size, spike and LFP data were both available every 50ms. Because only a single binary classification was needed, we wished to extract the clearest possible gross, movement-related signal from the LFPs without concern for finer tuning properties (Hwang and Andersen, 2012). To this end, we averaged the power spectra of all available channels during each time bin. Averaging resulted in one value for each frequency bin for each time bin. A frequency bandwidth of 11 Hz yielded 9 frequency bins between 0 and 100 Hz. Higher frequency bins were discarded. Example, trial-averaged neural data are shown in **Figure 3.2.2.3-1**.

### 3.2.2.3 Behavioral Task

The behavioral task (**Figure 3.2.2.3-1**) was designed to mimic human use of a GUI (Revechkis et al., 2014). First, the primate was presented with a single, icon-like face image as a sample at the center of the screen (Target 1). After selecting it with the cursor, a matching target (Target 2) appeared at one of 8 possible positions. Target positions were radially distributed at 45 degrees 9cm from the center of the screen. In the Crowd On task condition (illustrated in **Figure 3.2.2.3-1**) seven non-matching face icons appeared at the other target positions. In the Crowd Off condition (not illustrated in **Figure 3.2.2.3-1**) only the matching face appeared somewhere on the circle. After Target 2 appeared (with or

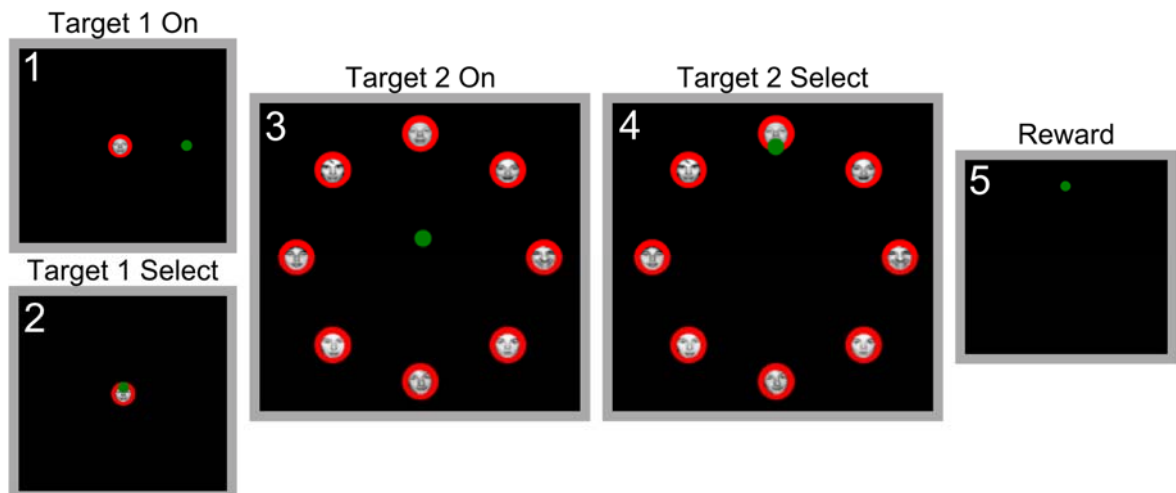


**Figure 3.2.2.3-1 Face in a Crowd Task Structure** Screenshots illustrate the behavioral task. Numbers were added in the upper left corner to indicate order. Titles indicate the event captured by the screenshot. Screenshots 3 and 4 are enlarged for clarity. The sample face icon, Target 1, appeared in the middle of the screen (1). After selecting it by overlapping it with the cursor (green dot) for 500ms (2), the same face icon appeared somewhere in the eight locations shown along with seven non-matching face icons (3). The NHP found and selected the matching face (in this case at the 12 o'clock position) by overlapping it for another 500ms (4). All targets then disappeared and a reward was delivered (5). Only the Crowd On task condition is illustrated. In the Crowd Off task condition, no other face icons appeared during the task aside from Target 1 and the matching Target 2.

without the Crowd), the primate had 20 seconds to select the matching face with the cursor. Selection of both Targets 1 and 2 was accomplished by visually overlapping the cursor with the target for a hold period of 0.5s.

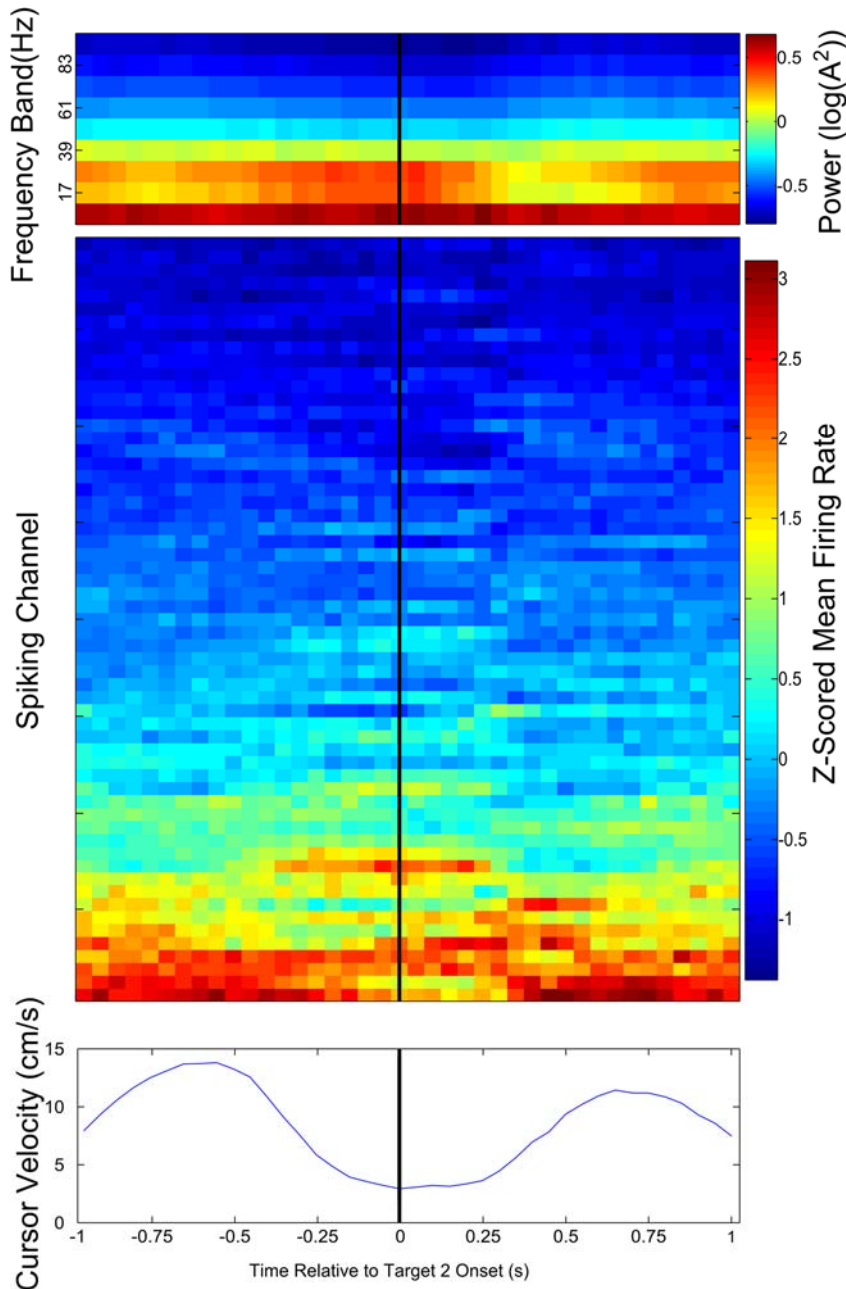


**Figure 3.2.2.3-1 Encoding of Movement versus Non-movement By the Neural Data** Both LFPs (top panel) and spiking activity (middle panel) reflected information about the overall movement state or velocity (bottom panel). These data, taken from training blocks when Brain Control was used with assistance, were used to train the State Decoder. Thereafter, the neural signals alone were used by the State Decoder to estimate whether or not cursor movement was intended at any given moment. That estimate was then used as a gate for the velocity decoder. Data for all panels was averaged across  $n = 222$  trials and aligned to the appearance of Target 2, indicated by the solid vertical line through all three panels. The top panel shows a spectrogram of the LFP frequency bands used. The labels on the vertical axis indicate the approximate middle of each frequency band marked. The middle panel shows z-scored mean firing rates for 55 of the most active spike channels available for decoding sorted from least to most active. The bottom panel displays mean decoded cursor velocity after trajectory assistance was applied.

### 3.2.2.4 Performance Measures

Task performance was quantified by measuring the time needed to perform each step of the task starting with the appearance of Target 2. Time to Acquire (TTA) measured the

duration between onset of Target 2 and the initial contact of the cursor with Target 2. Time to Hold (TTH), the primary measure addressed in the current study, measured the time between first contact with Target 2 and when reward was delivered, i.e., how long it took to successfully overlap Target 2 for the required hold period. This value could not be less than 0.5s by definition; however it could be greater if overlap of the cursor with the target was broken and reinitiated. Time to Reward (TTR) captured the time from Target 2 onset to completion of the trial and the concomitant juice reward.

#### **3.2.2.5 Statistical Tests**

Two-sample Kolmogorov-Smirnov tests were used to detect differences between performance measures in various task conditions. All  $p$  values reported herein were outcomes of this test unless otherwise noted.

#### **3.2.2.6 Decoder Training Procedure**

In order to train a decoder *de novo* for each session without physical movement (a clinically relevant scenario), observation of automated performance of the task was used to train an initial decoder. An automatic controller was programmed to simulate performance of the task by the NHP by moving the cursor with naturalistic, Gaussian velocity profiles to the instantaneous task goal. The cursor was left stationary when no goal was present on the screen. Reaction times were also simulated. The NHP received juice rewards for completed trials even while the automatic controller performed the task. Engagement in the task was enforced by requiring viewing of the screen. Breaking viewing of the 20cm

by 20cm region in the center of the display (the approximate extent of the task area on the display) for more than 3 seconds resulted in an abort of the current trial and a time out of 5-10s. In practice, this almost never occurred.

Neural data was recorded during a 250s Observation Block wherein the automatic controller performed the task in the Crowd Off condition. With the kinematics of the automatic cursor as responses and neural data as observations, a Velocity Decoder was computed (see below). This new decoder was then used as a Training Decoder during the subsequent Training Block as described in an earlier study (Revechkis et al., 2014).

After the Observation Block and the Training Block, a new Velocity Decoder was trained along with a State Decoder. They were then used by the NHP without assistance to perform the task in either the Crowd or No Crowd condition. The State Decoder was turned on and off in alternating blocks of 25-50 trials to assess its performance. This process of training both the Velocity and State Decoders and assessment of State Decoder performance constituted a single experimental session. One to three sessions were performed per day. Task condition did not vary within a session.

### **3.2.2.7 Velocity Decoder Computation**

For transforming neural activity into a cursor position, we used a linear predictor coupled with a linear model of the desired cursor dynamics,

$$\hat{x}_k = \mathbf{A}\hat{x}_{k-1} + \mathbf{B}z_k \quad (2)$$

where  $k$  denotes the time step,  $\hat{x} \in \mathbb{R}^{4 \times 1}$  is the predicted 4-dimensional kinematic state of the effector;  $z \in \mathbb{R}^{N \times 1}$  is an  $N$ -dimensional list of features derived from neural recordings;  $\mathbf{A} \in \mathbb{R}^{4 \times 4}$  is the state-space representation of the system dynamics of the effector motion; and  $\mathbf{B} \in \mathbb{R}^{4 \times N}$  addresses the influence of each feature upon each kinematic variable in  $\hat{x}$ .

The structure of the vector and matrix components of (2) is as follows for the  $m$ th degree of freedom (DOF) at time step  $k$ ,  $\hat{x}_k^m$ , and its derivative  $\dot{\hat{x}}_k^m$ :

$$\begin{bmatrix} \hat{x}_k^m \\ \dot{\hat{x}}_k^m \end{bmatrix} = \begin{bmatrix} 1 & dt \\ \alpha & \lambda \end{bmatrix} \begin{bmatrix} \hat{x}_{k-1}^m \\ \dot{\hat{x}}_{k-1}^m \end{bmatrix} + \begin{bmatrix} 0 & \dots & 0 \\ \beta^{m,0} & \dots & \beta^{m,N-1} \end{bmatrix} \begin{bmatrix} z_k^0 \\ \vdots \\ z_k^{N-1} \end{bmatrix} \quad (3)$$

In (3),  $dt$  is the step size of the discrete update equation in seconds,  $\alpha$  allows positional feedback onto velocity,  $\lambda$  is a smoothing parameter,  $\beta^{m,n}$  are the weights applied to the  $N$  neural features for the  $m$ th degree of freedom, and  $z_k^n$  are the neural features at time step  $k$ . The terms  $\beta^{m,n}$  were fit by regressing neural activity against cursor velocity using regularized linear regression. The regularization term was chosen to be the value that minimized cross-validated prediction error. In practice,  $dt$  was set to 0.05 s reflecting our choice of 0.05 s time bins. To prevent the cursor from drifting out of the workspace,  $\alpha$  was set to a small negative value of -0.05.  $\lambda$  was chosen to reject high-frequency noise without causing excessive delays. This typically led to a value of  $\lambda = 0.7$ . The final form of this decoding method is nearly identical to that described by Gilja and colleagues (Gilja et al., 2012).

### 3.2.2.8 State Decoder Computation

The same threshold crossing data was supplied to the State Decoder as well as the Velocity Decoder. The State Decoder also used the channel-averaged power spectra as input (**Figure 3.2.2.3-1**). Principal component analysis was used to reduce the dimensionality of the input data. The number of principal components required to capture at least 95% of the variance in the data were supplied to the classifier.

A naïve Bayesian classifier with uniform priors was trained on the neural data (observations) and movement state (responses). The response categories were determined using the same procedure described in previous work (Revechkis et al., 2014, Gilja et al., 2012) for interpreting the subject's instantaneous intentions during the Training Block. If no target was on the screen the intended velocity was assumed to be 0, and the response was categorized as Rest. Otherwise, the response was Movement. Reaction times were taken into account by delaying changes in intended state after target onset according to reaction times measured during manual control of the cursor in preliminary training sessions. The classifier assumed normality of the observation data and therefore estimated only the mean and standard deviation for each element of the input data for each movement state.

In order to prevent noisy switching between Movement and Rest on timescales unlikely to be useful, a gain ranging between 0 and 1 was applied to the output of the Velocity Decoder at every time bin. The output of the State Decoder was used to modulate this gain in a

linear, step-wise fashion. If in a given time bin, the State Decoder classified the current neural signals as Movement, the gain was increased by 0.4 to a maximum of 1. If Rest was decoded, the gain was decreased by 0.2 to a minimum of 0. The asymmetry in step size allowed fast initiation of movement but smooth, gradual deceleration. This way, noisy errors in the state classification would suddenly accelerate or halt movement less often than if the State Decoder output itself directly determined the gain.

### **3.2.3 Results**

We examined whether the NHP was able to manipulate the cursor to perform the task during Brain Control without hand movement. Cross-validated  $R^2$  values between neural cursor kinematics and measured hand kinematics, though at times statistically significant, never exceeded 0.03 in any session for any dimension. We therefore concluded that the NHP was not able to affect the neural cursor using physical movement of the limb.

Sixteen total sessions were run. Half included assessment of the State Decoder in the Crowd On condition and half with the Crowd Off. The overall effect of the State Decoder on the various performance measures in each task condition are shown in Figure 3.2.3-1. The results are similar for both task conditions.

The State Decoder significantly reduced the mean TTH in both Crowd On ( $p = 1.3e^{-13}$ ) and Off ( $p = 8.4e^{-11}$ ) from about 1.5s to 1.0s. Overall trial length as measured by mean TTR was reduced in both task conditions: from 3.51s to 3.04s with the Crowd Off ( $p = 1.2e^{-3}$ ),

and from 3.65s to 3.33s with the Crowd On ( $p = 8.9e^{-3}$ ). The estimated probability distributions of Time to Reward (Figure 3.2.3-1, 3<sup>rd</sup> column) indicated that the State Decoder helped flatten the tails of the distributions, i.e., reduce the frequency of longer trials in the 5 and 6-second ranges in the Crowd Off and On conditions, respectively.

A small but significant increase in mean TTA was measured as a function of the State Decoder. With the Crowd Off, TTA increased by 0.178s ( $p = 2.3e^{-7}$ ). With the Crowd On, TTA increased by 0.190s ( $p = 2.6e^{-4}$ ). While this delay in the ability to acquire the target undesirably hampered performance, it was outweighed by the reduction in TTH.

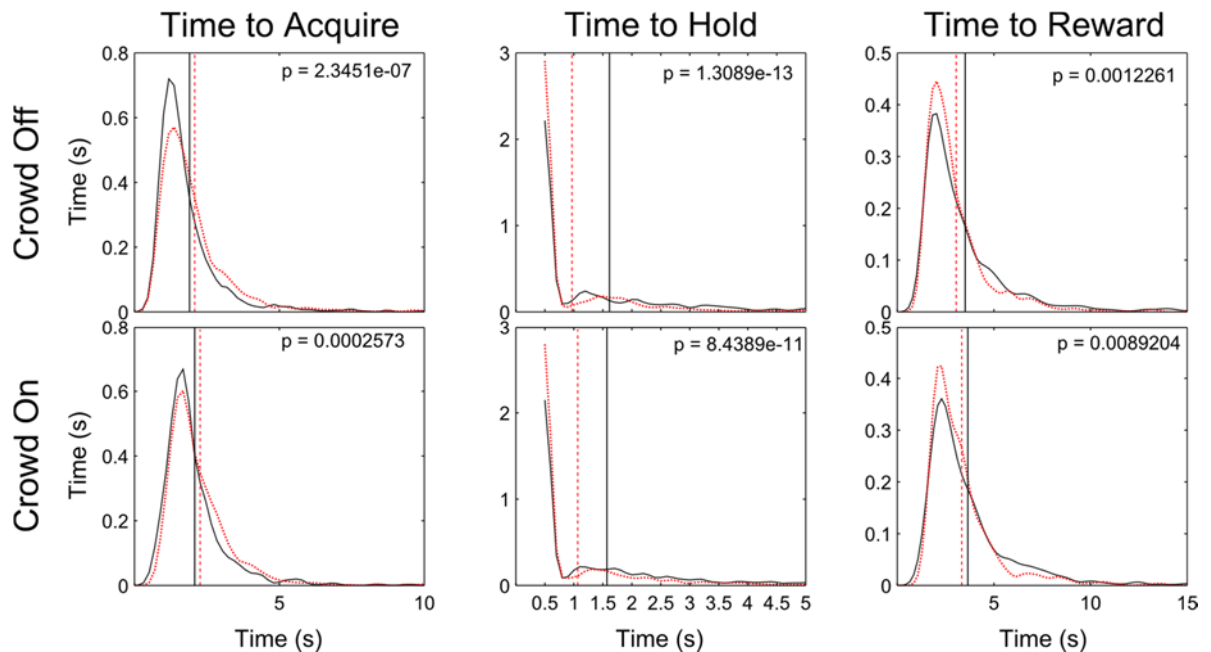


**Figure 3.2.3-1 Summary State Decoder Performance.** Smoothed probability density estimates for each behavioral measure (columns) for both task types (rows). Solid black traces indicate probability estimates for trials without the State Decoder. Dashed red traces are for estimates with the State Decoder on. Vertical lines indicate means of the distributions with the corresponding color and line type. P values for the two-sample KS test for differences in distributions for each panel are shown at the top right. The State Decoder substantially reduces Time to Hold (middle column) in both Task Conditions with only a slight penalty to Time to Acquire (left column), resulting in an overall decrease in Time to Reward (right column) and thus total trial time. Plots in top row summarize  $n = 1917$  trials across 8 sessions. Plots in bottom row summarize  $n = 1745$  trials across 8 sessions.

While the overall effects were significant across all sessions, a more nuanced relationship was evident when observing the effects of the State Decoder on a session-wise basis (**Figure 3.2.3-2**, left panel). While the State Decoder significantly improved TTH for 12 out of 16 sessions (6 after Bonferonni correction), it seemed that the State Decoder only substantially improved TTH when the initial TTH without the State Decoder was poor. To quantify this relationship, we examined the session-wise improvement in TTH as a function of the initial TTH without the State Decoder (**Figure 3.2.3-2**, right panel). Linear regression demonstrated a strongly positive and significant relationship ( $\beta = 0.67$ ,  $p = 2.4e^{-7}$ ). Thus, the State Decoder helped “rescue” poor performance as measured by TTH but imparted less benefit when the Velocity Decoder itself performed well.

Example videos show the readily apparent improvement in performance caused by the State Decoder on a day of poor initial performance (Video 3.2-1). We also include video of task performance with State Decoding when initial performance was already strong for reference (Video 3.2-2).

To determine the relative effectiveness of the LFPs and spikes, we retrained decoders for each training set in the study using just Spikes or just LFP data. (The existing decoders used both Spikes and LFPs.) True Positive rate for the detection of movement in the training data was computed and compared across all three groups. State Decoders based

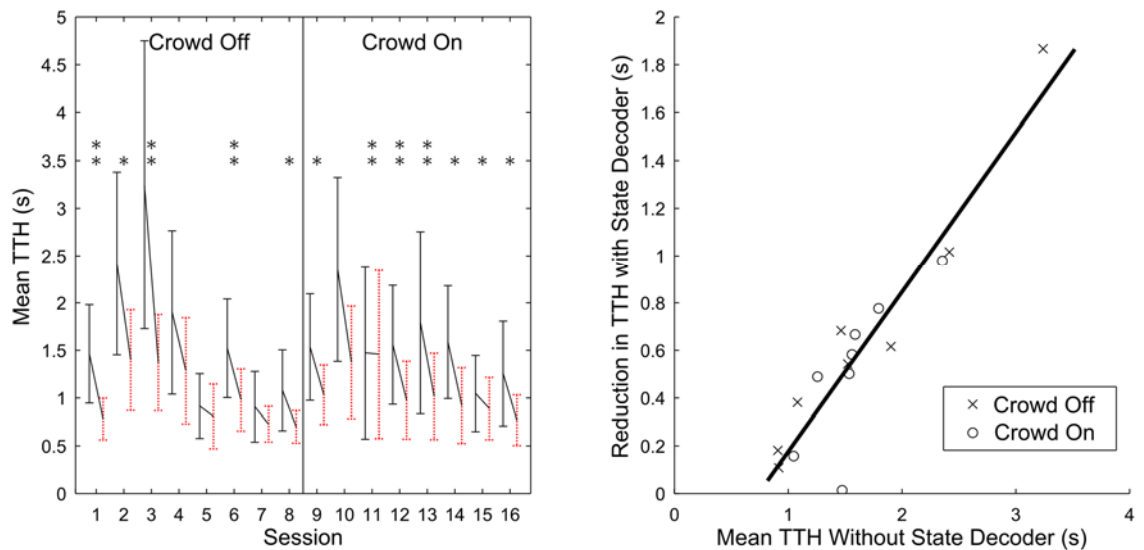


**Figure 3.2.3-2 Effect of State Decoding on TTH Per Decoder** The left panel shows the effect of state decoding on TTH for each session. Error bars indicate mean and 95% confidence interval of TTH within each session when the State Decoder was Off (solid, black error bars) and On (dotted, red error bars). Groups within each session are joined by a line connecting the means. Sessions are grouped by task condition and separated by the vertical, central line. Sessions are not shown in chronological order. Each session consists of at least 200 trials and therefore at least 100 trials per mean and error bar. \*:  $p < 0.05$ , \*\*:  $p < 0.0031$ . Right panel: reduction in TTH due to the State Decoder for each session plotted as a function of TTH without the state decoder. Each data point corresponds to one pair of error bars in the left panel. Linear regression (solid line) indicated a strong linear relationship:  $\beta = 0.67$ ,  $p = 2.4e-7$ . Thus, the worse the initial performance was without the State Decoder, the greater the reduction in Time to Hold achieved by using the State Decoder.

on LFPs alone (mean TP rate = 52.04%, S.D. = 6.04%) did not detect movement significantly better than the chance level of 50% ( $p = 0.26$ , T-test). Furthermore, the Spikes and LFPs group (mean = 68.40%, S.D. = 5.15%) did not perform significantly better than Spikes alone (mean = 68.15%, S.D. = 4.67%,  $p = 0.36$ , Two-sample KS test). This indicated that the spiking activity drove the state detection and that LFPs did not contribute.

### **3.2.4 Discussion**

Use of the State Decoder benefitted performance of the neural interface. While it did not have a large effect in all sessions, it dramatically improved target selection when performance was initially poor. The time required to select targets averaged across all trials decreased from approximately 1.5s to one second in both the GUI-like Crowd On task condition and the more basic Crowd Off condition. This effect was strong enough to drive a decrease in overall trial times despite a slight penalty to the speed of initial target acquisition.

The ability to successfully select targets will be integral to neural control of cursors in GUI interfaces in future applications. Whether accomplished via holding or clicking and whether driven by multi-unit activity or LFPs, the techniques described here would contribute to the speed and usefulness of such interfaces. By reducing the likelihood of struggling to select a target due to noise, subjects using prosthetics that employ these methods could also experience less frustration over time.

Decoding and training of both the velocity and state decoders were accomplished in the absence of physical movement. This is a likely clinical scenario, as patients who could benefit and have benefitted from neural prosthetics are those who lack any motor function. Furthermore, the task we designed involved operations similar to those employed in a modern GUI, e.g., browsing and selecting options from many possible alternatives with a cursor. The training, decoding, and task used in the current study strongly suggest that our results would likely be applicable and beneficial in a practical, clinical context.

These enhancements would allow a patient utilizing a GUI-based neural prosthetic to accomplish many of the tasks performed on devices such as smartphones and tablet computers. Effective control of such devices would grant paralyzed individuals access to a massive variety of applications, games, and tools, and through them, a degree of control over their environments and higher quality of life.

### 3.2.5 References

- Aggarwal V, Mollazadeh M, Davidson AG, Schieber MH, Thakor NV. "State-based decoding of hand and finger kinematics using neuronal ensemble and LFP activity during dexterous reach-to-grasp movements." *J Neurophysiol.* 2013 Jun;109(12):3067-81. doi: 10.1152/jn.01038.2011.
- Bremner, L.R. and Andersen, R.A. (2012). Coding of the Reach Vector in Parietal Area 5d. *Neuron.* 75, 342-351.
- Darmanjian, S., Kim, S.P., Nechyba, M.C., Morrison, S., Principe, J., Wessberg, J., Nicolelis, M.A.L., "Bimodal brain-machine interfaces for motor control of robotic prosthetics," in *Proc. 2003 IEEE/RSJ Int'l Conf. on Intelligent Robots and Systems*, vol. 4, Las Vegas, NV, pp. 3612-17.
- Gilja, V., Nuyujukian, P., & Chestek, C (2012). A high-performance neural prosthesis enabled by control algorithm design. *Nature*, 15(12), 1752-1758.
- Hwang, E. J., & Andersen, R. A (2009). Brain Control of Movement Execution Onset Using Local Field Potentials in Posterior Parietal Cortex. *Journal Of Neuroscience*, 29(45), 14363-14370. doi:10.1523/JNEUROSCI.2081-09.2009
- Ifft, P., Shokur, S., Li, Z., Lebedev, M., & Nicolelis, M (2013). A Brain-Machine Interface Enables Bimanual Arm Movements in Monkeys. *Science Translational Medicine*, 5(210), 210ra154-210ra154.
- Kemere, C., Santhanam, G., Yu, B. M., Afshar, A., Ryu, S. I., Meng, T. H., et al (2008). Detecting Neural-State Transitions Using Hidden Markov Models for Motor Cortical Prostheses. *Journal Of Neurophysiology*, 100(4), 2441-2452.
- Kim SP, Simeral JD, Hochberg LR, Donoghue JP, Friehs GM, Black MJ. Point-and-click cursor control with an intracortical neural interface system by humans with tetraplegia. *IEEE Trans Neural Syst Rehabil Eng.* 2011 Apr;19(2):193-203.
- Peirce, JW (2007) PsychoPy - Psychophysics software in Python. *J Neurosci Methods*, 162(1-2):8-13.
- Revechkis, B., Aflalo, TNS, Kellis, S, Pouratian, N, & Andersen, RA (2014). Parietal neural prosthetic control of a computer cursor in a graphical-user-interface task. *J Neural Engineering* 11 066014.
- Shenoy KV, Meeker D, Cao S, Kureshi SA, Pesaran B, Buneo CA, Batista AP, Mitra PP, Burdick JW, Andersen RA. Neural prosthetic control signals from plan activity. *Neuroreport.* 2003 Mar 24;14(4):591-6.
- Vargas-Irwin CE, Shakhnarovich G, Yadollahpour P, Mislow JM, Black MJ, Donoghue JP. Decoding complete reach and grasp actions from local primary motor cortex populations. *J Neurosci.* 2010 Jul 21;30(29):9659-69.
- Wang W, Collinger JL, Degenhart AD, Tyler-Kabara EC, Schwartz AB, Moran DW, Weber DJ, Wodlinger B, Vinjamuri RK, Ashmore RC, Kelly JW, Boninger ML. An electrocorticographic brain interface in an individual with tetraplegia. *PLoS One.* 2013;8(2):e55344.

## **4. Human Parietal Cortex**

### **4.1 Selectivity for Hand Movement Execution and Feedback in Human Parietal Neurons and Local Fields**

#### **4.1.1 Introduction**

Significant progress has been made in recent years towards clinically useful human motor neuroprosthetics. While most studies have focused on motor cortex (Collinger et al. 2013, Kim et al. 2011), some have explored parietal cortex as an alternative in non-human primates (Hauschild et al. 2012, Revechkis et al. 2014, Hwang and Andersen 2009) and recently in human subjects (Aflalo et al. in press, Andersen et al. 2014). One question not yet addressed in either area to date is the relevance of the appearance of the device being manipulated with a prosthetic. Can a patient neurally control an abstract effector such as a computer cursor just as ably as an anthropomorphic device such as a robotic limb? While numerous studies have implicated parietal subregions in motor control (Rizzolatti, Fogassi, and Gallese 1997, Seal, Gross, and Bioulac 1982, Mountcastle et al. 1975), parietal areas also appear to be involved in a combination of visual (Graziano, Cooke, and Taylor 2000, Iriki et al. 2001, Kalaska, Caminiti, and Georgopoulos 1983, Mulliken, Musallam, and Andersen 2008b) and somatosensory (Jones and Powell 1969, Sakata et al. 1973) feedback control and/or self-monitoring. We therefore hypothesize that parietal cortical activity driving a prosthetic device might respond more strongly to attempted manipulation of a (visible) effector that more closely resembles a hand.

To test this hypothesis, we designed a variety of tasks to test selectivity of parietal neural signals in human volunteers as part of an FDA-approved clinical study of neuroprosthetics. In the Limb Tuning task, the subject was asked to attempt movements of their limbs to mimic the movements of a computer animated character presented on a monitor. Various joints of all limbs were tested to test for specificity to any particular parts of the body.

We sought to compare decoding of willed movements of a 3D anthropomorphic arm to a two-dimensional or abstract cursor, similar to what would be used in a computerized neural prosthetic. In order to present the most life-like anthropomorphic limb for the patient, we utilized a head-worn, stereoscopic display to place the subject in a virtual environment in which an anthropomorphic avatar could be presented from a 1<sup>st</sup> person perspective. This would create the illusion of “owning” a virtual representation of the body. This illusion has been utilized in past experiments regarding body ownership (Banakou, Groten, and Slater 2013). Recent advances in virtual reality displays and computer graphics have made this a simpler alternative to physical, robotic limbs.

Several tasks were designed to take advantage of the virtual reality environment. In the Delayed Reach task, a simple reaching task in a vertical plane was employed. Such a paradigm is common in training and testing of motor neural prosthetics (Collinger et al. 2013, Hochberg et al. 2006, Kim et al. 2011). The movement effector was varied between arm of the subject’s avatar, a floating “cursor”, and no movement effector at all. With this task, we could assess the effect of visual feedback about an effector during attempted

movements. Because much of this could be explained by the substantial visual differences between a small floating cursor and an entire arm viewed from the first person perspective, the Gesture Task was designed to more carefully tease apart differences in neural responses to the different effectors during observation and attempting of arm motion. Finally, the Online Gesture Control task was designed to detect if the type of effector used during closed-loop online control would affect performance.

## **4.1.2 Methods**

### **4.1.2.1 Human Subject Recruitment**

A quadriplegic volunteer was recruited to participate in an FDA-approved clinical study. All NIH and FDA guidelines were followed. The subject had suffered a traumatic injury resulting in complete transection of the spinal cord at the C3-C4 vertebrae six years prior to recruitment for the study. The subject was ventilator independent and retained only muscle control of her head, neck, and to a limited degree, the shoulders.

An fMRI-based targeting paradigm and behavioral task were used to identify areas of the left superior parietal lobule that were active during attempted movement of the right arm (Appendix B). Two 96-channel Neuroport micro-electrode arrays (Blackrock Microsystems, Salt Lake City, UT) were surgically implanted in those areas identified on August 29, 2014. After approximately one month of recovery and healing, the patient participated in experimental sessions 2 to 3 times per week.

#### **4.1.2.2 Experimental Setup**

Two Neuroport data acquisition systems (Blackrock Microsystems, Salt Lake City, UT) were used to amplify, digitize, and record action potentials and local field potentials from each array. Basic details regarding the neural populations recorded are provided in Appendix A.2. Behavioral tasks and neural decoding were implemented and controlled by MATLAB software (The MathWorks Inc., Cambridge, MA). Spikes were extracted on each channel by detecting voltage crossings below  $-4.5$  times the RMS of the raw signal.

For the Delayed Reach and Online Gesture Control tasks, sorting was performed at the start of each day using time-voltage windows in the Central software (Blackrock Microsystems, Salt Lake City, UT). This was only performed for channels that had clearly discernible neural units as determined by overlaid spike waveforms. For the Limb Tuning and Gesture Tasks, spike sorting was performed offline using custom software by clustering the spike waveforms in the first two dimensions (principal components) of PCA space.

### 4.1.2.3 Behavioral Tasks

#### 4.1.2.3.1 Effector Specificity in Decoding Delayed Reaches

The subject wore an Oculus Rift DK2 virtual reality headset (Oculus VR, LLC, Menlo Park, CA). The headset, using stereoscopic images independently presented to each eye on a head-worn LCD panel, created the illusion of depth in an immersive virtual reality (Figure 4.1.2.3.1-1). The headset's display subtended  $\sim 106$  degrees visual angle. The interpupillary distance of the rendered world was calibrated to the subject's physical eye separation. An accessory infrared tracking camera detected any movement of the subject's head and adjusted the computer rendered perspective accordingly, creating the illusion of

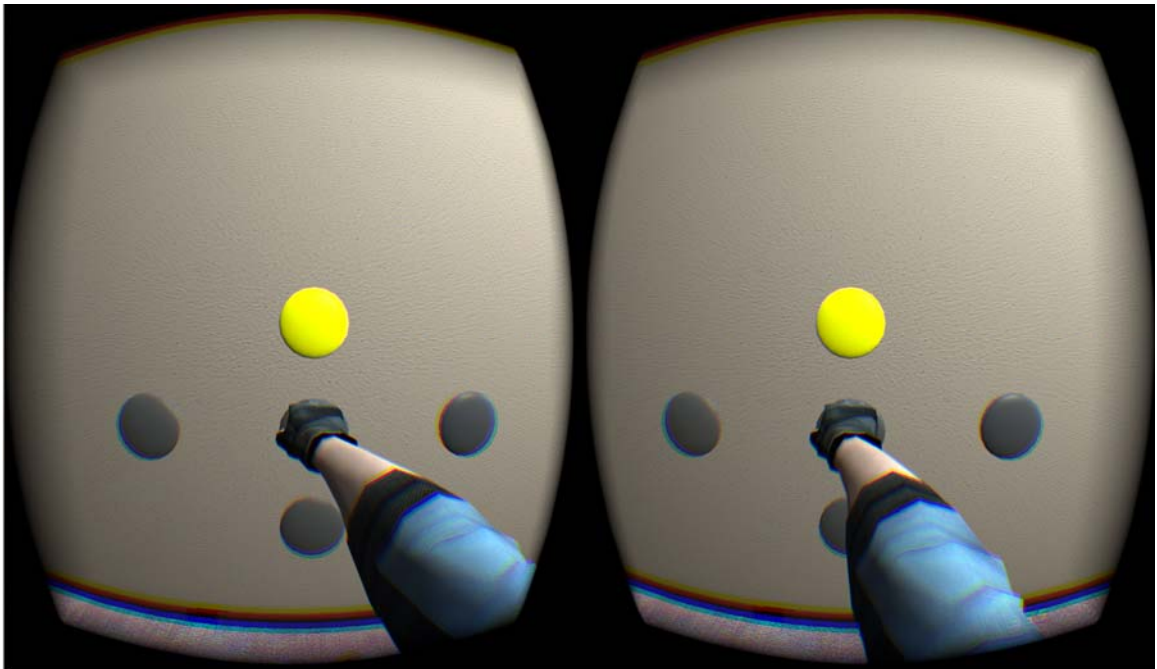


**Figure 4.1.2.3.1-1 Example Frame from Stereoscopic Display.** This image constitutes one frame presented on the Oculus Rift display at a particular instant during task performance. Each half of the image is presented to each eye independently at 75 fps. The black border around each image is not as it exceeds the portion of the internal LCD that falls within the subject's FOV after the image passes through correcting lenses built in to the headset.

“being inside” the virtual world. Head movement was not required during the task and was minimal.

The computer generated environments for all tasks in this study were designed, animated, and rendered with the Unity3D development platform (Unity Technologies, San Francisco, CA). The environment consisted of a plain interior of a small office. The subject’s virtual body, or avatar, was seated facing a plain wall at a distance of approximately 4 feet. The majority of the avatar, with the exception of the arm, was usually below the subject’s FOV, just as one’s body when seated and looking straight ahead is not immediately in view. At arm’s length in front of the subject were 4 grey, circular, targets: one central, and one in each cardinal direction in the vertical plane. No substantial features or furniture were visible other than the wall, floor, the avatar, and task elements.

This task employed a standard delayed reach paradigm. When a trial began, one of the peripheral targets turned yellow for 1 second (Cue phase) and then returned to grey. After a variable length delay (Delay phase) of 1-1.2 seconds, the central target turned green, signaling the subject to attempt a whole right arm movement at the shoulder to the peripheral target indicated (Go phase.) The Go phase lasted 2 seconds. After that duration, the green target reverted to grey and the trial concluded. The subject relaxed during the inter-trial interval of 1.5 – 2 seconds.

The subject moved three different “effectors” during the Go phase of this task. The first was “None”, meaning that nothing moved. The subject tried to make a whole arm movement during the Go phase, but nothing in the virtual world moved during that period. With the “Cursor” effector, the central green target was itself the effector. It moved to the peripheral target during the Go phase in a ballistic fashion under automatic computer control. At the start of the ITI, the Cursor effector turned back to grey and moved in a similar fashion back to its starting position at the center of the workspace.

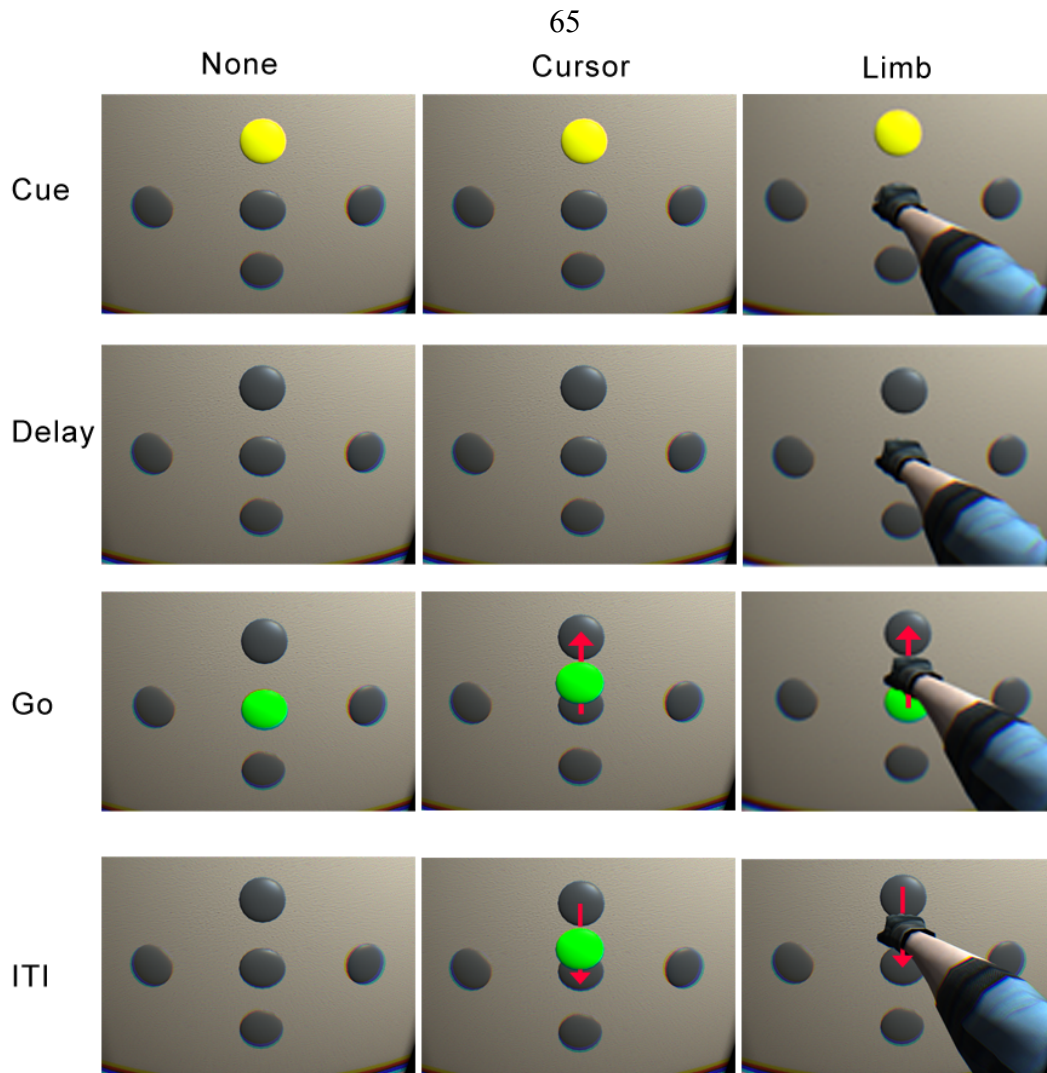


**Figure 4.1.2.3.1-2 Reaching Task Progression.** Rows show progression of task phases. Columns show the three different effectors that were used. Red arrows were added to emphasize motion but did not appear during task performance. Each image is the rendering taken from one eye (the left) only and cropped. See Video 4.1-1. Which effector to use was determined by blocking.

With the Limb effector, the avatar's right arm was held straight out with relaxed fingers, such that the knuckles were held just short of the central target. It remained in this posture throughout the Cue and Delay. During the Go phase, when the central target turned green, the arm made a ballistic movement towards the indicated peripheral target. At the start of the ITI (when the central target reverted to grey,) the arm moved back to the central position.

Effectors were compared in interleaved pairs: None versus Cursor, and Cursor versus Limb. The subject performed 4 trials, one in each direction with a given effector. Then, the effector was switched to the other in the pair being tested. Use of the Limb effector was clear because the Limb would remain in view. When the Limb effector was not being used, it returned to a relaxed position out of the subject's view. Switching between Cursor and No Effector was less obvious, but the subject would expect the Cursor to switch between being used (when compared with No Effector) every 4 trials. The pairs of comparisons were run in 2 blocks with 32 trials per block. This yielded 8 trials per target direction per effector for a session on a given day.

Offline decoding in this task was performed using a linear discriminant classifier to detect the direction of movement on each trial across a single session for a single effector. Data were preprocessed by summing all the spikes that occurred during the Go phase of each trial for that session. Cross validation was performed session-wise to test the generalization performance of the trained decoders on randomly and repeatedly selected held-out trials. These cross-validated estimates for each session were then pooled across sessions and compared across effectors.

#### **4.1.2.3.2 Limb Tuning Task**

This task consisted of repeated trials of viewing a movement by a computer rendered character on a (traditional, 2D) computer monitor and then repeating that movement. The subject was seated directly in front of a 27" widescreen LCD monitor.

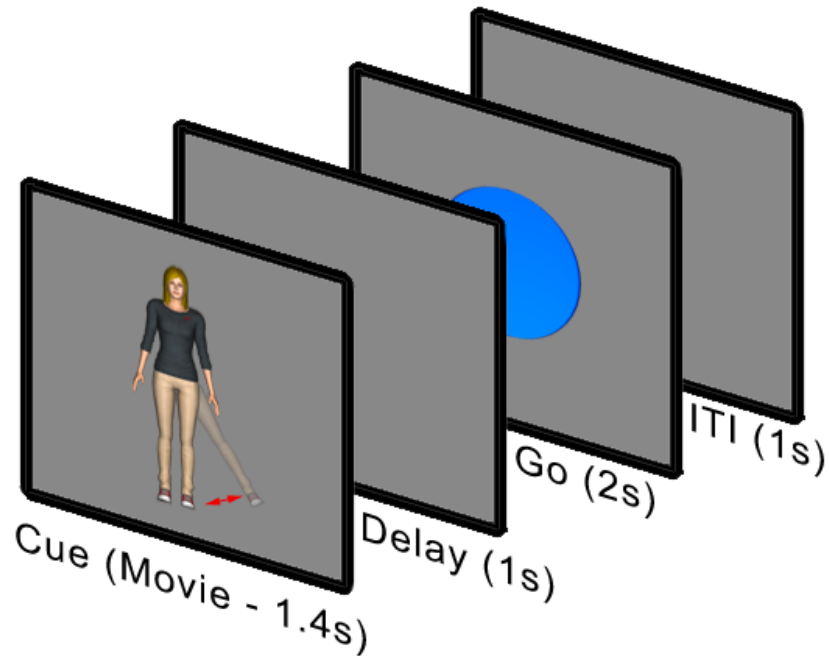


**Figure 4.1.2.3.2-1 Limb Tuning Task Diagram.** A snapshot of each phase of the task is shown. Time proceeds from left to right. The Cue phase consists of a movie of articulation of one joint. A ghosted frame of a leg movement trial and red arrow have been superimposed for illustration purposes.

A trial began (**Figure 4.1.2.3.2-1**) with a Cue Phase in which a computer generated female character appeared on the otherwise grey screen and immediately made a simple movement articulating one of 11 possible joints on either side (when applicable): wrist (pronation/supination), elbow (flexion/extension), shoulder (shrug), leg (abduction/adduction), knee (flexion/extension), or the neck (rotation). Each movement consisted of a simple back-and-forth motion. Motion amplitude varied from joint to joint for clarity. All movements lasted 1.4 s. When the movement was complete, the on-screen character disappeared. The screen remained blank for a one second (Delay Phase). After this Delay, a large blue circle appeared on the screen for two seconds (Go Phase). This was the subject's signal to attempt to execute the movement demonstrated earlier in the trial during the Cue Phase. The subject would attempt to repeat the movement using the corresponding part of her own body. After two seconds, the blue Go cue disappeared and

an inter-trial interval of 1 second occurred before the beginning of the next trial. After initial practice runs, the subject paced her movements to match the pacing demonstrated in the Cue phase. However, the Go phase was extended to about 2 seconds to allow for any variation and ensure the subject had adequate time to return attention to the screen to observe the end of the Go phase.

Due to her injury, the subject was only able to successfully perform the neck movements. All others were simply attempted in the absence of motor output. The subject mirrored the actions displayed by the on-screen character, e.g., the character moving its left wrist corresponded to the subject attempting to move her right wrist for that trial. Trials were run in 2 blocks of 55 yielding 10 trials per joint. Joint ordering was interleaved within each block. See videos for example stimuli (Video 4.1-2).

#### 4.1.2.3.3 Effector Specificity in Hand Gestures

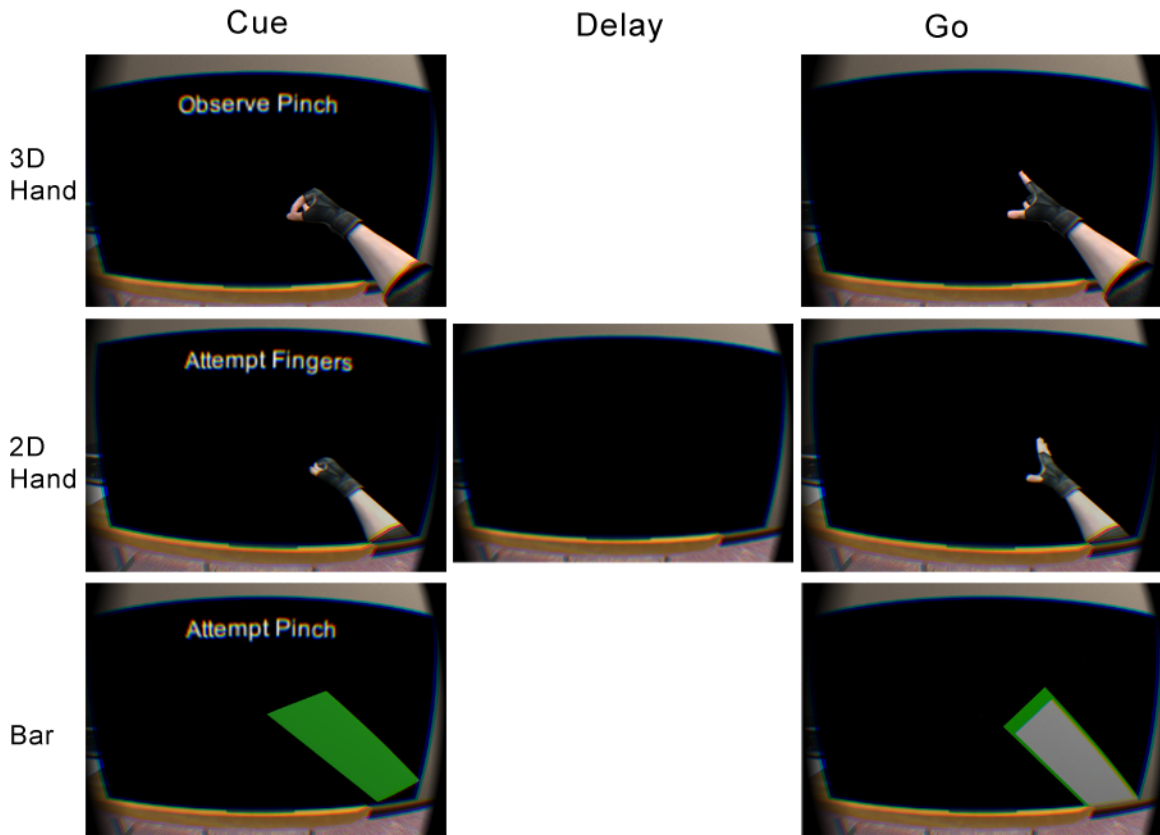


**Figure 4.1.2.3.2-1 Gesture Task Progression.** Screenshots taken from one eye during various phases (columns) and effectors (rows) in the Gesture Task. The Delay phase looked the same for all gestures. Screenshots are taken from only the left eye, but two independently rendered perspectives were presented to each of the subject’s eyes. Multiple gestures were performed (Pinch, Fingers, Flex, Roll,) but only Pinch and Fingers are pictured.

The Gesture Task compared observation and execution of (non-ballistic) hand movement as well as the relevance to such attempted movements of the effector being controlled. This task once again utilized the Oculus Rift DK2 virtual reality headset (see 4.1.2.2.1). For this task, the virtual environment also consisted of a small office. The subject was seated in front of a large virtual “screen” that occupied nearly the entire FOV (**Figure 4.1.2.3.2-1**). The subject’s virtual “body” or avatar in the task was in the seated position with arms

relaxed at the sides. It is important to emphasize that the “screen” referred to herein was a virtual representation of a large monitor placed in the VR environment—not the physical display in the headset. This virtual screen allowed the presentation of 2D images in a way that mimics the presentation of 2D images on a computer monitor. This was desirable to allow trial-by-trial variation of such flat, 2D images to a full 3D representation of an arm without the need to don and remove the physical virtual reality headset.

This task employed three different possible movement effectors: an abstract, 2D, green bar displayed on the virtual screen, a 2D arm presented on the virtual screen, and a 3D arm and arm “attached” to the subject’s avatar in the virtual environment. The 3D hand was lifted up when in use to appear between the subject’s viewpoint and virtual monitor. See videos for examples (Video 4.1-3). The virtual screen was scaled and placed such that all three effectors occupied similar size visual areas (**Figure 4.1.2.3.2-1**). The extra extent of the 3D arm that extended beyond the limits of the “virtual” monitor (thus making it slightly bigger than the 2D hand) was at or beyond the edge of the area of the head-mounted display that was visible to the subject. Thus the change in size between the 2D and 3D limbs were negligible.

The green bar is an abstract cue meant to correlate with the subject’s motion but not represent it explicitly. The “motion” of the abstract cue consisted of an expanding, inner, white rectangle that changed the bar from green to white (**Figure 4.1.2.3.2-1**, Video 4.1-3). The subject, through initial practice with the task, learned to perform the instructed

movements in sync with the expansion and contraction of the abstract cue. Thus, the timing of the subject's attempted movements was the same across all effectors. The 2D hand is an anthropomorphic but flat image of the hand not "attached" to the viewing subject that shows movements explicitly. The 3D limb is an anatomically correct 1st person view of an arm, i.e., the same view an individual typically has of their own arm when performing movements. They only differed in that one visualization was a disembodied, 2D representation of the hand while the other was an anatomically correct, 3D, fully embodied representation of the hand.

The trial structure of this task employed the same phases as tasks described above: Cue, Phase, Go, and ITI. During the 2s long Cue period, the subject was instructed 1) whether movement would be attempted or observed, 2) the hand gesture to be performed (or observed), and 3) which effector to use (or observe) for the movement. Whether or not to move was indicated by the word "Observe" or "Attempt" at the top of the virtual screen (**Figure 4.1.2.3.2-1**, left column). Which movement or gesture to make was indicated by the word "Flex", "Fingers", or "Roll" also appearing at the top of the monitor. "Flex" referred to flexion and extension of the wrist. "Fingers" referred to opening and closing the fingers into a fist or a squeezing gesture. "Roll" indicated pronation and supination of the hand and forearm. Which effector would be "used" during the motion was indicated by the appearance of one of the three possible effectors during the Cue: the green bar, the 2D hand on the virtual screen, or the 3D hand. During the Cue phase, the effector for the given trial simply appeared and disappeared without any motion occurring.

After the Cue phase, all the information just presented about the trial disappeared from the virtual screen for a 1 second Delay phase. In trials where the 3D limb was in use, it returned out of view to the resting position during the Delay. After the Delay phase, the effector specified for the given trial appeared, performed the gesture specified, and disappeared. All gestures took 2 seconds. During “Observe” trials, the subject was simply passively viewing the motion. During “Attempt” trials, the subject was actively trying to perform the motion along with the effector. For trials using the abstract green bar, the timing of the change from green to white and back to green was identical to that of the 2D or 3D hands performing their respective movements. The subject learned to associate the timing in preliminary training trials in which both the green bar and hand appeared. Once learned, the subject could easily recall the proper pacing of movement execution with only the abstract effector. For Observe trials in which the Bar effector was used, no gesture was applicable since the subject passively watched the Bar change color with no gesture attempted or implied.

Trials were run in 3 blocks of 56 with short breaks in between blocks. Effector and attempting/observing movement were interleaved within each block. Gestures (Flex, Fingers, or Roll) were separated across blocks as they were not compared directly. This yielded a total of 8 trials per effector per gesture per movement condition.

#### **4.1.2.3.4 Online Gesture Control**

To test whether closed-loop neural control would be influenced by the effector being used, we devised an online analog to the previous test. Here, a simple text-based task was used to train a binary classifier (**Figure 4.1.2.3.4-1**, top row). The text task, displayed using the HMD, consisted of a simple Cue-Delay-Go paradigm. The cue was a text instruction as to what gesture to perform: “squeeze” or “pinch”. Here, squeezing was identical to the “fingers” gesture in the previous task. This Cue was displayed for 1s, after which a Delay

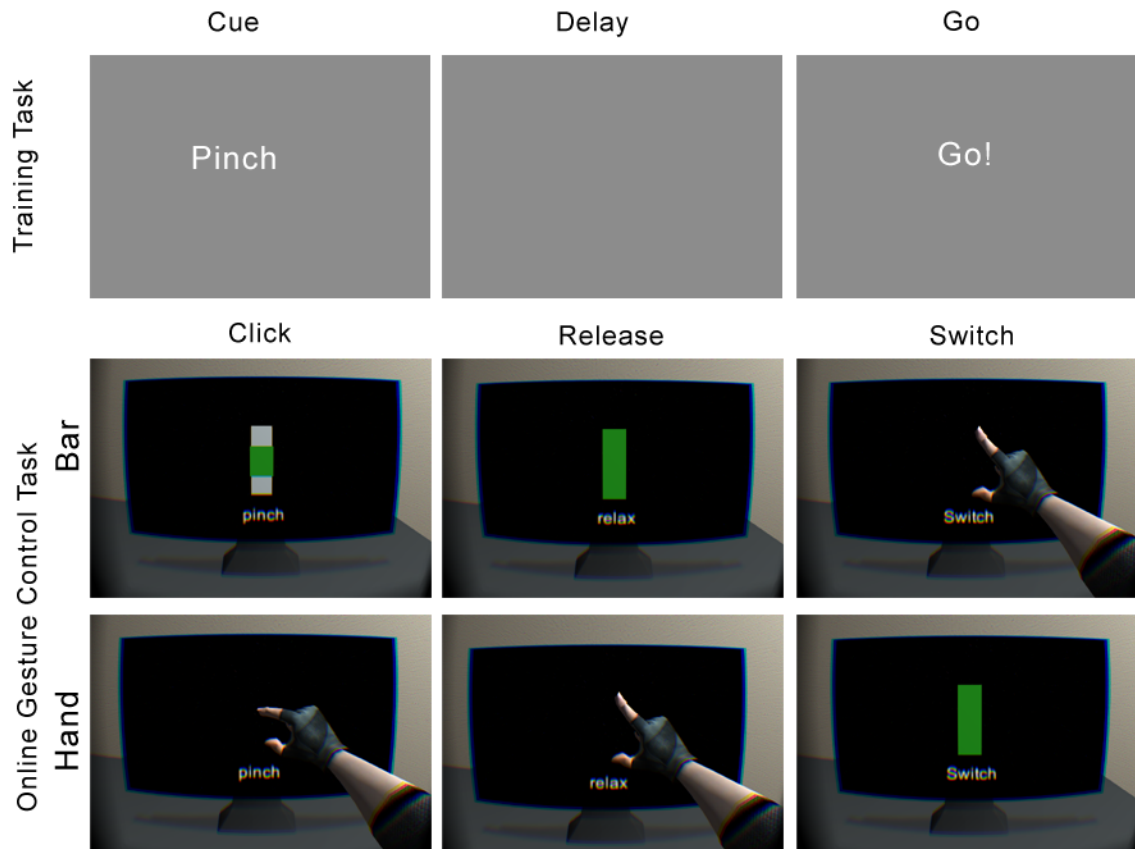


**Figure 4.1.2.3.4-1 Online Gesture Control Task And Training Task.** Top Row: Training Task. Text cues on an otherwise blank subject instruct the subject what action to perform (Cue Phase,) and when to perform it (Go phase.) Not shown is an inter-trial interval during which “relax” was displayed. Bottom two rows: Online Gesture Control task. A binary neural decoder controlled the aperture of either a green bar (middle row) or 1<sup>st</sup> person hand (bottom row). “Click” phase required the subject to perform the gesture and attempt to close the aperture for the duration of the phase. “Release” phase required doing nothing to obtain a maximally open aperture. Click and Release phases were performed in pairs of five for 4-5s each before switching to the other effector during a brief “Switch” phase. For both effectors, the halfway closed state is pictured for Click, and maximally open state is pictured for Release and Switch.

of 1-1.5s occurred. The Go phase was signaled by the appearance of the text “Go!” during which time the subject performed the indicated gesture for 2 seconds. An inter-trial interval of 3 seconds followed wherein the word “relax” appeared in place of the previous text cues. After the ITI, a new trial began. Ten trials per gesture were performed in an interleaved order. The text commands appeared in 3D using the HMD, but on an empty grey screen. Thus the text appeared to the subject to be “floating” in otherwise empty, grey space. This was done to facilitate easy shifting from this to the following task without the need to physically reconfigure equipment and don the HMD. The task itself did not necessitate any 3D component.

A linear classifier was then trained on the data for each gesture. Spikes from the latter 1s of the Go phase (“click” data) were summed for each channel (feature) and for each trial (observation). The null distribution (“release” or “relax” data) was taken from the middle 1s of the inter-trial interval. These two classes were fit with a linear classifier for each gesture. The classification performance was tested offline using cross validation. The gesture with the highest cross-validated performance was then used for the online portion of the task. For consistency across gestures, detecting the action being instructed will be referred to as a “click”, while not detecting performance of the gesture will be referred to as “release”.

The online control task consisted of a virtual environment of the same office and monitor used in the tasks in previous sections (**Figure 4.1.2.3.4-1**). In this task, the subject was

asked to repeatedly perform the gesture trained in the text training task while receiving closed-loop visual feedback about the decoding output from one of two possible virtual effectors: a green vertical bar displayed on the “virtual” monitor or the virtual avatar hand viewed from the first-person perspective.

Each trial consisted of one Click Phase and one Release Phase. A trial began with a 4-5s Click phase wherein the name of the gesture (“squeeze” or “pinch”) appeared on the virtual monitor within the environment, instructing the subject to perform the gesture. The subject tried to actively perform the gesture for the duration of the phase. A 4-5s Release phase followed during which the subject could relax and stop performing the gesture. The word “relax” appeared in the same location for the duration of the phase. No explicit inter-trial interval was used for this task. The Release phase served a similar function.

Five trials were performed with each effector before a 5s “Switch” phase occurred. The current effector disappeared from the screen, and the other appeared in the fully “released” state. During the Switch Phase, the effector did not change as a function of the decoder output and remained still in the fully “open” or released state. After the Switch phase, another block of 5 trials began. This alternation was performed 4 times per run. At least two runs per session were performed, yielding at least 20 click and release trials per session.

The decoder inferred the subject’s motor intention (Click or Release) every 50ms throughout the task (except during the Switch phase) using the last 1 second of spike data.

If the decoder decoded that the gesture was being performed (a “click”), the hand effector responded by closing the aperture for the current gesture. For pinching, this meant the hand would move the thumb and index finger closer together. If the hand and thumb were already at their maximal proximity, the hand remained in that state. If no performance of the gesture was detected by the classifier (a “release”), the hand effector was moved closer to the fully open or relaxed confirmation. For the pinching, this meant thumb and index finger maximally spread apart. Again, the release state was limited once the fully open conformation was reached (**Figure 4.1.2.3.4-1**, bottom row, middle panel).

When using the bar effector, a “click” resulted in shrinking of the bar. The lower limit of the bar size was a small sliver. Decoding “release” resulted in expansion of the bar until its maximum vertical extent was reached (**Figure 4.1.2.3.4-1**, middle row, middle panel). Both the hand effector (for all gestures) and bar effectors were broken up into 20 evenly spaced intervals for control. For example, to go from fully open to fully closed, the decoder would need to output “click” for 20 consecutive time bins (50ms/time bin, therefore 1 second). The size of the bar was adjusted so that its vertical visual extent matched the aperture of the hand when fully open for both squeeze and pinch (Video 4.1-4).

### **4.1.3 Results**

#### **4.1.3.1 Delayed Reach Task**

In this task, reaches in the vertical plane were attempted in a Delayed Reach style paradigm. Three different effectors were used and moved (by automatic computer control) during the Go phase to provide simulated effector feedback during the attempted movement. The three effectors were “none”, meaning no actual effector moved or was present, a cursor effector, or a full anatomically correct limb effector viewed from the 1<sup>st</sup> person (**Figure 4.1.2.3.1-2**).

The offline decoding performance summary is shown in **Figure 4.1.3.1-1**, left panel. Neural data for decoding was taken from the last 1.25 seconds of the Go phase. A substantial and significant increase in cross-validated offline decoding performance of the reach target was observed for the cursor (mean = 75.83% +/- 5.3% s.d.) over no movement

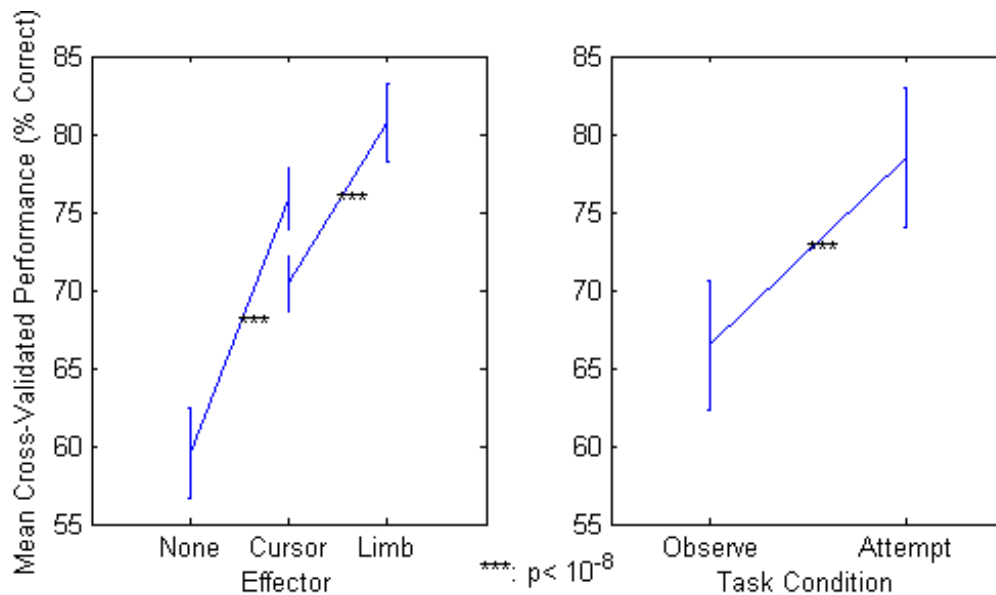


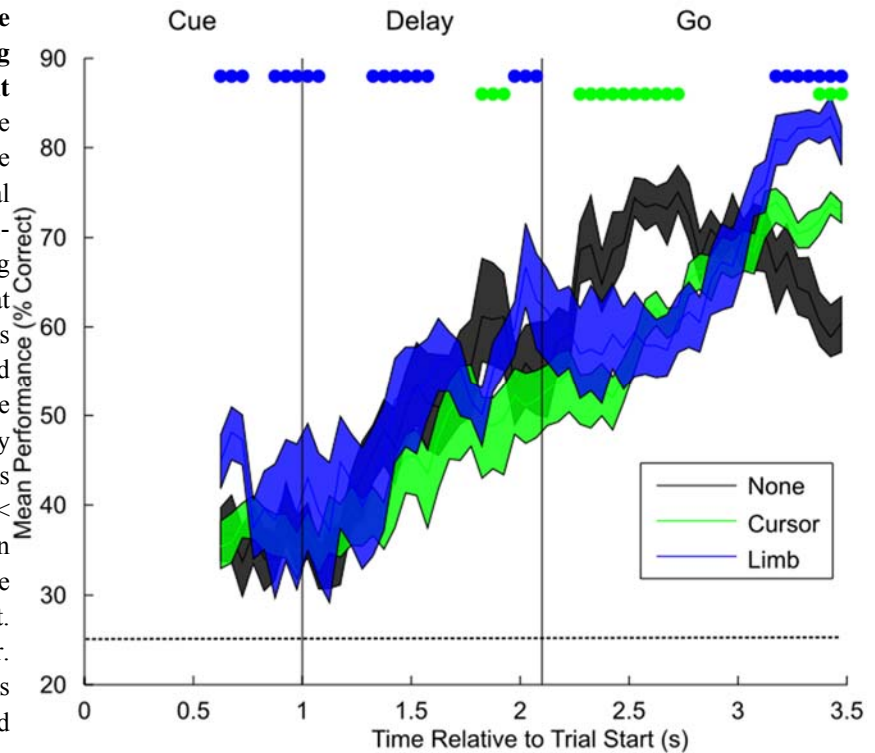
**Figure 4.1.3.1-1 Delayed Reaching Task Offline Decoding Performance.** Left Panel: Performance by effector. Mean cross-validated performance and its 95% confidence interval is plotted for each effector. The cursor effector appears twice in the plot because the effectors were compared using independent pairwise comparisons (None vs. Cursor and Cursor vs. Limb.) Horizontal lines join the means for each pair. Data for each item plotted was taken from 96 trials collected across 3 sessions run on different days. Right Panel: Decoding performance of trials with passive observation vs. normal task performance with the Limb effector. This indicated substantial visual tuning to the Limb even in the absence of overt movement. N = 240 trials per category. Chance performance (not shown) is 25% given that there are 4 possible targets.

effector at all (mean = 59.58% +/- 7.7% s.d.,  $p < 10^{-10}$ , T test), and an increase was observed for the limb effector (mean = 80.72% +/- 6.8% s.d.) over the cursor effector (mean = 70.41% +/- 4.83% s.d.,  $p < 10^{-8}$ , T test). The cursor effector appears twice in this plot because the effectors were compared in a pairwise manner independently for each pair. All effectors greatly exceeded chance level of 25%. For detailed decoding statistics and tuning properties of the neural population, see Appendix A.2.

Part of this performance difference could be accounted for by the simple influence of visual motion during the Go phase when the Cursor or Limb effectors are used. When no effector is present, there was no visual motion during the Go phase. Thus, any spatially tuned neurons selective for visual motion would express a difference with moving effectors. Thus, we also compared the decoding of which target was used on a given trial in another way (**Figure 4.1.3.1-1**, right panel). We interleaved regular trials with the Limb effector (“Attempt trials”) with “Observe” trials in which the subject simply watched the effector perform the movements to the four targets. Performance of decoding the spatial target during these trials (mean = 67.18% +/- 11.97 s.d.), while substantially above chance level of 25%, was significantly less than during Attempt trials (mean = 78.36% +/- 12.73 s.d.,  $p < 10^{-12}$ , T test.)

**Figure 4.1.3.1-2 Time Course of Decoding Performance Throughout the Trial.**

Each band is the bootstrapped ninety-five percent confidence interval of the mean of the cross-validated decoding performance for that effector. Decoding is averaged across trials and shown throughout the three task phases, divided by vertical black lines. Dots above bands indicate  $p < 0.05$  after FDR correction of  $p$  values of two-sample Kolmogorov-Smirnov test. Blue dots: Limb vs Cursor. Green dots: Cursor vs None. Horizontal dotted line indicates chance level.



We also examined the offline decoding performance as a function of the time window used for neural decoding (Figure 4.1.3.1-2). Cross-validated decoding performance was calculated based on a 1.25 s wide sliding window with a step size of one time bin (0.05s). FDR-corrected significance testing was performed using the two-sample Kolmogorov-Smirnov test. Durations not exceeding significance for at least 3 consecutive time bins were thrown out. This analysis revealed that, while the decoding performance at the end of the Go phase (the same shown in Figure 4.1.3.1-1) had one ordering, performance immediately after the Go cue actually had a different arrangement. At that time, having no effector actually yielded the best decoding performance, and there was no difference between the Cursor and Limb. This result suggested that the “better” decoding for the Cursor and Limb at the end of the Go phase was either a function of the visual feedback received during that part of the trial or somehow delayed the expression of the motor plan in the neural

responses. It is also interesting to note, however, that target decoding performance was slightly but significantly better during the earlier parts of the trial (Cue and Delay) for the Limb over the Cursor, despite the lack of target specific visual information during those task phases.

These results indicated that, though there was a strong visual component for when the first-person limb moved around the screen with no contribution from the subject, attempting to move the arm to the current target was reflected in the neural activity. This enhanced response, even if it was visual, was more pronounced for a whole limb than a floating cursor. However, an alternative explanation of simple visual tuning could have (though did not necessarily) accounted for these results. Determining how exactly that feedback affected the responses required a more finely tuned examination in the subsequent tasks.

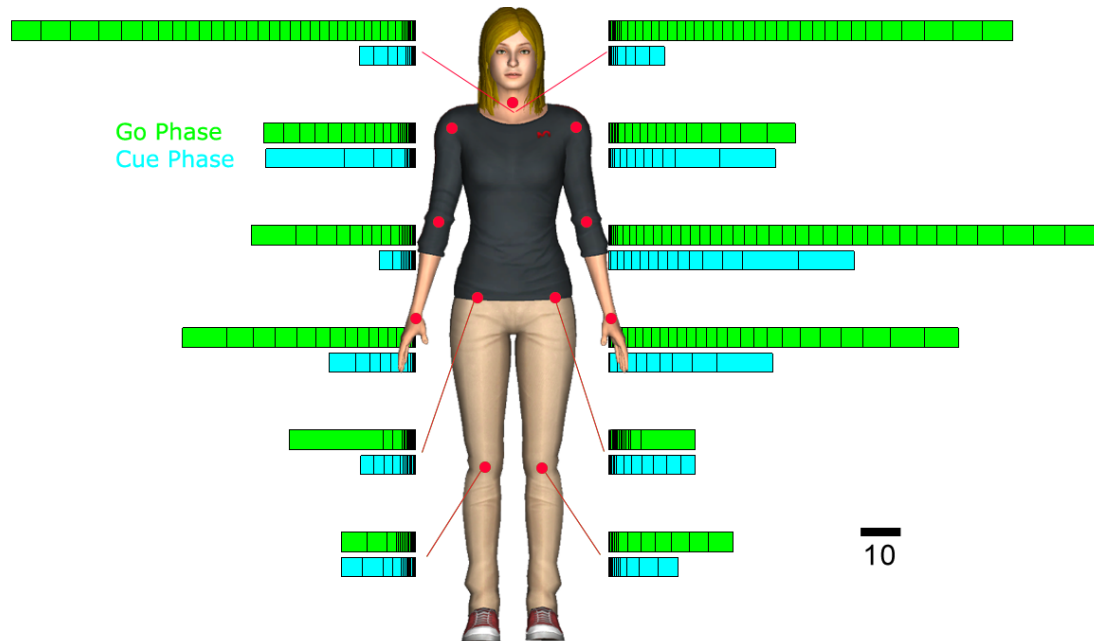


**Figure 4.1.3.1-3 Limb Tuning Task Results.** The figure illustrates the spiking responses during the Limb Tuning Task. Each block or section within within each row of blocks represents one neural unit that was significantly modulated for that particular joint for that phase when compared to its firing rate during the ITI. The width of each block represents the ratio of the firing rate during the indicated phase (Cue, cyan, or Go, green) to the average firing rate during the ITI for that particular unit. A block, shown for scale, corresponds to the width of a block if the unit it represented fired 10x more spikes for a given condition than it did during the ITI. The character used for cueing is reproduced and movement joints highlighted with red dots (and lines where needed for clarification). The responses for the neck joint have been doubled on either side to aid visual comparison. Note that the subject mirrored the cued joints, so the character's left side corresponds to the subject's right side. Also note that the same neural unit can be represented in any row (but not more than once per row.)

#### 4.1.3.2 Limb Tuning Task

In order to determine if tuning to the Limb effector in the prior task resulted from sensitivity to any anthropomorphic body parts or specifically to the hand, we designed a follow-up task to address differences in tuning between viewing and attempting to move different body parts. The Limb Tuning task required the subject to watch a brief movie of a computer generated character perform a simple, one-joint, back-and-forth motion, then repeat that movement after a delay (**Figure 4.1.2.3.2-1**). We compared neural responses to the various joints by simply comparing the total number of units activated by a given effector during

either the Cue phase or Go phase (Figure 4.1.3.1-3). Activation was measured per neural unit per joint by comparing the number of spikes fired during the Cue and Go phases for that joint to the number of spikes fired during the inter-trial intervals for that unit with a Mann-Whitney U test. If that neuron had a  $p$  value of less than .05 for that phase and for that joint, the ratio of the average firing rate for that phase to the average rate during the ITI was taken and included further analysis. The ratios of neurons meeting this criterion for any effector for any trial phase are pictured in Figure 4.1.3.1-3. Each neuron could be included in the pool for either phase for any joint. The exact  $p$  value used was not critical here, as we were interested in the relationships between numbers of neurons exceeding threshold in subsequent comparisons.

We then compared the numbers of units passing this test between task phases and between joints. We found more units tuned to movements and cueing of the subject's right side than left ( $p = .02$ ), more units responding during the movement period than the Cue period ( $p = .00014$ ), and more units preferring movement and cueing of the arms versus the legs ( $p = .019$ , Mann-Whitney U test.) These patterns are evident in the figure. The only joint the subject could actually move was the neck joint, so it is unsurprising that neck trials are relatively overrepresented relative to other joints (but only during the Go phase). Additionally, movement of the neck resulted in movement of the subject's gaze away from the screen, which could have further enhanced the responses of any visually sensitive neurons specifically during the Go phase of neck trials. This pattern of responses supported the notion that the neurons recorded by the implant are movement and arm tuned with a

bias towards the subject's right arm. This bias was true when attempting movements with no visual feedback regarding the movement, or when watching the on-screen character perform the movements.

#### **4.1.3.3 Gesture Task**

The Gesture Task required observing or attempting motion (“Movement Condition”) with three different movement Effectors (a green bar, 2D hand, 3D hand) in one of 4 possible previously learned gestures. In this task, we found both local field potentials as well as single neurons responding preferentially to the 3D hand in the LFPs and both the 2D and 3D hands in the spike activity.

##### **4.1.3.3.1 LFP Response**

The local field potentials reflected different aspects of the task in different frequency bands. LFP power in the beta band (15Hz-35Hz) and gamma band (60Hz-100Hz) were computed and averaged across all electrodes on the recording array. Power between 0.25s and 1s after the start of each phase was averaged for each trial. Multiple linear regression was performed on the averaged power for each band for each phase. The p values reported in the following paragraphs all refer to the significance of the F tests for that model.

The beta band significantly responded to whether a trial was an Observe or Attempt trial (Movement Condition) during all three phases of the trial ( $p \ll 10^{-10}$ , **Figure 4.1.3.3.1-1**). Power in the beta band was high between trials and dropped at the onset of the Cue. For Attempt trials, it remained low throughout the trial. For the Observe trials, the beta band power quickly recovered after onset of the Cue to nearly the same level as during the inter-trial interval. The beta band was not significantly tuned to effectors in the Delay or Go phase. The beta band's response to the 3D Hand did just barely reach significance for the Cue phase ( $\beta = -0.05$ ,  $p = 0.0496$ ). For both Observe and Attempt trials, the beta band remained at a constant level and dipped only slightly at the onset of the Go phase. The beta band has been reported to drop on the onset of movement and remain high between trials

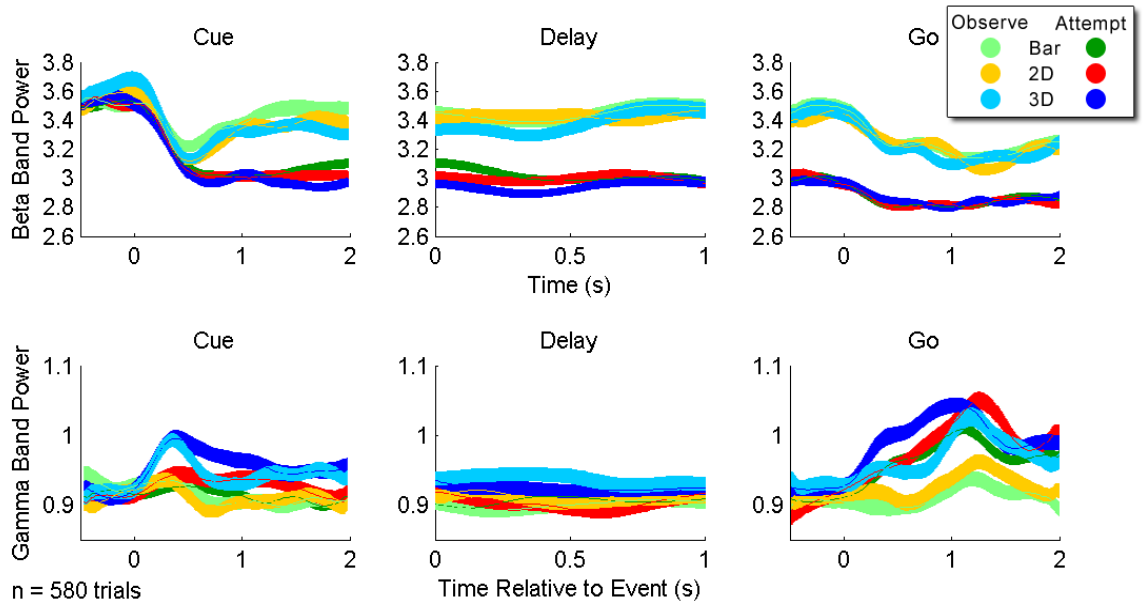


**Figure 4.1.3.3.1-1 Responses in the Local Field Potentials of Array 1 to Task Variables.** Power in the Beta Band (top row) and Gamma Band (bottom row) averaged across all electrodes on Array 1 are shown aligned to the onset of the Cue phase (left column), Delay phase (middle), and Go phase (right column). The beta band reflected Movement Condition (Attempt or Observe) in all three phases ( $p \ll 10^{-10}$ , multiple linear regression, all phases), whereas the gamma band was tuned to the Effector during all phases ( $p \ll .001$ , multiple linear regression, all phases) as well as Movement Condition during Cue ( $p < 10^{-5}$ ) Go ( $p < 10^{-25}$ ). Width of each trace corresponds to standard error of the mean. Responses are averaged across  $N = 580$  trials.

previously in non-human primates (Hwang and Andersen 2009, Scherberger, Jarvis, and Andersen 2005). It is worth noting that this dip still occurred even during Observe trials when no movement was attempted by the subject.

We ran a separate regression that incorporated trial phase in addition to the other task variables to test differences in power across phases. Relative to the Cue phase, beta band was significantly elevated during the Delay phase ( $\beta = 0.043$ ,  $p = 0.0072$ ) and attenuated during the Go phase ( $\beta = -0.15$ ,  $p < 10^{-23}$ ). See Supplementary Figure C-1.

The gamma band was also tuned to Movement Condition, but only for the Cue and Go phases ( $\beta = 0.021$ ,  $p < 10^{-5}$  and  $\beta = 0.064$ ,  $p < 10^{-25}$ , respectively.) As opposed to the beta band which contained higher power during Observe trials, the gamma band was activated more strongly for Attempt trials. It was also significantly modulated by only the 3D Hand throughout all trials (Cue phase:  $\beta = 0.052$ ,  $p < 10^{-15}$ ; Delay phase:  $\beta = 0.023$ ,  $p < 10^{-4}$ ; Go phase:  $\beta = 0.048$ ,  $p < 10^{-11}$ ). It was not significantly modulated by the 2D Hand in any phase. Though the effect appears to trend in a graded fashion from bar to 2D hand to 3D hand, the signal-to-noise of LFPs and number of trials recorded may have prevented this difference from reaching statistical significance. Curiously, the beta band also showed this stepped (but not significant) trend in its response during the Delay period (**Figure 4.1.3.3.1-1**, top row, middle panel).

As with the beta band, we tested for meaningful modulation in the gamma band across phases, which seemed apparent. Unlike the beta band, the gamma band was, relative to the Cue phase, attenuated during the Delay phase ( $\beta = -0.023$ ,  $p < 10^{-8}$ ) but then enhanced during the Go phase ( $\beta = 0.023$ ,  $p < 10^{-8}$ ).

Array 2, located a few centimeters away (Appendix B), did not record any spiking activity. However, the beta band recorded on that array (Figure C-2) during performance of the task followed nearly the same pattern described above. While highly tuned for Movement Condition in all three phases (Cue Phase:  $\beta = 0.090$ ,  $p = 0.0013$ ; Delay phase:  $\beta = 0.26$ ,  $p < 10^{-15}$ ; Go phase:  $\beta = 0.32$ ,  $p < 10^{-22}$ ) the beta band on this array was only selective for the Effector (both 2D,  $\beta = -.072$ ,  $p = 0.028$  and 3D limb,  $\beta = -.074$ ,  $p = 0.024$ ) during the Cue phase. The confidence intervals for  $\beta$  for the 2D and 3D hands overlapped, so the beta band was equally activated for either the 2D or 3D hands during the Cue phase on this array. It has been observed that power in the gamma band of the LFP correlates well with multi-unit spiking activity recorded in the same area (Berens et al. 2008). Therefore, it is unsurprising that Array 2, because it was unable to pick up spike activity, showed minimal responsiveness to the task in the gamma band (Figure C-2 and Figure C-3).

#### **4.1.3.3.2 Single/Multi-Unit Response**

Four example sorted units are shown in Figure 4.1.3.3.2-1. We observed two main classes of neurons. The first class echoed the gamma band response of the LFP (Figure 4.1.3.3.2-1, top two rows). The second class preferentially responded to Observation of either the 2D

or 3D Hands (Figure 4.1.3.3.2-1, bottom two rows). To quantify these responses across the population, we applied generalized linear regression (Poisson distribution, logistic link function) to the responses for each sorted neural (single or multi) unit. Because we were not specifically concerned with differences in responses to the different hand gestures, responses to each gesture were analyzed separately for each unit to preserve statistical power. Direct comparisons across gestures were not made. The analysis was restricted to neural responses during the Go phase.

We compared the distributions of the absolute values of beta coefficients for the 2D and 3D hands for all recorded units that were significantly modulated by at least one hand effector for at least one gesture. While these distributions are already (by definition) likely to be different from zero, the distributions for the 2D hand ( $m = 0.21$ ,  $sd = 0.21$ ) and 3D hand ( $m = 0.26$   $s.d. = 0.27$ ) were also significantly different from each other ( $p = 0.018$ , two-sample Kolmogorov-Smirnov test). This suggests that the population was potentiated by the 2D hand relative to the bar, and even more so for the 3D hand relative to the 2D hand. This stepped population response, visible in the example units in the Figure 4.1.3.3.2-1, matches that of the gamma band in the LFPs, though the gamma response to

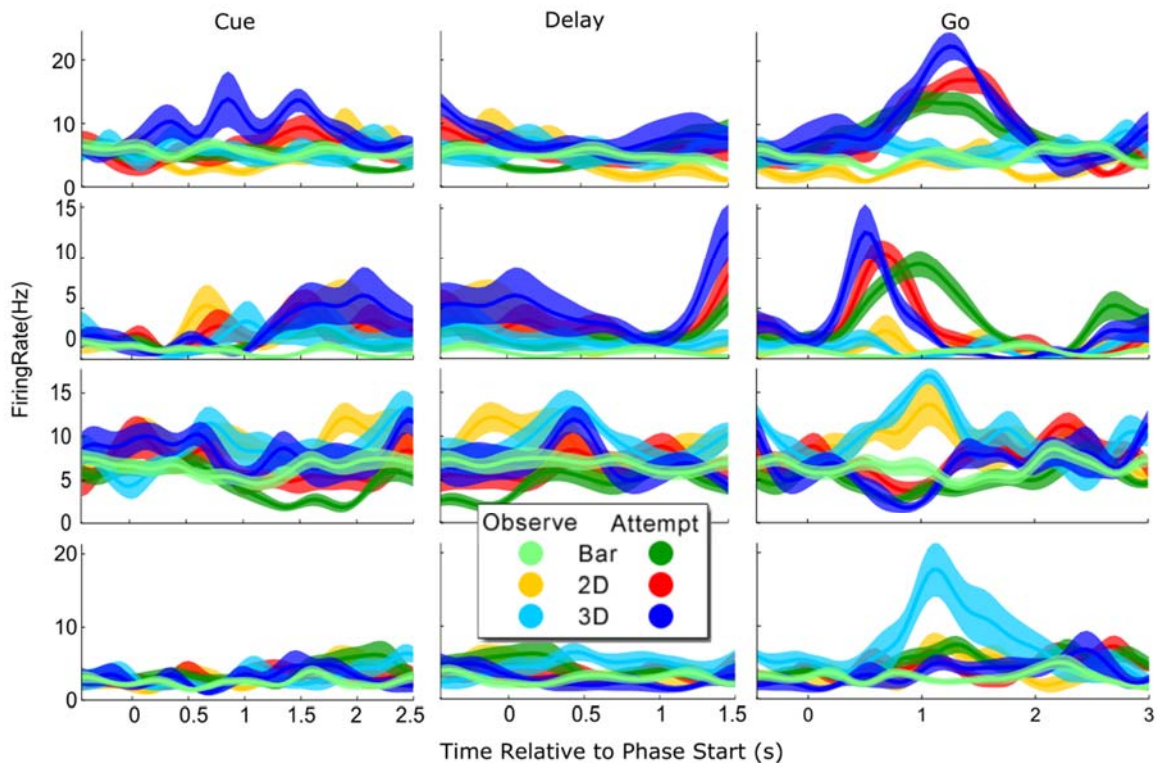


**Figure 4.1.3.3.2-1 Example Neural Responses during the Gesture Task.** Four example neurons' responses to the Gesture task during the Cue, Delay, and Go phases. Each row is one unit's response to  $n = 8$  trials under the color-coded condition. Trace widths are standard error of the mean. Color scheme is the same as Figure 4.1.3.3.1-1. All neurons shown showed significant modulation ( $p < 0.05$ , multiple linear regression, FDR corrected) for Movement Condition (Observe vs Attempt) and 3D Limb (relative to the Bar) after FDR controlled significance testing. The unit in the row 3 was also significantly activated by the 2D hand relative to the Bar.

the 2D hand did not reach significance. Individual neurons preferring the 2D Hand or even Bar did exist, but they were relatively rare.

We examined the distribution of beta coefficients for Movement Condition for all units with significant modulation to that variable. While applying the criterion of significance ensures the beta coefficients will have a distribution *not* centered on zero, it is nonetheless informative to determine the sign of the divergence from zero. The distribution had a mean of 0.17 and s.d. of 0.53, indicating a bias towards potentiation for Attempt rather than Observe Trials. However, 37.7% of the significantly tuned coefficients were nonetheless less than 0. These Observe-preferring neurons were common amongst the tuned population, and also showed a strong bias to observing the 2D or 3D Hand. Two such units are shown in Figure 4.1.3.3.2-1 (bottom two rows).

#### **4.1.3.4 Online Gesture Control Task**

The preference found for representation of and visual feedback regarding the hands in previous tasks lends itself to an additional question. Will these tuning properties have any effect during online decoding of movement intentions? In other words, will performing closed-loop control of a hand improve decoding? To this end, we designed the closed-loop,

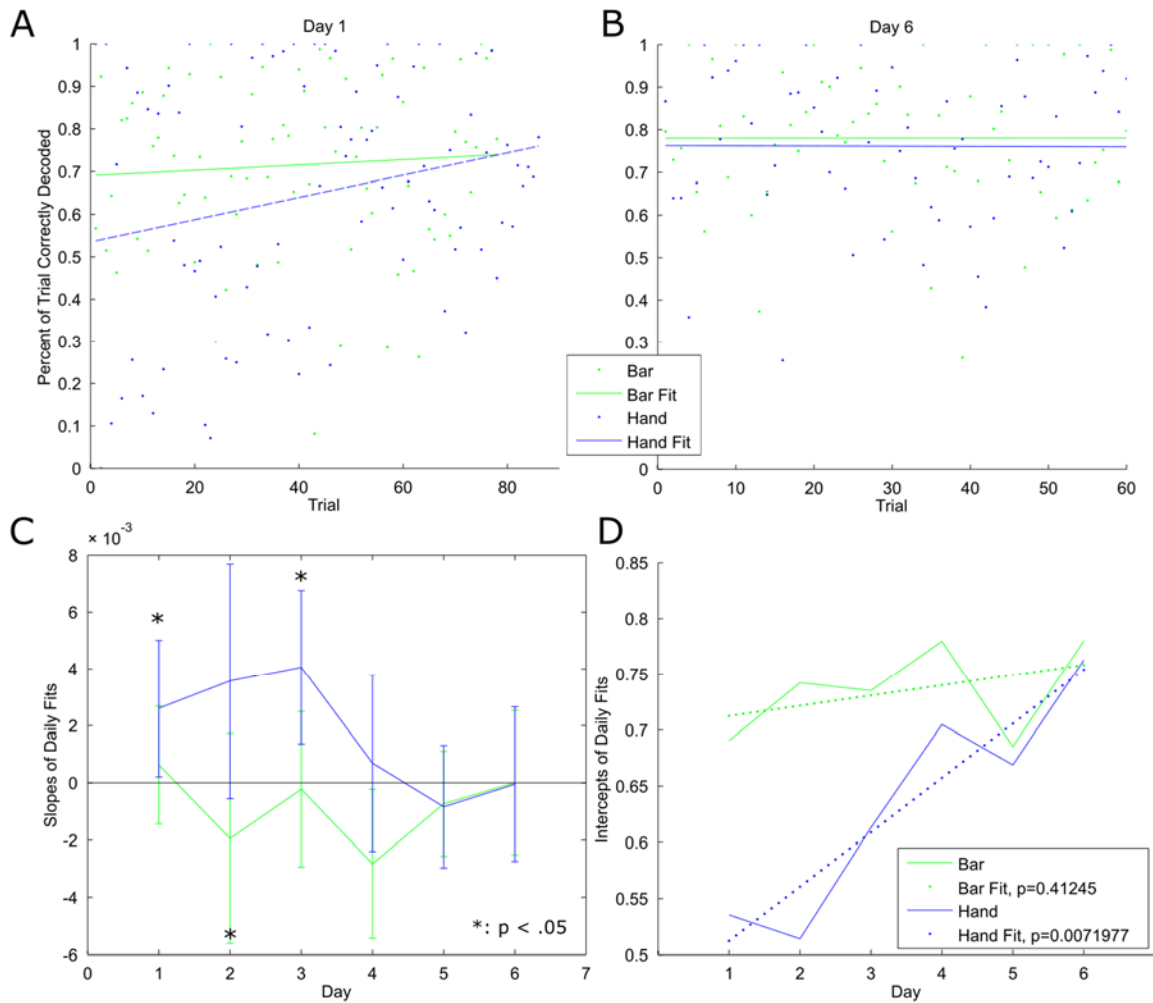


**Figure 4.1.3.4-1 Online Gesture Control Performance Summary.** **A,B** Because effector actuation was decoded in 50ms bins for each trial phase lasting 4-5s, it was possible to calculate the number of bins in each phase (Click or Release) that decoded the correct action for that phase. Each dot is thus the percentage of bins in a given phase that were (correctly) decoded as the instructed action. Lines represent linear fits. Slope of broken lines differs significantly from 0. For all panels, blue corresponds to Hand trials, green to Bar trials. **C** Slopes and their corresponding 95% confidence intervals for daily performance linear fits segregated by effector. Asterisks denote days wherein slope of fit for indicated effector significantly differed from zero. **D** Daily initial performance represented by intercept of the daily linear fit segregated by effector. Intercepts for Bar trials did not change significantly, but intercepts for the Hand fits did ( $p = 0.0072$ ). First and last data points in **C, D** correspond to panels **A, B**.

online analog of the Gesture Task (4.1.2.3.4). Here, we found significant improvements in decode performance within and across days when controlling the Hand, but not the Bar.

The first several days showed a clear trend wherein the subject's neural control of the hand was poor, but noticeably improved throughout the day. Linear fits of performance for each effector for each day revealed that (**Figure 4.1.3.4-1**) performance within a day either improved significantly (Days 1 and 3) or remained equal for the Hand and decreased significantly (Day 2) or remained roughly equal for the Bar. On days 3 and 4, performance during the last 20 trials of the day was significantly better for the Hand than the Bar ( $p < .05$ , ANOVA), despite having the reverse (but not significant) trend at the start of the day.

Across all days, the slopes for the fits for Hand trials (blue trace) were significantly greater than the slopes for the Bar trials (green trace,  $p = 0.028$ , ANOVA, **Figure 4.1.3.4-1, C**). Overall, this pattern indicated a change in neural control was occurring within the course of a day. These changes only manifested as increased performance for the Hand and decreased performance for the Bar. But, this initial disparity in performance went away across days. By Day 6, the initial performance of the Hand was equal to that of the Bar, and performance did not change for either effector. This effect is discernible overall in the changes in slopes and intercepts of the fit lines across days (**Figure 4.1.3.4-1, C and D**). Thus, though control of the Hand started out poorer, it seemed to improve both within and across days to the point where no difference was measured. It should be noted that the initial superior performance of the abstract effector seems to contradict the earlier result

with the Delayed Reach task (4.1.3.1) wherein offline performance seemed to be superior. The result in the current task supports interpreting the former result an artifact of differing degrees of visual feedback during the task. The current task is more likely to accurately reflect the nature of closed-loop effector control.

Individual (unsorted) spiking channels used by the decoders were observed to alter their firing from the initial 20 trials of a session to the last 20 trials. Firing rates were calculated in 50ms bins for each Click and Release phase for each trial separated by effector. Firing rates were smoothed and compared in each time bin with a paired sample t-test. Groups of time bins meeting the threshold of  $p = 0.05$  were included only if at least 5 contiguous time bins exceeded the threshold. Two example channels are shown (**Figure 4.1.3.4-2**). In the first example channel (**Figure 4.1.3.4-2**, top 4 panels), the channel's firing rate was attenuated during the course of the day exclusively for the Click phase of trials using the

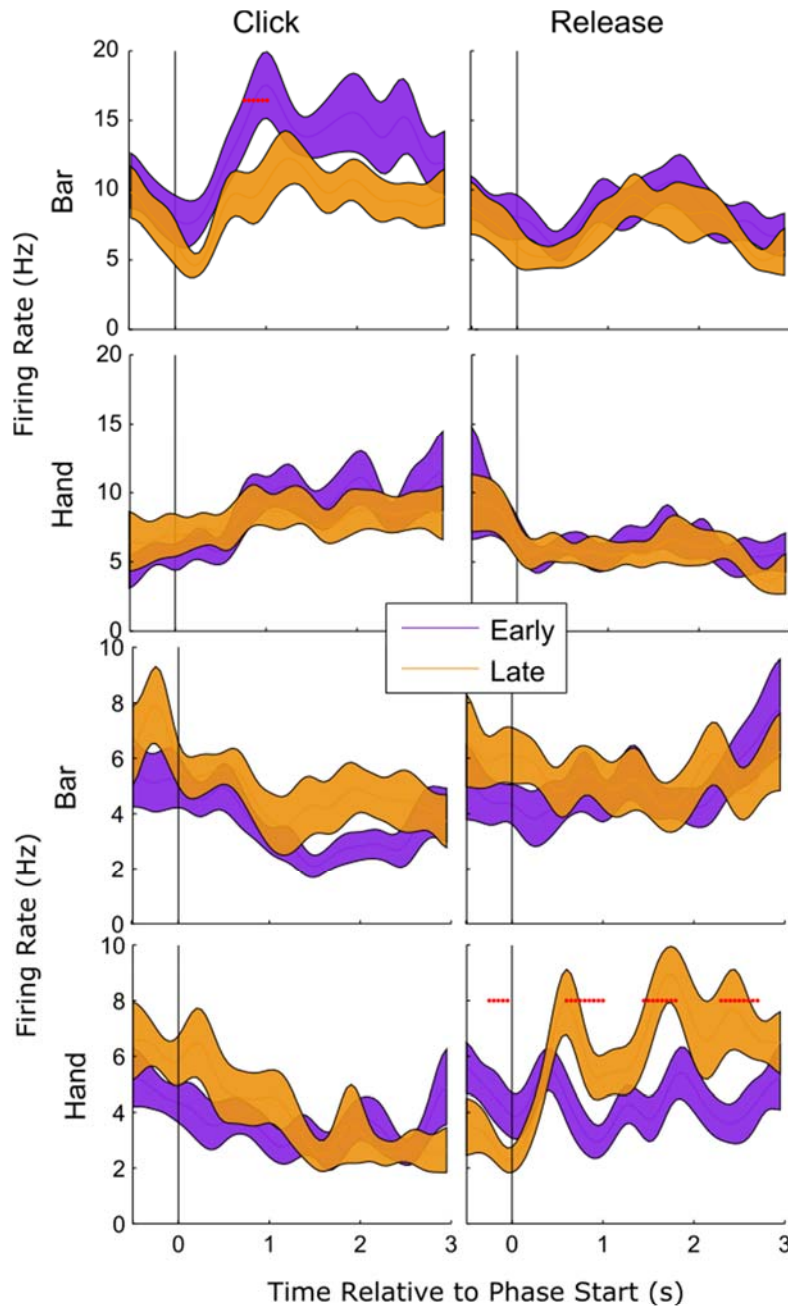


**Figure 4.1.3.4-2 Change in Activity of Units Used For Decoding.** PSTHs of two example units used for decoding during the Online Gesture Control Task. Traces represent smoothed firing rates averaged across first (purple) and last (orange) 20 trials of the respective unit's sessions. Traces are separated by Effector and Phase for each unit. Red dots above traces indicate significant difference ( $p < 0.05$ ) according to a paired sample t test. Top 4 panels correspond to one spiking channel. Bottom 4 panels are a second example. Width of each patch corresponds to bootstrapped 95% confidence interval of the mean. We believe the same units were recorded due to consistency of most tuning properties.

Bar effector (top left panel). The second example neural channel (bottom 4 panel) potentiated its response exclusively during the Release phase of Hand trials (bottom right panel).

#### 4.1.4 Discussion

Throughout these tasks, the first-order component of the neural responses was the presence or absence of an intended movement by the subject. A significant but second-order component was the “handness” of the movement effector.

These results were reflected in both the spike activity and local field potentials of the recorded signals.

In the Gesture Task, we observed a partial dissociation of task variables with respect to the two bands of the LFP investigated. The beta band on both recording arrays was tuned to Movement Condition through all phases of the Gesture Task, but just barely reached significance during the Cue phase for Effector specificity. The gamma band, on the other hand, was tuned to Movement Condition during only the Cue and Go phases, but highly significantly tuned to the Effector throughout the task phases. The gamma band was most active during the Cue and Go phases, while the beta band was most highly activated during the Delay phase. This pattern of results for the beta band dovetails with the growing body of evidence for the notion that beta band activity plays a broad inhibitory or movement withholding related across far flung sections of cortex (de Hemptinne et al. 2013, Engel and Fries 2010) and also does so in the parietal areas. This result also constitutes the first report of field potentials recorded with extracellular electrodes in human parietal cortex.

The responses of neurons at the single-unit level largely mirrored the structure of the response of the gamma band response in the LFP. While activated more highly in trials wherein movement was attempted, neurons also showed sensitivity to the effector and showed a preference for the hand effectors. There was also a further increase in neural unit responses between the 2D, disembodied representation of the hand to an anatomically correct, first-person view of a 3D hand attached to the subject's virtual body. This graded

response was also a visible trend in response of the gamma band of the LFP, but the difference between the 2D and 3D hands did not reach significance (possibly due to the lower SNR of LFP recordings).

Additionally, neurons were found that responded preferentially to observation of hand movement when the subject intended no movement. While this pattern of tuning makes it unlikely that they contributed to decoding, their presence suggests interesting possible functions of the areas recorded in monitoring the motion of others.

Results during the Online Gesture Control further strengthened the notion that neurons recorded in this area are specialized for control of hands. Neural control, though initially poorer for the anthropomorphic Hand than the abstract Bar, significantly improved within and across days. This suggests that the neurons being used for online control were a part of a feedback control loop that adjusted the neural response throughout the day for the preferred effector. The net effect of these changes was to influence the decoder such that the desired state of the end effector was achieved more consistently.

It is possible that these changes in individual neurons used for decoding may have also occurred in neurons not directly used for decoding. This would account for the improvement across days. Because neurons detectable by the recording electrodes varied with days and even hours, it is highly unlikely that same neurons were used for decoding across the month long period throughout which experimental sessions were carried out.

While the daily improvements were a relatively robust effect, it is possible the random shuffling in the recorded neural population across experimental weeks may have driven the apparent long term learning effect across sessions. More data and repetition with other subjects will help determine which the case is.

This pattern of results suggested that, by using fMRI to target hand movement signals in the parietal cortex, we were able to target neural signals specialized for motor control and feedback. These areas, while preferentially tuned to movement of the contralateral arm itself, also appeared to incorporate visual information regarding the state of that (virtual) limb. The response of the signals in the area seemed to have a bias for anthropomorphic looking hand effectors rather than cursors or other abstract representations of movement. It is plausible that this bias was the result of years of specialization of the area to feedback control of the hand acquired throughout life, despite the patient's loss of motor control years prior. Motor cortex has also been found to retain tuning even years after high spinal cord injury resulting in tetraplegia (Truccolo et al. 2008).

The pattern observed in the various tasks indicate that, while decoding intended movement of a hand endpoint effector may activate an endogenous self-monitoring feedback loop, *not* doing so by using an abstract effector did not handicap decoding. As the Online Gesture Task demonstrated, performance of the abstract effector started out high and remained that way across days. The decoders, trained daily on a text-based open-loop task, may therefore

be able to capture a “pure” motor intention before information on the specific nature of the effector has any influence on the neural activity.

#### 4.1.5 References

- Aflalo, T. N. S., R. A. Andersen, S. Kellis, and C. Klaes. in press. "Decoding Motor Imagery from the Posterior Parietal Cortex of a Tetraplegic Human." *Science*.
- Andersen, R. A., S. Kellis, C. Klaes, and T. Aflalo. 2014. "Toward more versatile and intuitive cortical brain-machine interfaces." *Curr Biol* 24 (18):R885-97. doi: 10.1016/j.cub.2014.07.068.
- Banakou, D., R. Groten, and M. Slater. 2013. "Illusory ownership of a virtual child body causes overestimation of object sizes and implicit attitude changes." *Proc Natl Acad Sci U S A* 110 (31):12846-51. doi: 10.1073/pnas.1306779110.
- Berens, P., G. A. Keliris, A. S. Ecker, N. K. Logothetis, and A. S. Tolias. 2008. "Comparing the feature selectivity of the gamma-band of the local field potential and the underlying spiking activity in primate visual cortex." *Front Syst Neurosci* 2:2. doi: 10.3389/neuro.06.002.2008.
- Collinger, J. L., B. Wodlinger, J. E. Downey, W. Wang, E. C. Tyler-Kabara, D. J. Weber, A. J. McMorland, M. Velliste, M. L. Boninger, and A. B. Schwartz. 2013. "High-performance neuroprosthetic control by an individual with tetraplegia." *Lancet* 381 (9866):557-64. doi: 10.1016/S0140-6736(12)61816-9.
- de Hemptinne, C., E. S. Ryapolova-Webb, E. L. Air, P. A. Garcia, K. J. Miller, J. G. Ojemann, J. L. Ostrem, N. B. Galifianakis, and P. A. Starr. 2013. "Exaggerated phase-amplitude coupling in the primary motor cortex in Parkinson disease." *Proc Natl Acad Sci U S A* 110 (12):4780-5. doi: 10.1073/pnas.1214546110.
- Engel, A. K., and P. Fries. 2010. "Beta-band oscillations \textemdash signalling the status quo?" *Current opinion in neurobiology*.
- Graziano, M. S., D. F. Cooke, and C. S. Taylor. 2000. "Coding the location of the arm by sight." *Science* 290 (5497):1782-6.
- Hauschild, M., G. H. Mulliken, I. Fineman, G. E. Loeb, and R. A. Andersen. 2012. "Cognitive signals for brain-machine interfaces in posterior parietal cortex include continuous 3D trajectory commands." *Proc Natl Acad Sci U S A* 109 (42):17075-80. doi: 10.1073/pnas.1215092109.
- Hochberg, Leigh R., Mijail D. Serruya, Gerhard M. Friehs, Jon A. Mukand, Maryam Saleh, Abraham H. Caplan, Almut Branner, David Chen, Richard D. Penn, and John P. Donoghue. 2006. "Neuronal ensemble control of prosthetic devices by a human with tetraplegia." *Nature* 442 (7099):164--171.
- Hwang, E. J., and R. A. Andersen. 2009. "Brain Control of Movement Execution Onset Using Local Field Potentials in Posterior Parietal Cortex." *Journal of Neuroscience* 29 (45):14363-14370. doi: Doi 10.1523/Jneurosci.2081-09.2009.
- Iriki, A., M. Tanaka, S. Obayashi, and Y. Iwamura. 2001. "Self-images in the video monitor coded by monkey intraparietal neurons." *Neurosci Res* 40 (2):163-73.
- Jones, E. G., and T. P. S. Powell. 1969. "CONNEXIONS OF THE SOMATIC SENSORY CORTEX OF THE RHESUS MONKEY." *Brain* 92 (3):477-502.

- Kalaska, J. F., R. Caminiti, and A. P. Georgopoulos. 1983. "Cortical mechanisms related to the direction of two-dimensional arm movements: relations in parietal area 5 and comparison with motor cortex." *Exp Brain Res* 51 (2):247-60.
- Kim, S. P., J. D. Simeral, L. R. Hochberg, J. P. Donoghue, G. M. Friehs, and M. J. Black. 2011. "Point-and-click cursor control with an intracortical neural interface system by humans with tetraplegia." *IEEE Trans Neural Syst Rehabil Eng* 19 (2):193-203. doi: 10.1109/TNSRE.2011.2107750.
- Mountcastle, V.B., J. C. Lynch, A. Georgopoulos, H. Sakata, and C. Acuna. 1975. "Posterior parietal association cortex of the monkey: command functions for operations within extrapersonal space." *Journal of Neurophysiology* 38 (4):871-908.
- Mulliken, G. H., S. Musallam, and R. A. Andersen. 2008b. "Forward estimation of movement state in posterior parietal cortex." *Proc Natl Acad Sci U S A* 105 (24):8170-7. doi: 10.1073/pnas.0802602105.
- Revechkis, B., T. N. Aflalo, S. Kellis, N. Pouratian, and R. A. Andersen. 2014. "Parietal neural prosthetic control of a computer cursor in a graphical-user-interface task." *J Neural Eng* 11 (6):066014. doi: 10.1088/1741-2560/11/6/066014.
- Rizzolatti, G., L. Fogassi, and V. Gallese. 1997. "Parietal cortex: from sight to action." *Curr Opin Neurobiol* 7 (4):562-7.
- Sakata, H., Y. Takaoka, A. Kawarasaki, and H. Shibutani. 1973. "Somatosensory properties of neurons in the superior parietal cortex (area 5) of the rhesus monkey." *Brain Research*.
- Scherberger, Hansjrg, Murray R. Jarvis, and Richard A. Andersen. 2005. "Cortical Local Field Potential Encodes Movement Intentions in the Posterior Parietal Cortex." *Neuron* 46 (2):347--354.
- Seal, J., C. Gross, and B. Bioulac. 1982. "Activity of Neurons in Area-5 during a Simple Arm Movement in Monkeys before and after Deafferentation of the Trained Limb." *Brain Research* 250 (2):229-243. doi: Doi 10.1016/0006-8993(82)90417-6.
- Truccolo, W., G. M. Friehs, J. P. Donoghue, and L. R. Hochberg. 2008. "Primary Motor Cortex Tuning to Intended Movement Kinematics in Humans with Tetraplegia." *Journal of Neuroscience* 28 (5):1163--1178.

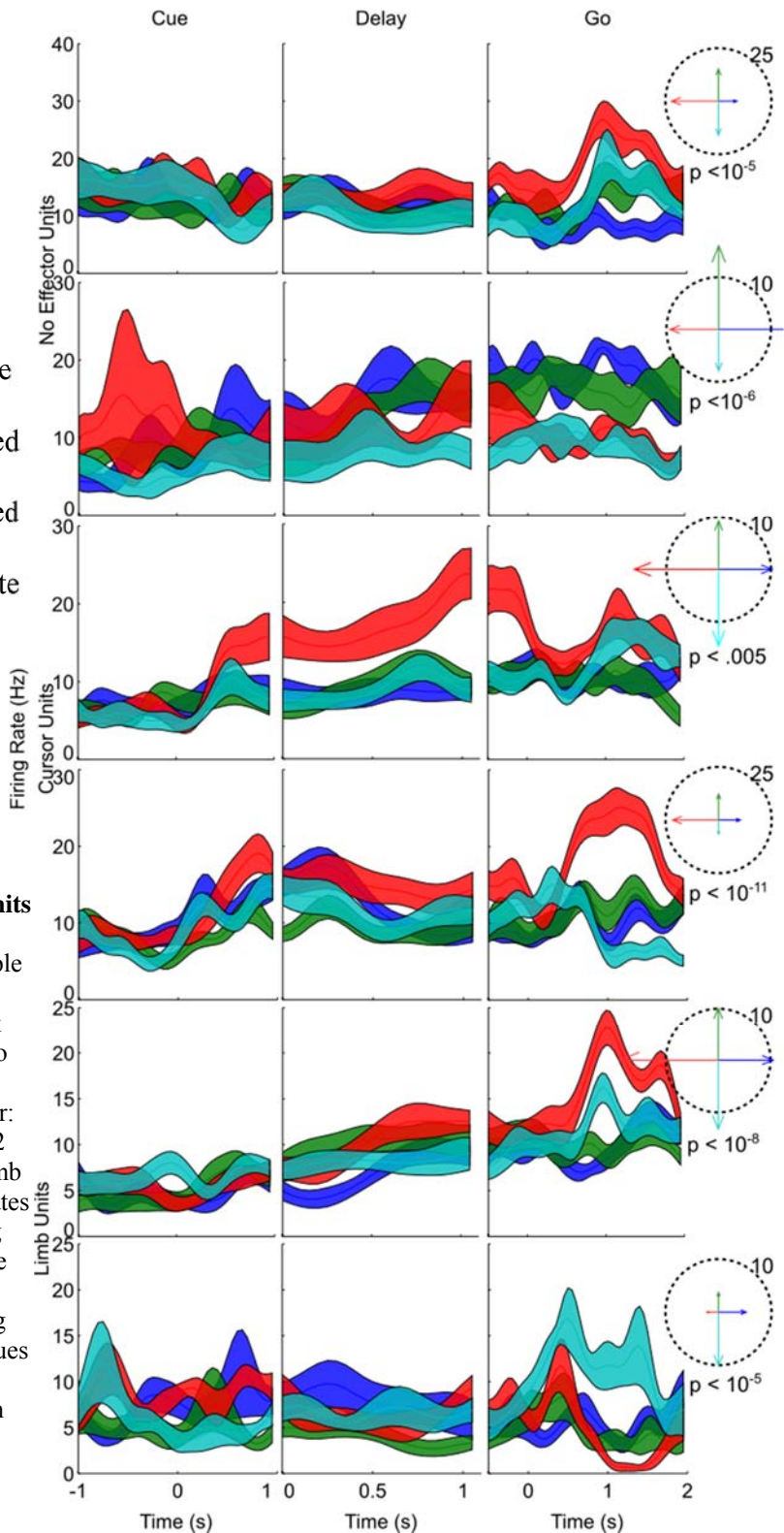
**Appendices**

**A. Tuning and Decoding Properties of Neural Populations**

**1. Human Neural Population**

Before inclusion in offline decoder for the Delayed Reach task, units were tested for minimum firing rate differences of 1 Hz between at least 2 targets. Across days and

**Figure A-1 PSTHs of Tuned Units Used for Offline Decoding of Delayed Reach Task.** Six example traces of firing rate for each of 4 targets in the Delayed Reach task aligned to the Cue, Delay, and Go phases. Each pair of rows corresponds to a different effector: top 2 rows: No Effector, middle 2 rows: Cursor, bottom 2 rows: Limb effector. Inset: Each arrow indicates magnitude of neural firing during Go for that neuron for trials in the arrow's direction. Dotted circle denotes noted magnitude of firing rate at the indicated radius. P values shown correspond to one-way ANOVA applied to firing rates in compass plot.



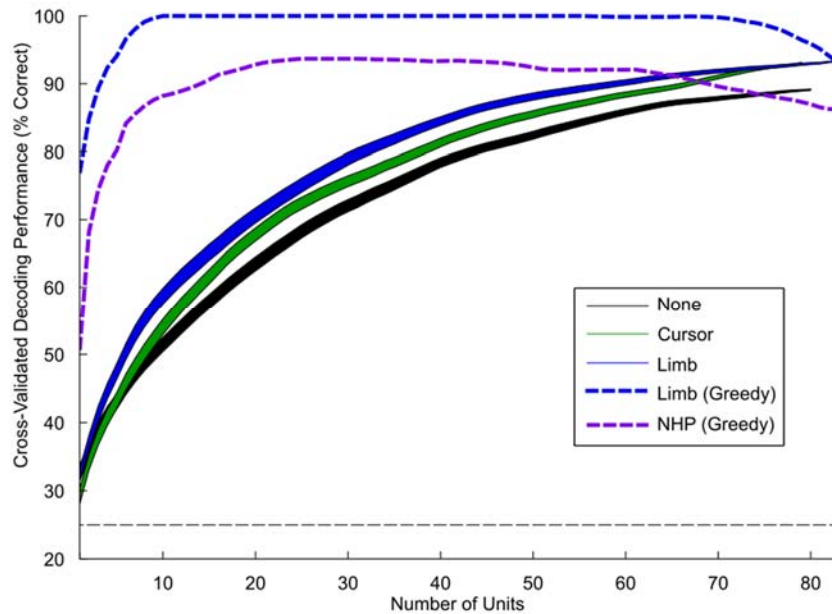


**Figure A-1 Neuron Dropping Curves for Delayed Reach Task By Effector.** Spiking (single and multi) units across 3 days were pooled performance was calculated by selecting features at random (solid ribbons) or greedily (dashed lines). Random feature selection was repeated 100 times per effector. Width of ribbon indicates standard error. Average result is shown. Dashed lines represent greedy feature selection performed once (pooling all days) and smoothed for human subject data with the limb, and for comparison, with NHP data in a similar task (See Appendix A.2). Chance level of 25% is indicated by the horizontal dashed line. Actual daily identified units averaged 25 and yielded approximately the same performance range (Figure 4.1.3.1-1) indicated by this curve in the 20 – 30 unit range. Time windows for spikes were the first 1.25 s of the Go period for No effector, and the last 1.25s of the Go period for the Cursor and Limb effectors. These time windows were chosen for peak performance per effector. See Figure 4.1.3.1-2.

effectors, an average of 25 +/- 4.57 s.d. spiking (single or multi) units were identified for offline decoding of reach direction. The inclusion criteria caused an average of 60% of the units used in decoding to pass significance testing on a single channel level when tested later (Figure A-1).

We calculated neuron dropping curves using both random and greedy feature selection (Figure A-1) by pooling neurons recorded during performance of the Delayed Reach task across three days. The same relationship between effectors was observed if optimal decoding windows were chosen for each. We also compare these results to neuron dropping

curves calculated for a similar delayed center-out reaching task for the NHP data from Chapter 3. Trials were randomly sub selected to match the number of trials performed with the human subject. Because the NHP implant had a higher neural yield, only 1 days' worth of data was required to match the information content of 3 days' worth of neural signals from the human subject.

## 2. NHP Neural Population

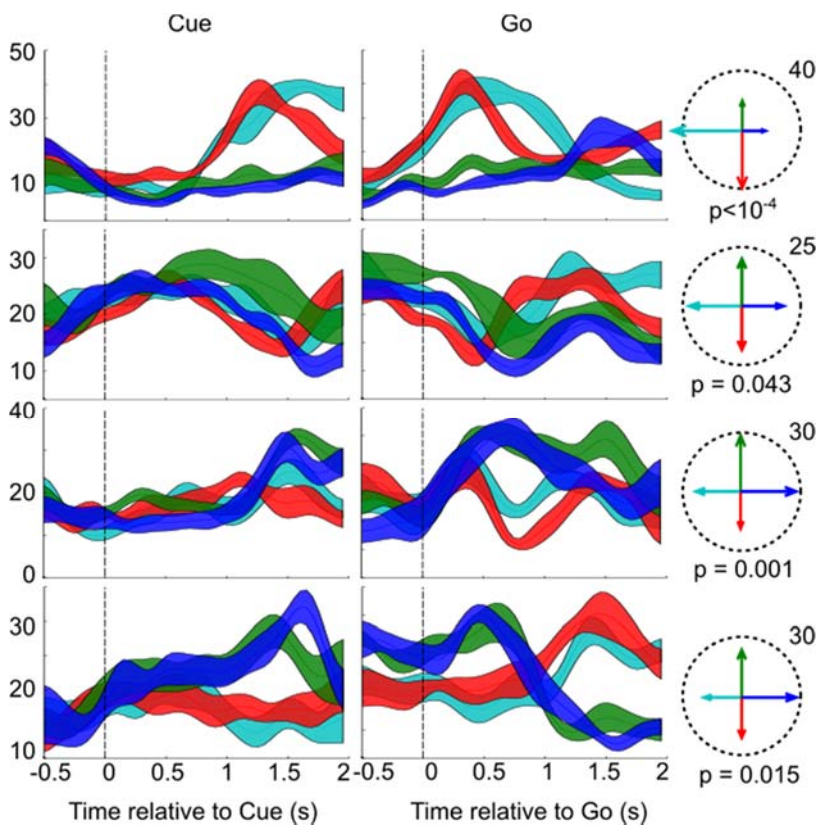


**Figure A-2 PSTHs of Tuned Neurons Recorded during a Delayed Reach Center-Out Task.** PSTHs as in Figure A-1 of neurons recorded during manual performance of a similar Center-Out Delayed Reach task performed with a primate.

For comparison, example neural units from a primate task (similar to the Delayed Reach task performed with the human subject) are shown in Figure A-2. This task also involved

Cue, Delay, and Go phases, but the trial target was not extinguished during the delay period. Thus, Cue and Delay are shown as one phase in the figure.

## **B. Clinical Implant Targeting Methodology**

The following task descriptions and results are adapted with permission from “Aflalo, Bonaiuto, and Andersen. *Functional Localization for Neuroprosthetic Control. Poster presented at: Society for Neuroscience 2012; November 13 2013; Washington, D.C.*” and T. Aflalo (*personal communication*). The scanner used was a Siemens Tim-Trio 3 Tesla MR scanner with an 8 channel head coil. Anatomical sequence: T1-weighted MP-RAGE sequence (TR = 1590 ms; TE = 2.7ms; fov = 176 x 256 x 256 mm; 1 mm isotropic voxels). Functional sequence; T2\*-weighted single-shot echo-planar acquisition sequence (TR = 2000 ms; slice thickness = 3 mm; in-plane resolution = 3x3mm; TE = 30ms; flip angle = 80; fov = 192 x 192mm; matrix size = 64 x64; 33 slices (no-gap) oriented 20 degrees relative to ACPC line). Signals were analyzed with GLM using AFNI’s afni\_proc.py processing pipeline. Functional runs were slice scan-time corrected, 3D motion corrected, spatially smoothed (4 mm full-width half-max), masked to only include voxels within the brain, converted to percent signal change, and detrended. Predictors aligned to stimulus onset were generated with AFNI’s BLOCK function with two second duration. Motion correction parameters were included in the regression models. All statistical maps were created with an FDR correct of  $q \leq 0.05$ . Freesurfer (<http://surfer.nmr.mgh.harvard.edu/>) was used for cortical surface reconstructions.

Three tasks were performed while the clinical subject underwent functional MRI scanning to localize areas in the parietal cortex specifically tuned for reaching. Task stimuli and instructions were presented on an LCD monitor. Gaze position was tracked to ensure task compliance.

Task 1 consisted of a simple, red or green circle cue appearing periodically on the screen while the subject was scanned. When the green circle was on the screen, the subject was instructed to attempt to reach out towards the screen. When the circle was red, the subject was instructed to relax. The subject also relaxed between presentations of the colored circles. BOLD signal was compared between the green and red circle conditions (Figure B-2, A).

Task 2 presented the subject with either scrambled or whole images of every-day, graspable objects. When the image was scrambled, the subject was instructed to identify the object. When the image was whole, the subject was asked to imagine reaching out and grasping the object. The graspable objects consisted of tools, utensils, and other small objects. For this task, the BOLD signal was compared between grasping trials and identification/looking trials (Figure B-2, B).

Task 3 consisted of several more phases (Figure B-1). A trial began with the subject fixating on a central dot for 3 seconds. The subject was asked to maintain fixation throughout each trial, the Rest phase excepted. Next, during the Cue phase, a single letter instruction “R” or “A”, appeared at the middle of the screen for 1 second. The Stimulus phase followed, during which the subject was presented with two rods presented to the left and right of fixation. One rod was broken and the other was whole. For R trials, the subject imagined reaching with the right arm to grasp the (unbroken) rod. The subject was to

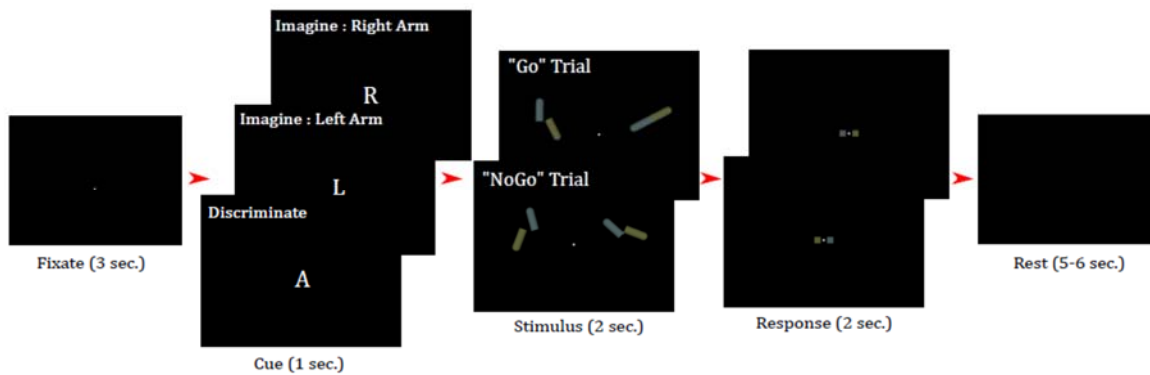


**Figure B-1 Targeting Task 3 Schematic.** Task Progression of Targeting Task 3. Figure reproduced with permission from “Aflalo, Bonaiuto, and Andersen. Functional Localization for Neuroprosthetic Control. Poster presented at: Society for Neuroscience 2012; November 13 2013; Washington, D.C.”. “L” trials were excluded as we targeted the left hemisphere (right arm) only. Response phase was only used during pre-scan behavioral training.

imagine grasping the rod in the most comfortable hand orientation possible. During the Response phase that followed, the subject reported verbally whether her thumb pointed to the left or to the right when imagining grasping the rod. On intermittent “No Go” trials,

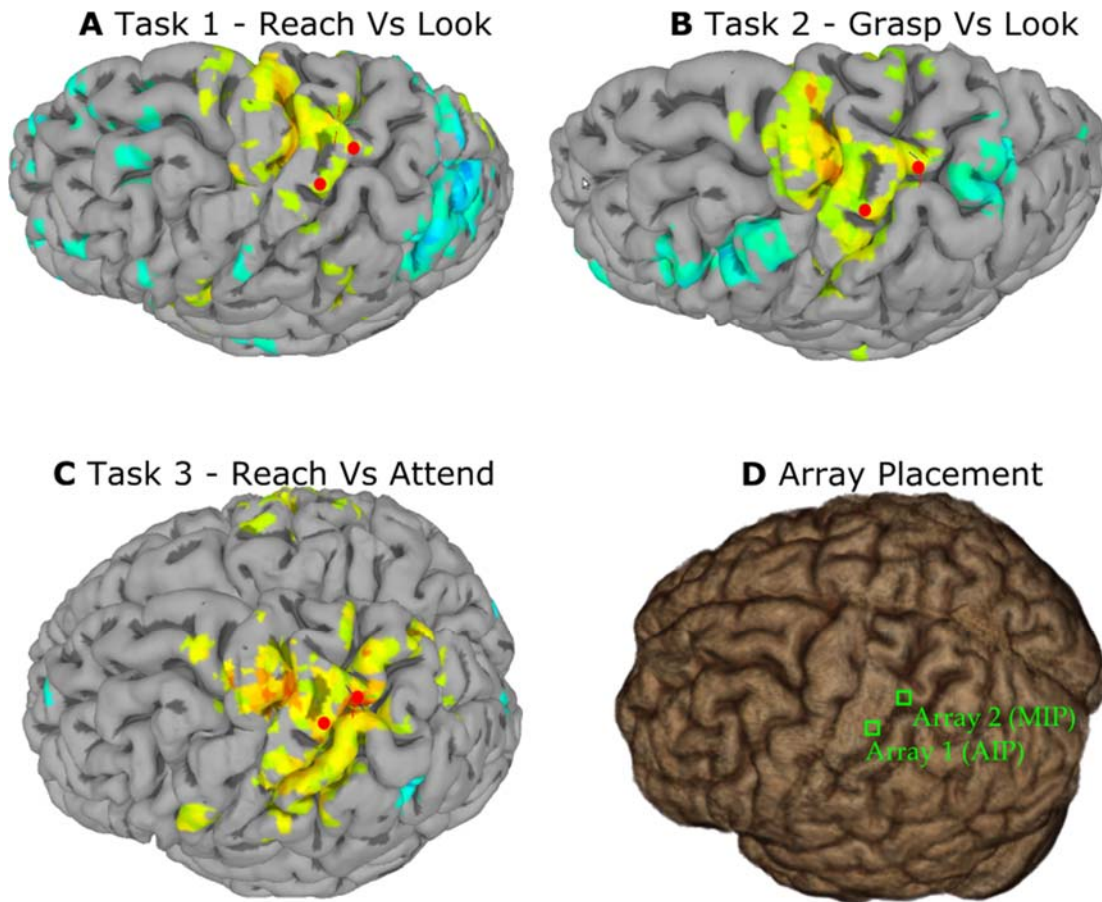


**Figure B-2 fMRI Results and Array Implant Locations.** A,B,C Results from fMRI tasks overlaid on 3D reconstruction of the subject's brain. Hotter colors indicate greater magnitude BOLD activation. All colored areas were significantly modulated by the condition indicated (after FDR correct with  $\alpha = .05$ ). **D** Reconstructed anatomical scan. **A** and **B** show left hemisphere only. **C** and **D** show the entire brain. Approximate array implant locations are overlaid as red dots in **A,B,C** and indicated with green squares in **D**. Array 1 had electrodes with 1.0mm long shanks. Array 2 had 1.5mm long shanks.

both rods appeared broken. The subject was instructed to simply maintain fixation during these trials. The subject was only asked to make a verbal response during a behavioral training set of sessions. The subject's behavior was confirmed to be accurate in these sessions. In the scanner, the response phase was skipped and the subject's behavior was assumed to be correct.

If the A cue appeared during the Cue phase (“A” for “attend”), the subject was asked to make a sensory discrimination during the Stimulus phase. Specifically, the subject was to determine which half of the unbroken rod, blue or green, was brighter. During pre-scan training, the subject made her response verbally during the Response phase. During scans, the Response phase was skipped. Finally, a 5-6 rest phase occurred during which the subject could relax. All trial types were counterbalanced.

The results from all three tasks (Figure B-2, A, B, C) identified a variety of brain areas activated preferentially for reaching and grasping and not just looking or attending. The areas showing the greatest overlap for all three tasks were chosen as the potential implant sites before surgery and are superimposed on the fMRI results. Figure B-2, D shows the actual sites located and used for implant.

### C. Supplementary Data

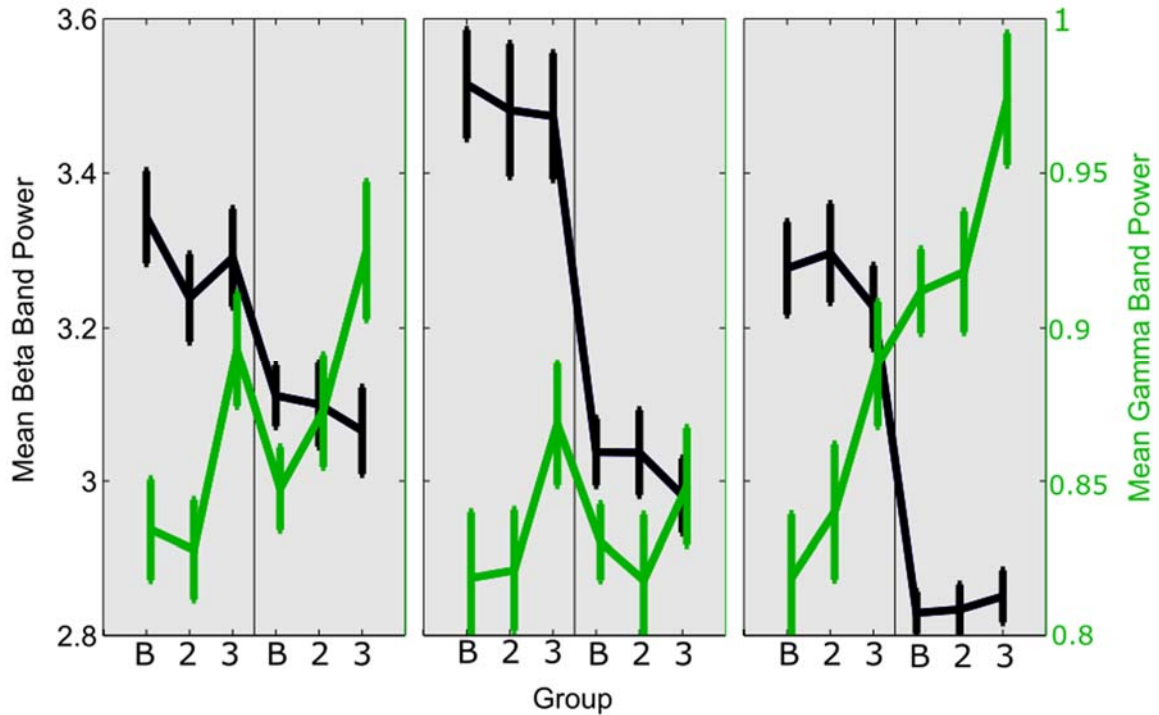


**Figure C-1 Local Field Potential Power for Array 1 During the Gesture Task, Collapsed in Time.** LFP power in beta band (black) and gamma band (green) recorded on Array 1 and averaged across electrodes during the three phases of the Gesture task. Left: Cue, Middle: Delay, Right: Go. Error bars indicate 95% confidence interval of the mean. Left half of each figure panel is Observe trials. Right half is Attempt trials. Effector is noted at the bottom of the figure (B: Bar, 2: 2D Hand, 3: 3D Hand). Note the strong tuning of beta band to Observe/Attempt throughout the task and the tuning to both task variables in the gamma band during the Go phase.

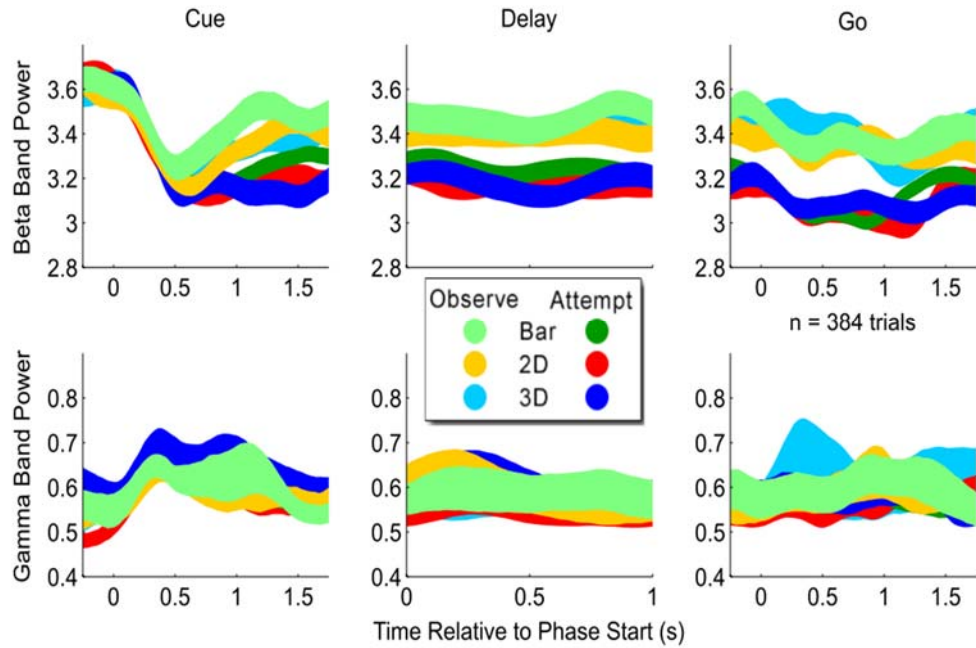


**Figure C-2 Local Field Potentials of Array 2 During the Gesture Task.** Same as Figure 4.1.3.3.1-1 except tracer are for LFP power averaged across Array 2.

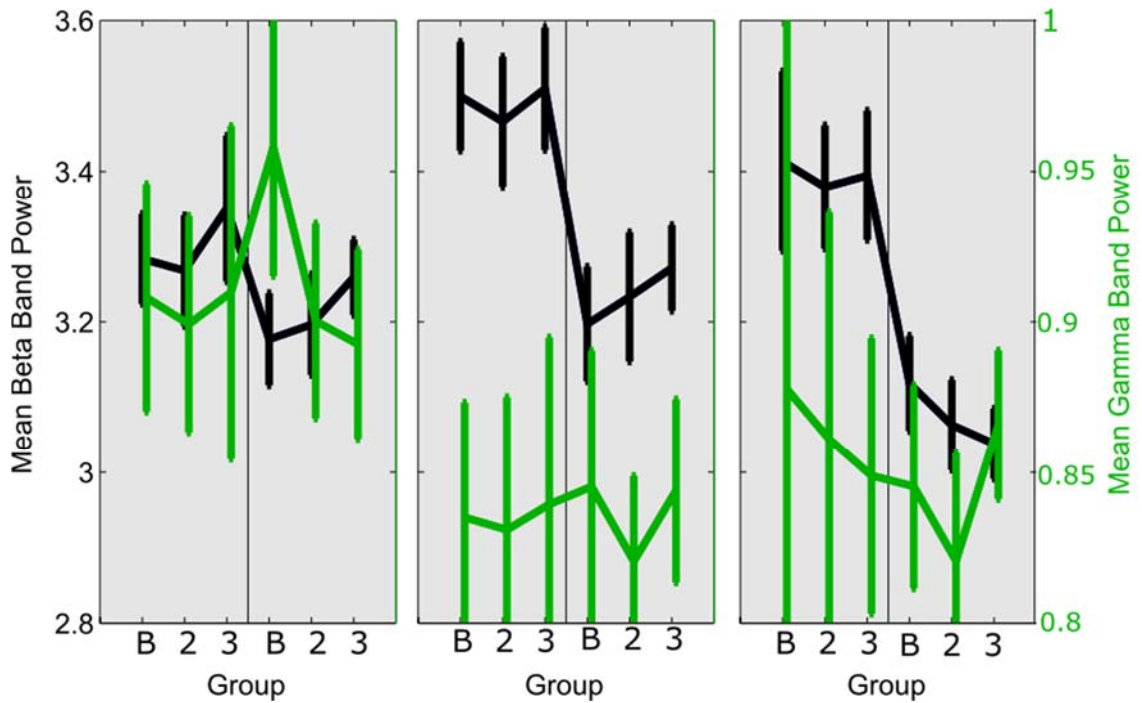


**Figure C-3 Local Field Potential Power for Array 2 During the Gesture Task, Collapsed in Time.** Same as Figure C-1, except for Array 2.

#### **D. Descriptions of Video Files**

**Video 3.1-1** Brain Control performance of the task in the Crowd On condition. Video was regenerated from recorded behavioral data and played back in real-time. The images appear almost exactly as they were viewed by the subject, with one exception: the behavioral clock was superimposed in the top left corner post hoc for reference.

**Video 3.1-2** Brain Control performance of the task in the Crowd On condition as in Video 3.1-1. Here, the Gaze Position has been superimposed post hoc to demonstrate the subject's eye behavior. The video plays back once in real-time and then again at half speed for clarity.

**Video 3.1-3** Brain Control performance of the task in the Crowd On condition as in Video 1. In this sample, the Inter-trial Intervals were set to 1s to demonstrate the subject's ability to return the cursor to the center of the screen in anticipation of the next trial and without visible visual goals. Unrelated to the current study, task performance in this video also included use of a State Decoder.

**Video 3.1-4** Brain Control performance of the task in the Crowd On condition with the targets on a 3 x 3 grid, generated as in Video 3.1-1.

**Video 3.2-1** Comparison video of Brain Control during task performance with State Decoder on versus Off. Videos were regenerated from saved behavioral data and decoder output. Both clips were taken from the same day. The video is identical to what the NHP viewed while performing the task excepting two items added for reference: the time in the upper left corner and titles indicating usage of the State Decoder.

**Video 3.2-2** Video of performance generated as for Video 3.2-1. In this clip, only performance with the State Decoder on is shown. This data was taken from a day when initial performance was already good, and the State Decoder's effect did not reach statistical significance.

**Video 4.1-1** Clips of virtual reality shown to the subject during performance of the 2D reaching task with the various effectors. The full stereoscopic image has been cropped to only show the perspective from one eye. Surrounding black borders are present in the image displayed on the Oculus Rift's internal display, but these borders are outside the subject's field of view.

**Video 4.1-2** Example visual stimuli viewed by the patient on a flat-screen LCD monitor for the Limb Tuning Task. Part of the grey area has been cropped to reduce file size. One of each joint movement is demonstrated in the video, though not for both sides of the body.

**Video 4.1-3** Example trials of the Gesture Task viewed by the subject in virtual reality. The full stereoscopic image is shown in this video to make observable the slight difference between the 2D and 3D Hands. One trial with each trial type (Observe/Attempt) and Effector is shown (Abstract/2D/3D). Slight movement of the image is due to normal small head movements of the subject during task performance.

**Video 4.1-4** Example control during the Online Gesture Control Task. Clips are taken from the beginning of Session 3, the end of Session 3, and the beginning of Session 6, as indicated by the titles added post hoc. These videos show the subject's perspective (again cropped) as she saw it in virtual reality. A simultaneously recorded video of the patient wearing the headset was superimposed post hoc for the first clip. Note the correspondence between her head movements and turning of the perspective in virtual reality.